Oxide-based High Temperature Thermoelectric Generators - Development of Integrated Design Technique and Construction of a Thermoelectric Module

Wijesooriyage, Waruna Dissanayaka

Publication date:
2015

Document Version
Publisher's PDF, also known as Version of record

Oxide-based high temperature thermoelectric generators - Development of integrated design technique and construction of a thermoelectric module

AALBORG UNIVERSITY
DENMARK

Waruna Padmendra Wijesekara Dissanayaka Wijesooriyage

Dissertation submitted to the Faculty of Engineering and Science
in partial fulfilment of the requirements for the degree of

Doctor of Philosophy (Ph.D.)

Aalborg University
Department of Energy Technology
Aalborg, Denmark

Thesis submitted:	07th October 2015
Ph.D. Supervisor:	Professor Lasse Rosendahl Aalborg University, Aalborg, Denmark
Ph.D. Assessment Committee:	Professor Dr. rer. nat. Eckhard Müller, German Aerospace Center (DLR), Cologne, Germany and Justus Liebig University Giessen, Germany
	Professor Nini Pryds, Technical University of Denmark (DTU), Roskilde, Denmark
	Associate Professor Thomas Condra, Aalborg University, Aalborg, Denmark
Ph.D. Series:	Faculty of Engineering and Science, Aalborg University, Aalborg, Denmark
ISBN:	978-87-92846-67-9

Published by:
Department of Energy Technology
Aalborg University
Pontoppidanstraede 101
Aalborg, DK-9220, Denmark
http://www.et.aau.dk
Email: wwd@et.aau.dk

Printed in Denmark by Aalborg University Press

Contents

Mandatory Page

Thesis title : Oxide-based high temperature thermoelectric generators - Development of integrated design technique and construction of a thermoelectric module

Name of PhD student : Waruna Padmendra Wijesekara Dissanayaka Wijesooriyage

Name and title of supervisor and any other supervisors: Lasse Rosendahl, Professor.

List of published papers :

- Paper 1: Waruna Wijesekara, and Lasse Rosendahl: "Expanding the reduced current approach for thermoelectric generators to achieve higher volumetric power density" Phys. Status Solidi A 212, No. 3, 591–599 (2015), DOI 10.1002/pssa.201431335
- Paper 2: Waruna Wijesekara, Lasse Rosendahl, David R. Brown and, G. Jeffrey Snyder: "Unileg thermoelectric generator design for oxide thermoelectrics and generalization of the unileg design using an idealized metal", Journal of Electronic Materials, Vol. 44, No. 6, 1834-1845 (2015), DOI: 10.1007/s11664-014-3569-4
- Paper 3: Waruna Wijesekara, A. Rezania, Lasse Rosendahl: "Simple engineering design for complex thermoelectric generators based on reduced current approach", Energy, 86, 455-466 (2015), doi:10.1016/j.energy.2015.04.058

Conference Contributions:

- Waruna P. Wijesekara, Lasse A. Rosendahl, NingYu Wu, Li Han, Rasmus Bjørk, and Ngo V. Nong: "Performance and Stress Analysis of Oxide Thermoelectric Module Architecture Designed for Maximum Power Output": International Conference on Thermoelectrics – ICT 2013, Kobe, Japan.
- Waruna Wijesekara, Lasse Rosendahl, and G. Jeffrey Snyder: "Altering the designing technique of TEG to generate higher power output while reducing the size the module": 2013 MRS Fall Meeting & Exhibit, Boston, Massachusetts, USA.
- Waruna Wijesekara, Lasse Rosendahl, David R. Brown, and G. Jeffrey Snyder: "Unileg thermoelectric generator design for oxide thermoelectrics and generalization of the unileg design using an idealized metal": International Conference on Thermoelectrics – ICT 2014, Nashville, Tennessee, USA.

This present report combined with the above listed scientific papers has been submitted for assessment in partial fulfilment of the PhD degree. The scientific papers are not included in this version due to copyright issues. Detailed publication information is provided above and the interested reader is referred to the original published papers. As part of the assessment, co-author statements have been made available to the assessment committee and are also available at the Faculty of Engineering and Science, Aalborg University.

Preface and Acknowledgments

This thesis is submitted in partial fulfilment of the requirements for the Doctor of Philosophy in Energy Technology at Aalborg University. This work has been carried out in the period from December 2011 to October 2015 under supervision of Professor Lasse Rosendahl, and is funded by the Danish Council for Strategic Research, Program Commission on Sustainable Energy and Environment through OTE-Power project (Contract No. 10-093971).

I would like to thank all those who support me throughout my doctoral studies. Foremost on this list, I am greatly thankful to Professor Rosendahl for his advice and support during the research. My special thanks go to Professor Jeffrey Snyder for his interest in this work during my stay at Materials Science, California Institute of Technology, 1200 East California Boulevard, Pasadena, CA 91125, USA. I am most thankful to Dr. Alireza Rezaniakolaei, my colleagues and the secretaries at the Department of Energy Technology, for all their kind assistance and support.

I greatly dedicate this thesis to my parents, my wife, my brother, and my relatives for their love, and endless support through all my life from the day that I born to the day that you read this; also to all my teachers for their encouragement at all the time; and also to all my friends who be with me all through my life and sharing all my tears and joys and bring me up to this level by their shoulders.

October 2015
Aalborg, Denmark
Waruna Padmendra Wijesekara Dissanayaka Wijesooriyage

List of Publications

Journal Publications

- Paper A: Waruna Wijesekara, and Lasse Rosendahl: “Expanding the reduced current approach for thermoelectric generators to achieve higher volumetric power density" Phys. Status Solidi A 212, No. 3, 591–599 (2015), DOI 10.1002/pssa.201431335

- Paper B: Waruna Wijesekara, Lasse Rosendahl, David R. Brown and, G. Jeffrey Snyder: “Unileg thermoelectric generator design for oxide thermoelectrics and generalization of the unileg design using an idealized metal”, Journal of Electronic Materials, Vol. 44, No. 6, 1834-1845 (2015), DOI: 10.1007/s11664-014-3569-4

- Paper C: Waruna Wijesekara, A. Rezania, Lasse Rosendahl: “Simple engineering design for complex thermoelectric generators based on reduced current approach”, Energy, 86, 455-466 (2015), doi:10.1016/j.energy.2015.04.058

Conference Contributions

- Waruna P. Wijesekara, Lasse A. Rosendahl, NingYu Wu, Li Han, Rasmus Bjørk, and Ngo V. Nong: “Performance and Stress Analysis of Oxide Thermoelectric Module Architecture Designed for Maximum Power Output”: International Conference on Thermoelectrics – ICT 2013, Kobe, Japan.

- Waruna Wijesekara, Lasse Rosendahl, and G. Jeffrey Snyder: “Altering the designing technique of TEG to generate higher power output while reducing the size the module”: 2013 MRS Fall Meeting & Exhibit, Boston, Massachusetts, USA.

- Waruna Wijesekara, Lasse Rosendahl, David R. Brown, and G. Jeffrey Snyder: “Unileg thermoelectric generator design for oxide thermoelectrics and generalization of the unileg design using an idealized metal”: International Conference on Thermoelectrics – ICT 2014, Nashville, Tennessee, USA.

Abstract

In the field of energy management, thermoelectrics are niche candidates for electrical generator devices. For decades, scientists have been focused on thermoelectric (TE) material development. Thus TE module design techniques are still in relatively virgin state when comparing to the TE material development. This thesis is focused on development and optimization of thermoelectric generator (TEG) design techniques for high temperature (> 700 °C) applications. Some of the main targets of this optimization process are to achieve higher volumetric power density (VPD), and reduce the cost-per-Watt. Oxide based TE materials were used as the core of the TEG due to the focus on high temperature applications and the requirement that the TE materials should be stable at those temperatures. However, p- and n-type oxide TE materials do not perform (zT values) at the same level and it is one of the major challenges identified in this project. Thus, the proposed TEG optimizations should address this challenge in an appropriate manner. The work has established a new TEG optimization strategy based on the existing well-known TEG design technique Reduced Current Approach (RCA). This extended version of RCA is able to produce TEGs with higher VPD, compared to RCA, when the p- and n-leg of the TEG has difference performance levels (zT value) and thus the cost-per-Watt of the TEG can be reduced. Furthermore, the PhD project introduces the Unileg-TEG (U-TEG) concept for the oxide TEGs to address the issues of the thermoelectrically mismatched materials. U-TEG removed the weaker TE material and replaced it with a conductor. It is shown that U-TEG is a valuable concept to increase the VPD of a TE device that has mismatched TE materials. Moreover, U-TEG design is generalized using an idealized metal. Furthermore, well-known Ioffe's method and RCA are compared using the temperature independent TE properties. This comparison opens up a new strategy to reduce the cost-per-Watt of the TEG, by increasing the dominancy of the cheaper TE material in a TEG design. In addition, the work has introduced an engineering approach for complex TEG designing technique RCA, to define the TEG architecture in a simple and time saving manner.

Abstrakt på Dansk

Termoelektriske generatorer er enheder der omsætter en temperaturforskel til elektrisk strøm igennem den såkaldte Seebeck effekt. Disse generatorer, der er kendetegnet ved forholdsvist lave virkningsgrader men høj robusthed, viser sig at være velegnede til niche områder indenfor konvertering af varme til el. I årtier har forskerne primært været fokuseret på udvikling af termoelektriske (TE) materialer. Således er design af selve TE modulet stadig et relativt jomfrueligt forskningsområde, når man sammenligner med TE materiale udvikling. Denne afhandling omhandler udvikling, modellering og optimering af termoelektriske generatorer (TEG) til høj temperatur (> 700 °C) applikationer hvori disse indpasses. Oxidbaserede TE materialer har været brugt som kernen i TEG på grund af fokus på højtemperatur applikationer, og disse materialers høje stabilitet under sådanne forhold. Arbejdet har inkluderet udvikling af nye optimeringsstrategier baseret på eksisterende TEG design teknikker. Numeriske modelleringsmetoder er blevet anvendt til at opstille beregningsmetoder, der er blevet udviklet i løbet af dette arbejde. Unileg TEG konceptet blev introduceret til oxide thermoelectrics for at håndtere misforholdet mellem p og n benets termoelektriske ydeevne, og fordelene ved dette koncept er blevet undersøgt igennem brug af de udviklede desingmetoder. En sammenligning af Reduced Current Approach og Ioffe's metode til at beregne det optimale arealforhold har resulteret i udvikling af en ingeniørmæssig tilgang til arbejdet med at designe komplekse TEG, hvilket resulterer i en mere direkte og resultatorienteret beregningsgang.

1. Introduction

One of the most important considerations in the modern world is energy. The availability of low-cost, low-maintenance solid-state generators capable of converting temperature gradients directly into electricity are attractive in many applications. Thermoelectric generators (TEGs), based on semiconductor materials are such devices. However, TEGs are typically hampered by relatively low conversion efficiencies, which limits their competitiveness, compared to other technologies, to certain niche applications (*e.g.*, sensors that require low-power, remote or autonomous systems; low-grade heat recovery; and high-temperature applications). Their advantages are that they are maintenance free, they have a long lifetime, and they produce a stable DC power output. Furthermore, when the TEG operates with a highly fluctuating input source, the thermal latency of the TEG will act as a filter to minimize the fluctuations in the DC power; unlike PV cells, which respond almost instantly to changes in input.

TEGs are semiconductor devices consists of two p- and n-type semiconductors that are connected thermally in parallel and electrically in series, as shown in Figure 1.1 [1]. The semiconductors, that are thermally and electrically connected to each other by using metal interconnectors, are sandwiched between two ceramic layers. These semiconductor materials are known as thermoelectric (TE) materials and are the core of the TEG.

When the device is subjected to a temperature difference TE effects converts part of the heat crossing the TEG into electricity. The performances of a TE material is measured by the TE Figure-of-Merit (zT), which is defined as the $zT = \frac{\alpha^2}{\rho\kappa}T$, where α is the Seebeck coefficient, ρ is the electrical resistivity, κ is the thermal conductivity, and T is the absolute temperature [2].

Though TE materials are the core of the TEG, the design of the TEG device must also be carefully considered for a particular TEG device. Therefore, the TEG design is important as well as the choice of TE materials, in the field of thermoelectricity.

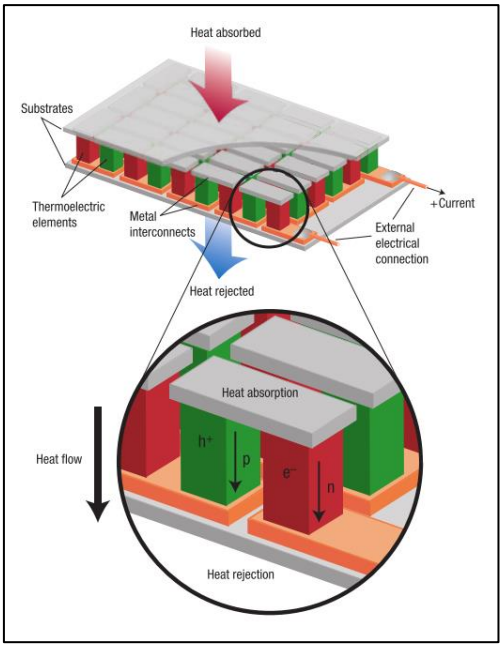

Figure 1.1: Conventional TEG design [1].

1.1 Thermoelectric Generator Applications

TEGs can be applied over a wide temperature range, from room temperature up to above 1000 °C. At room/low temperatures, TEGs often operate in battery-like applications, such as in pacemakers, wrist watches, or wearable thermoelectrics powered by a TEG using body heat [3,4]. Solar powered TEGs are used to meet household energy requirements, using a combined system consisting of a solar thermal collector and a TEG [5–25]. Wood or gas fired heaters could also be combined with TEGs, serving as a good source of power for domestic use. These uses are beneficial for areas isolated from the grid, which can provide lights and power electrical appliances, such as TVs, water pumps, vacuum cleaners, and small kitchen alliances [26–30].Similarly TEGs as a portable power source to power small electronic devices are popular TEG applications. Explorers, people living in remote areas, and soldiers benefit from these devices, and their heat sources are generally microcombustors [31–39].

Energy recovery from vehicle exhaust gas using a TEG can increase the energy efficiency of a vehicle. This technology is currently applied to cars and light vehicles, heavy machinery powered by diesel engines, and military vehicles [3,40–43]. Some other applications include energy recovery from industrial furnaces [44] and subsea level applications in oil wells [45]. TEs also play key roles in deep space applications. Beyond the planet Mars, the radiation from the sun is not sufficient to power a space craft using solar panels, and, radioisotope TEGs (RTEGs) are used [46]. Here, heat generated from the radioactive decay of a radioactive material is

directed to a TEG to generate electricity. RTEGs are not limited to space crafts but are also used to power the rovers used for exploration on Mars.

1.2 Project Scope and Hypothesis

This project is concerned with TEG energy recovery from high-temperature (> 700 °C) heat sources. Energy recovery from the cement kilns at cement manufacturing plants, electricity generation from domestic wood burning stoves, and self-powered air heating systems for tents are some of the applications which are part of the field of interest in this project. The main focus of this PhD project is to develop an integrated design technique for high-temperature TEGs and supply its numerical models. Thus the core part of this thesis is about the current TEG design techniques and optimization of those techniques using engineering approaches.

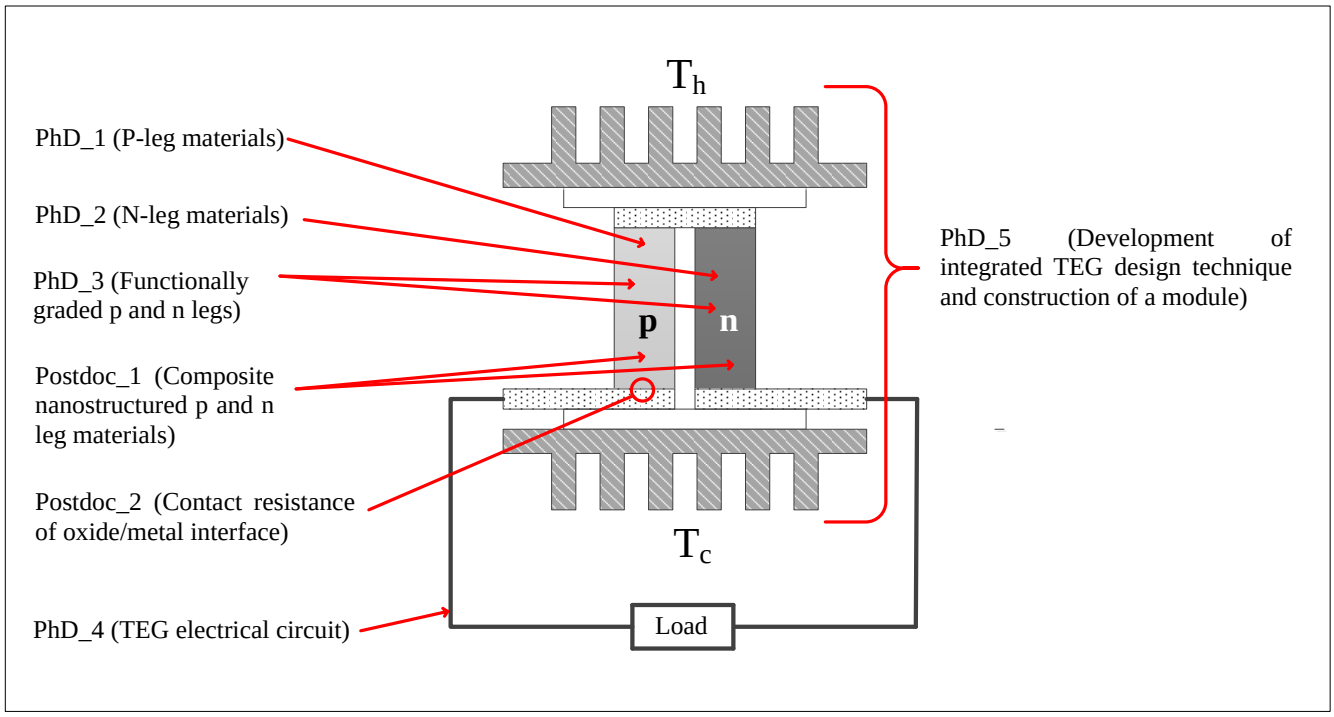

Figure 1.2: The distributed responsibilities of each PhD or Postdoc in the "OTE-Power" project

This PhD project is a subproject of the "OTE-Power" project. The abbreviation "OTE-Power" stands for "Oxide Thermoelectric Power", and the main class of TE materials used in this project is oxide TE materials. The entire OTE-Power project is concerned with every aspect of a TEG, from TE material development to prototype building. The OTE-Power project is funded by the Danish Council for Strategic Research. Three universities in Denmark are involved with the project: Aalborg University, Technical University of Denmark, and Aarhus University. Moreover, 5 PhD projects and 2 Postdoc projects were funded by the OTE-Power project, as shown in Figure 1.2. This PhD project concerns the development of an integrated TEG design technique and construction of a module, which is PhD_5 in Figure 1.2. Thus, one of the main responsibilities of this PhD

project is to combine the outcomes of PhD_1, PhD_2, PhD_3, Postdoc_1, and Postdoc_2 to provide a final TEG design for this high-temperature oxide TE module. The one of the preliminary targets, of the project is to build a TEG that can produce an output greater than 1 W and 4.5 V when the hot side of the TEG is at a temperature of 900 – 1200 K. Therefore, this PhD project is focused on altering the existing TEG design techniques using engineering approaches to make those techniques compatible with the operational, environmental and economic requirements of the OTE power project. This project further focuses on new TEG device technologies and prototype building.

The stability of oxide TE materials at high temperatures provides the freedom to work with high temperature heat sources; though these materials offer low zT values compared to the conventional intermetallic alloy TE compounds. However, oxide TE materials are cost effective compared to some of the intermetallic alloy TE materials [47,48]. Thus, the main TE materials studied in this PhD project, for the oxide TEGs, are p-type $Ca_3Co_4O_9$ and n-type Al doped ZnO [49,50].

As this PhD project focuses on the engineering aspects of the TEG, one of the main concerns is to minimize the cost-per-Watt ($/W) of the TEG, and thus the focus is to increase the volumetric power density (VPD) of the TEG. One of the major challenges to achieve this target is the TE property mismatch of the p- and n-leg TE materials chosen. In the OTE-Power project, the fact that $Ca_3Co_4O_9$ possess considerably higher zT values, in comparison to the Al-doped ZnO, gives rise to a potentially inefficient module. Therefore, this zT mismatch should be addressed by the TEG design method to produce higher power output at high temperatures. These challenges are addressed in this PhD project by modifying existing TEG design techniques, and by finding alternative economical material combinations for p- and n-legs. Considering the cost-per-Watt of the TEG, another focus is to identify and use the appropriate TEG design techniques for specific operating conditions to increase the cost effectiveness of a TEG.

To minimize the cost-per-Watt of the TEG, the first focus is to optimize the cross-sectional area ratio of the p- and n-leg of the TEG to obtain high VPD. The efficiency $\left(efficiency = \frac{Power\ output}{Heat\ input\ to\ the\ hot\ side\ of\ the\ TEG}\right)$ is one of the main focuses when designing a TEG, and thus the most efficient area ratio of p- and n-legs is essential [51–53]. However, for the applications at high-temperatures or with essentially free heat sources, the power output should be the main focus to minimize the cost-per-Watt of a TEG [54,55]. Moreover, reducing the length of the thermoelements will increase the power output, but will decrease the efficiency of a TEG [54,55]. The OTE-Power project is concerned with high-temperature applications. Thus, by considering the above facts, the maximum power output should be the main focus and not the efficiency when designing the TEG in this project. Therefore the concept of most efficient area ratio for the temperature dependent TE properties in the reduced current approach (RCA) proposed by Snyder et al. [51,52] is combined with the concept of reducing the thermoelement length to obtain higher power output by Min et al. [54,55], to develop the TEG for the OTE-Power project. This combining process results in a new TEG design technique based on RCA, called extended reduced current approach (ERCA). One of the important questions that this new method should address is how to combine thermoelectrically mismatched p- and n-leg TE materials in a TEG in an appropriate manner, because the p-type oxide TE materials have more superior TE properties than the n-type oxide materials. It has been proven that ERCA is a valuable method for the OTE-Power project and ERCA is able to produce a TEG with considerably higher VPD compared to the RCA at the same operating conditions, using the TE materials in the OTE-Power project. This new method and its limitations are introduced in Chapter 3 of this thesis, and the

journal article "Expanding the reduced current approach for thermoelectric generators to achieve higher volumetric power density" is attached to this thesis as Paper A.

To reduce the cost-per-Watt of a TEG, another focus of this PhD project is to find economical material combinations for p- and n-legs, either using only TE materials or using TE materials and metals. As mentioned earlier, the core TE materials used for the OTE-Power project are oxide TE materials. Thus, $Ca_3Co_4O_9$ was used as the p-type TE material, and Al-doped ZnO was used as the n-type TE material. Oxide TE materials have low zT values, and p-type oxide materials have more superior TE properties than n-type oxide materials, which can be a critical issue when making the TE devices, for many reasons. One reason is that a weaker TE material may not produce an output comparable to the superior material, and thus, the weaker material could act as a resistor, hindering the output of the superior material. Additionally, the weaker material could add a high cost-per-Watt to the TEG. Thus, it could be beneficial to replace the weaker TE material with a more common and inexpensive conductor (*e.g.* Copper, Nickel, Constantan, *etc.*). Of course, this could introduce thermal shortening (thermal short-circuiting) problems to the thermal circuit of the TEG, but those are questions that can be resolved by changing the design parameters. This concept is called unileg TEG (U-TEG) in this thesis. The U-TEG concept was already used in some other works such as Nemoto et al. They built a Mg_2Si based unileg TEG for the temperature range of 300 – 900 K [56]. Madan et al. presented a thick-film single element TEG based on Se-doped Bi_2Te_3 (with 2% Se and 1% Se) for the temperature range of 20 – 100 °C [57,58]. However, these studies did not systematically study the U-TEG concept or perform a comparison of U-TEG with a conventional unicouple TEG device. In this project, we performed a systematic study of the U-TEG concept, first combining Constantan with an oxide TE material and then combining three types of imaginary idealized metals with oxide TE materials. In addition, we performed a proper comparison of U-TEG with a conventional TEG. Based on all of these studies, we proved that U-TEG is a valuable concept for the OTE-Power project and can produce less expensive TEGs with a high power density. U-TEG will reduce the cost-per-Watt of oxide TEG devices. This U-TEG concept is introduced in Chapter 4 in this thesis and the attached the journal article "Unileg thermoelectric generator design for oxide thermoelectrics and generalization of the unileg design using an idealized metal" as Paper B.

Another focus of this PhD project is to identify and use the appropriate TEG design techniques for specific operating conditions to minimize the cost-per-Watt of the TEG. Two of the most established TEG design techniques have been considered in here are the method proposed by Ioffe in 1957 (Ioffe's method) [53] and the RCA in 2003 [51,52]. These two methods use different strategies to claim the most efficient area ratios for the p- and n-legs of a TEG. Therefore, this difference could lead to obtain different optimal area ratios that might open for some designs giving cost reductions when the unicouple have very different zT for the p- and n-legs. This project identifies an interesting relationship between Ioffe's method and RCA for the temperature independent TE material properties: when the TE properties of the p- and n-legs are the same, at the same operating conditions, the most efficient area ratios given by Ioffe's method and RCA are the same. Moreover, for the same total thermoelement area and thermoelement length, both methods predict the same power output and efficiency. However, when the TE properties of the p- and n-legs are different, at the same operating conditions, Ioffe's method and RCA do not predict the same p- and n-leg area ratio as the most efficient p- and n-leg area ratio (this can give rise to a significant area ratio difference, as explained in Chapter 5). Although for the same total thermoelement area and thermoelement length, both methods predict the same power output and efficiency. This

effect forms the basis of a comparison of the fundamentals of these two approaches, as well as a cost-reduction study based on the optimal material amounts for each leg predicted by the two methods in Chapter 5.

As described earlier, Ioffe's method is one of the established and earliest TEG design techniques that can be used for TEGs with temperature independent TE properties [53]. As stated in the previous paragraph and Chapter 5, the RCA is plays an important role even for TEGs with temperature independent TE properties, by defining different optimal TEG architecture (length and cross-section area of thermoelements) than the Ioffe's method that could increase the cost effectiveness of the TEG [51,52]. However, RCA is a more complex technique, compared to the Ioffe's method, and a high level of knowledge about the technique is needed to work with it. Thus a simple form of this complex and reliable technique would be very beneficial for researchers who do not have extensive knowledge of TEG design techniques. It would also be highly beneficial for TEG designers to make their initial predictions of the TEG architecture without requiring long and time consuming calculations. Therefore, simplified TEG design technique based on RCA is introduced in this work for temperature independent TE material properties. This method can predict the most efficient TEG architecture with a degree of agreement greater than 97% to the TEG architecture given by RCA for the majority of the possible temperature and zT ranges of current TEGs. This technique is introduced in Chapter 6 of this thesis and the attached journal article "Simple engineering design for complex thermoelectric generators: based on reduced current approach" as Paper C.

Originally, designing an OTE-Power prototype was a part of this PhD project. However, due to timing and coordination effects, this was not possible within the time frame. Therefore, data from the OTE-Power TEG module constructed early in the project was used to make the initial comparison between the ideal model and the real device. However, a prototype of an U-TEG have been developed, which is based on Zn_4Sb_3 and constantan, as these materials were gracefully provided by project partners Aarhus University and TEGnology. The laboratory facilities at Aarhus University were used to build the U-TEG device. Unfortunately, it has not been possible to produce module characterization data in time for this thesis.

As a consequence, the focus of this project has been shifted to on engineering aspects of the TEG, some of the main concerns of this PhD project are increasing the volumetric power density and decreasing the cost-per-Watt of a TEG. Therefore, a focus of this PhD project is to address the challenges of combination of two thermoelectrically mismatched materials in order to produce a TEG with higher volumetric power density by using two different approaches. The first approach defines a new TEG design technique that can produce high volumetric power density using thermoelectrically mismatched materials. The second approach replaces the weaker TE material with a well-known inexpensive conductor. Finally, the cost-per-Watt of a TEG is decreased by reducing the amount of expensive TE material in the TEG system by using different TEG design techniques, while keeping the volumetric power density constant. Additionally, this PhD project provides a simplification of the RCA.

2. Fundamentals and state-of-the-art of thermoelectrics and TEG modelling

2.1 Theory of Thermoelectric Materials

Since TE devices are based on TE materials, it is essential to understand the fundamental characteristics of TE materials. This understanding will help to identify the differences between good and poor TE materials, and the reasons behind these differences. Basically, TE properties depend on the temperature. Thus a TE material could be a poor TE material for a specific temperature range, but it may suitable for another temperature range. At the TE device stage, the usefulness of a TE material depends on many factors, such as, best performing temperature range, physical properties, ability of the TE material to combine with other TE or Non-TE materials, preferred working environment, *etc.* When considering these facts, both good and poor TE materials are important in the field of thermoelectrics. Therefore, how to utilize also the poor TE materials by themselves or together with good TE materials in TE devices is an important concern. Thus to identify and address these issues, an understanding about TE material fundamentals is important, before focusing on TE devices. This understanding includes basic TE material properties and physics behind them, common and potential TE materials, working temperature and other important physical properties of TE materials, *etc*.

In simple terms, a material which could generate electricity, when it subjected to a temperature gradient can be termed as a TE material. There are three main TE effects in a TE material: the Seebeck effect, Peltier effect, and Thomson effect. To outline these effects, two dissimilar conductors (a and b) that are connected thermally in parallel and electrically in series can be considered, as shown in Figure 2.1, which is a basic thermocouple.

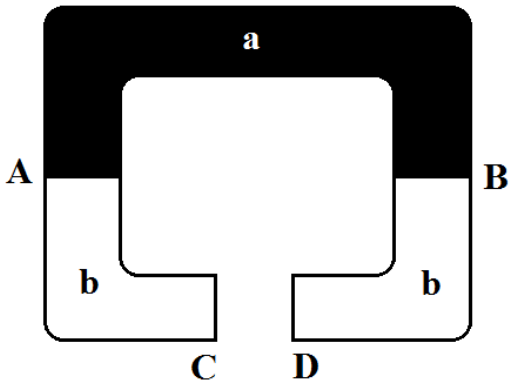

Figure 2.1: Basic thermocouple made of materials a and b.

If T_1 and T_2 are the temperatures of junctions A and B, respectively ($T_1 > T_2$), the open circuit electromotive force between C and D can be expressed as in Equation (2.1), which is the differential Seebeck coefficient (α_{ab}) between materials a and b. Thus, the Seebeck coefficient (α) is the voltage (V) that the material can generate per unit temperature difference (ΔT) [2]. The units of the Seebeck coefficient is *V/K*, more commonly given as $\mu V/K$.

$$V = \alpha\,(T_1 - T_2) \;\Rightarrow\; \alpha = \frac{V}{\Delta T} \tag{2.1}$$

When a potential difference is applied externally to C and D in Figure 2.1, an electric current (I) is produced. The rate of generation of heat (q) occurs at junction A or B, and the rate of cooling ($-q$) occurs at the other junction. In this system, the Peltier coefficient (π) is defined as the ratio between q and I, as shown in Equation (2.2). The unit of the Peltier coefficient is *W/A* or *volts* [2].

$$\pi = \frac{q}{I} \tag{2.2}$$

The Thomson effect describes the rate of generation of reversible heat (q) within a conductor when it is subjected to a temperature gradient (ΔT) while passing an electrical current (I) through it. The Thomson coefficient (β) can be expressed as in Equation (2.3), and the unit of the Thomson coefficient is *V/K* [2].

$$q = \beta\, I \Delta T \tag{2.3}$$

The Kelvin relations combine the above three thermoelectric effects as follows in Equations (2.4) and (2.5) for two dissimilar connected materials "a" and "b" [2].

$$\alpha_{ab} = \frac{\pi_{ab}}{T} \tag{2.4}$$

$$\frac{d\alpha_{ab}}{dT} = \frac{\beta_a - \beta_b}{T} \tag{2.5}$$

The thermoelectric material efficiency can be stated as in Equation (2.6) using the dimensionless TE "figure-of-merit (zT)". The zT of a material depends on the Seebeck coefficient, electrical resistivity (ρ) or electrical conductivity (σ), thermal conductivity (κ), and the absolute temperature. Moreover, $\alpha^2\sigma$ is defined as the power factor.

$$zT = \frac{\alpha^2}{\rho\kappa}T = \frac{\alpha^2\sigma}{\kappa}T \tag{2.6}$$

The behaviour of different TE properties with the carrier concentration is illustrated in Figure 2.2 [2]. Insulators have low carrier concentrations and the metals have high carrier concentrations. When the carrier concentration in a material increases, the Seebeck coefficient decreases, and the electrical conductivity increases. Thus, the power factor of a material will peak at the carrier concentrations of a semiconductor. Moreover, the electronic thermal conductivity increases with the carrier concentration, although the lattice thermal conductivity does not depend on the carrier concentration.

As stated earlier, the charge carrier concentration of a material also affects the TE properties of the material. The two types of carriers present in a material are electrons and holes. Negative carriers promote n-type conduction,

and positive carriers promote p-type conduction. When a material is subjected to a temperature gradient, carriers on the hot side tend to move to the cold side. This movement of carriers will generate a Seebeck voltage across the material. However, if a material contains equal numbers of n- and p-type carriers, the charge carriers will cancel each other out, and the generated Seebeck voltage will be zero. Insulators and semiconductors have high Seebeck coefficients, as shown in Figure 2.2. This behaviour is explained in Equation (2.7) [1], where n is the charge carrier concentration and m^* is the effective mass. Thus, when insulators and semiconductors have low charge carrier concentrations, they will have high Seebeck coefficients. Furthermore, the high effective mass will also increase the Seebeck coefficient based on Equation (2.7). Therefore, low n and high m^* will help to increase the Seebeck coefficient and increase the zT value of the material based on Equation (2.6). However, based on Equation (2.8), the electrical conductivity will decrease when the number of charge carriers is reduced [1]. Moreover, the carrier mobility (μ) will decrease when the charge carriers have a high effective mass. Therefore, low n and high m^* will decrease the electrical conductivity and have a negative effect on the zT value based on Equation (2.6).

$$\alpha = \frac{8\pi^2 k_B^2}{3eh^2} m^* T \left(\frac{\pi}{3n}\right)^{2/3} \tag{2.7}$$

$$1/\rho = \sigma = ne\mu \tag{2.8}$$

The thermal conductivity of a material is a combination of two different thermal conductivities, the electronic thermal conductivity (κ_e) and the lattice thermal conductivity (κ_l). The electronic thermal conductivity is the electron/hole contribution to the heat transfer, and the lattice thermal conductivity is the phonon contribution to the heat transfer. Thus, the thermal conductivity of a material can be stated as in Equation (2.9). The Wiedemann-Franz law describes the electronic thermal conductivity of a material and can be expressed as in Equation (2.10) [1].

$$\kappa = \kappa_e + \kappa_l \tag{2.9}$$

$$\kappa_e = \sigma L T = \frac{LT}{\rho} \tag{2.10}$$

where L is the Lorenz factor, which is equal to $2.8 \times 10^{-8}\ J^2/K^2C^2$ for free electrons.

However, the Lorenz factor depends on the carrier concentration. In general practice, the lattice thermal conductivity is calculated using the difference between the total thermal conductivity and the electronic thermal conductivity of the material. The electronic thermal conductivity is calculated using Equation (2.10), using the experimentally determined electrical conductivity. Thus, the exact value of the Lorenz factor is essential. For materials with low carrier concentrations, the Lorenz factor could be reduced by up to 20% of its free electron value [1,59].

The bipolar effect is another concern that affects the thermal conductivity of a material [1,60]. The bipolar effect arises because of the two types of charge carriers, *i.e.*, electrons and holes. The contribution of the three types of

thermal conductivity to the total thermal conductivity is shown in Figure 2.3 for a $Si_{80}Ge_{20}$ n-type semiconductor [60]. The bipolar effect increases with temperature due to the excitation of electrons from the valence band to the conduction band as the temperature increases, creating an equal number of holes. These electrons and holes will then move to the cold side and transport heat from the hot side to the cold side. However, the net electrical current is zero in this movement due to the equal numbers of opposite charges. Moreover, the presence of both electrons and holes will have a negative effect on the Seebeck coefficient. Thus, removing the bipolar effect helps improve zT in two different ways.

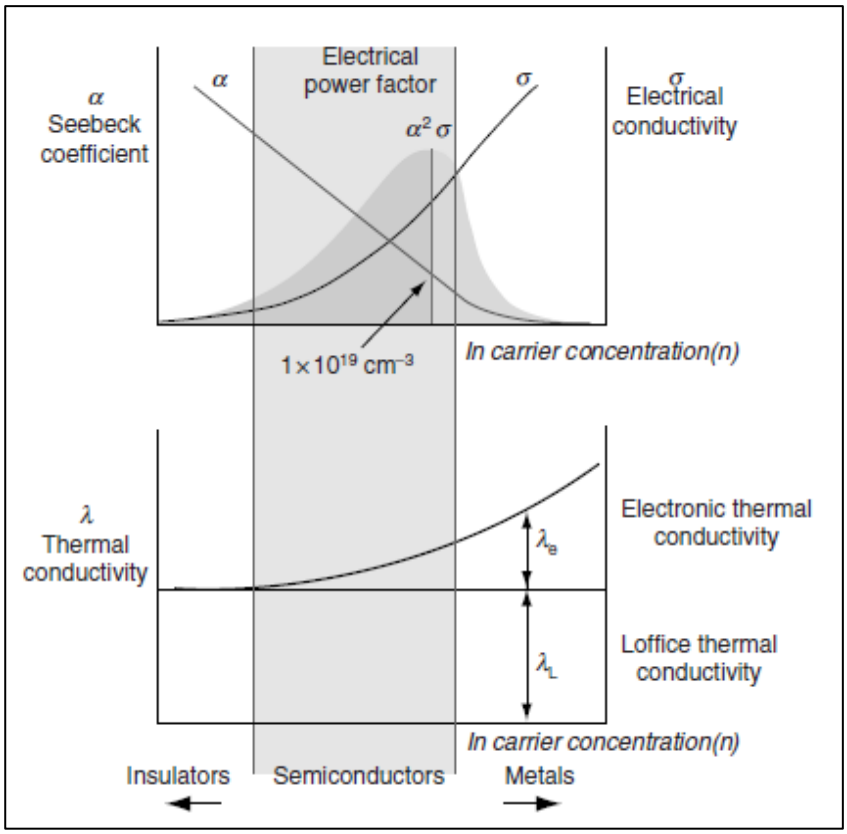

Figure 2.2: Variations of TE properties, Seebeck coefficient (α), electrical conductivity (σ), power factor ($\alpha^2\sigma$), and thermal conductivity (λ), with the carrier concentration [2].

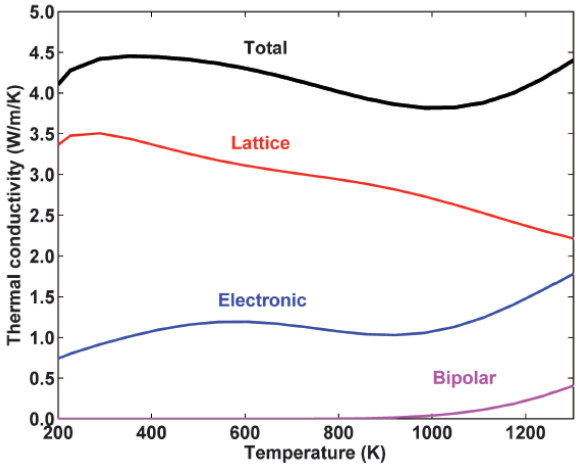

Figure 2.3: Contribution of lattice, electronic, and bipolar thermal conductivities to the total thermal conductivity for a $Si_{80}Ge_{20}$ n-type semiconductor [60].

2.2 State-of-the-art thermoelectric materials and properties

According to Equation (2.6), good TE materials should have a high electrical conductivity, high Seebeck coefficient, and low thermal conductivity. As shown in Figure 2.2, metals have a high electrical conductivity, but they have low Seebeck coefficients and high thermal conductivities, whilst insulators have high Seebeck coefficients and low thermal conductivities, but they have low electrical conductivities. Thus, neither metals nor insulators are suitable for use as TE materials. Due to their peak power factors and considerably low thermal conductivities, heavily doped semiconductors are the most suitable candidates as TE materials. Some state-of-the-art commercial TE materials are shown in Figure 2.4 [1].

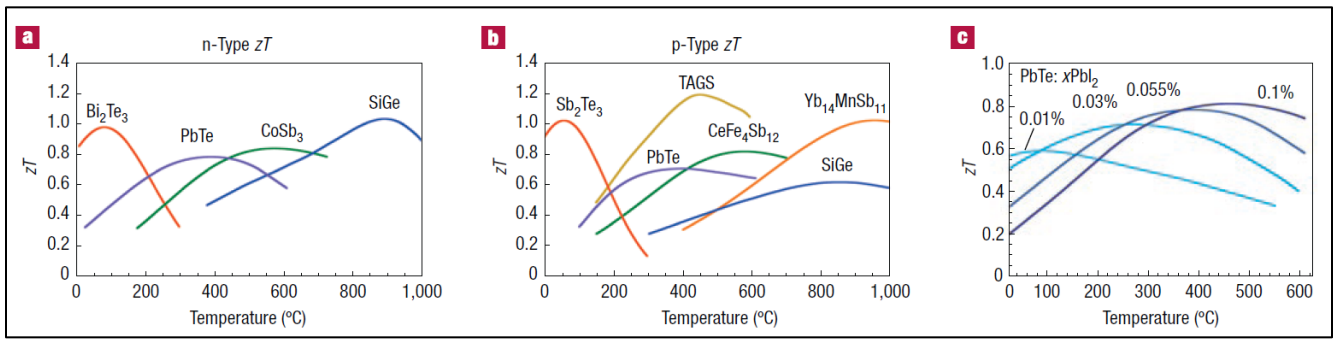

Figure 2.4: Some of the state-of-the-are commercial TE materials with their TE Figure-of-Merit (zT): (a) n-type TE materials, (b) p-type TE materials, and (c) effects of the dopant concentrations on PbTe in terms of zT and the temperature at which the highest zT occurs [1].

Some of the most famous and widely used TE materials are alloys of Bi_2Te_3 and Sb_2Te_3, for applications below 250 °C [6,10,13,15,17,27,29–31,45,61–64]. Different material development techniques were applied to produce these materials, and the majority of these techniques produced materials with *zT* values of approximately 1.0 [1,2,59,65–70]. Poudel et al. produced bulk nanostructured bismuth antimony telluride with a *zT* of 1.4 using the ball-milling technique [71]. Venkatasubramanian et al. produced p-type Bi_2Te_3/Sb_2Te_3 superlattice structures with a *zT* of 2.4 [72]. Another promising TE material is lead telluride (PbTe), which can produce a *zT* of approximately 1.0 at operating temperatures from 300 – 600 °C [1,2,70,73–76].

Clathrates are another class of TE materials that have low thermal conductivities with an open framework structure. Clathrates succeed in producing *zT* values of approximately 0.7, and the operating temperatures are in the range of 100 – 600 °C [1,2,59,75,77]. Skutterudites are another interesting class of materials for thermoelectrics. Some skutterudites could produce a *zT* of 1.0 at 600 °C, and these could operate at 300-800 °C [1,2,59,75,77–82]. Half-Heusler (HH) compounds are another interesting class of candidates for use as thermoelectric materials [1,75,77,83]. These intermetallic alloys are good candidates for high-temperature applications due to their high stability at elevated temperatures, with melting points of 1100 – 1300 °C and zero sublimation at 1000 °C. The HH alloy $Hf_{0.75}Zr_{0.25}NiSn_{0.975}Sb_{0.025}$ could produce a *zT* of 0.8 at 750 °C [75].

β-Zn_4Sb_3 is another thermoelectric material that has a low thermal conductivity [75,84]. Some researchers reported a *zT* value for β-Zn_4Sb_3 of 1.3 at 400 °C. The melting point of β-Zn_4Sb_3 is approximately 560 °C. However, one of the main drawbacks of β-Zn_4Sb_3 is that it decomposes to ZnSb and Zn at temperatures lower than its melting temperature. Undoped Mg_2Si is an n-type TE material that has low *zT* values below 400 °C [56,85–87]. The doping of Mg_2Si could increase the TE properties of the materials and would be able to increase the *zT* up to 0.5 [88]. Some other types of silicides available as TE materials are boron silicide [74], manganese silicide [89,90], chromium silicide, and cobalt silicide [90]. Silicon germanium (SiGe) is a material that can be used as either a p- or n-type thermoelectric material [1,2,74,82,91–93]. Reported *zT* values of n-type SiGe are approximately 0.9, and for the p-type, it is approximately 0.5 at operating temperatures of 600 – 1000 °C [1]. Further improvements to the material have also been reported that can increase the *zT* up to 1.3 for n-type and 0.95 for p-type materials [91]. Another interesting TE material is tin selenide (SnSe). Recent reports show that some crystal axes of SnSe could produce high *zT* values of up to 2.6 at 650 °C [94,95]. Organic thermoelectrics are another class of interesting TE materials that can produce flexible TE devices [96–102], suggesting applications as wearable thermoelectrics. Organic TEs have relatively low *zT* values, but some reports show a value of 0.4 for this class of materials [98].

As shown in Figure 2.5, Oxide-TE materials are another class of TE material and are popular for high-temperature waste heat recovery applications [50,75,81,103–110]. $NaCo_2O_4$ and $Ca_3Co_4O_9$ are promising p-type oxide TE materials that can produce *zT* values of approximately 1.0 [75,108]. These materials produce high thermopower at elevated temperatures, which helps to generate high *zT* values [75,103,108–110]. $SrTiO_3$, ZnO, and $CaMnO_3$ are n-type oxide TE materials [50,75,104,106,107] that have lower *zT* values than p-type oxide materials of approximately 0.3 [75]. In a TEG, oxide TE materials could cause problems in the oxide/metal electrode contact zones due to high contact resistances. Additionally, a high thermal expansion coefficient mismatch between the metal and oxide could cause cracking in the contact zones of the TEG during operation. Semiconductors and intermetallic alloy TE materials are composed of toxic or heavy elements, and at high temperatures, they undergo melting, sublimation or oxidation [75]. However, oxides are highly stable at elevated

temperatures. Moreover, they are prepared from low-cost, non-toxic raw materials, and the synthesis processes are relatively simple [81,109]. The OTE-Power project is concerned with high-temperature waste heat recovery applications. Thus, oxide TE materials are used as the core TE materials in the design of high-temperature TEGs in this project. As shown in the Figure 2.5, oxide TE materials have a poor performance at low temperatures. When oxide TE materials are used in large temperature gradients, the total efficiency of the TEG system decreases due to the poor performances of the oxides at low temperatures. Thus the OTE-Power project also focused on the segmented TE materials to tackle the poor performance at low temperatures [48]. In the OTE-Power project, segmentation is done by combining oxides with intermetallic alloy TE materials [48].

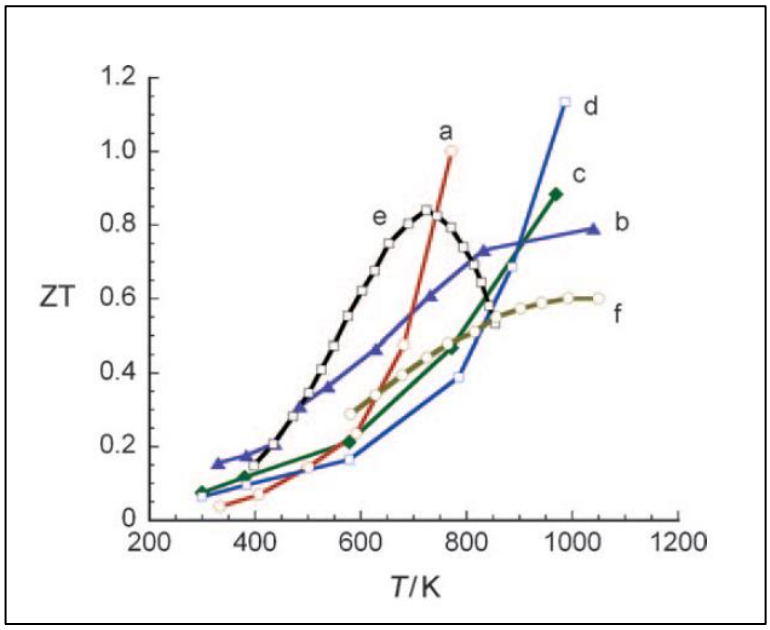

Figure 2.5: Variation of the zT of some of the oxides with temperature, (a) Na_xCoO_2 (crystal), (b) Na_xCoO_2 (ceramic), (c) $Ca_3Co_4O_9$ (crystal), and (d) $Bi_2Sr_2Co_2O_y$ (crystal) compared to the conventional TE materials, (e) PbTe and (f) $Si_{1-x}Ge_x$ [75]

2.3 Thermoelectric Devices

The power output of a TE material is essentially determined by the TE device. Thus, it is important to have a complete understanding of TE device technology [83,90,111–116]. As discussed in Section 2.1, Seebeck and Peltier discovered two basic phenomena of thermoelectrics, and thermoelectric devices are based on both phenomena. TE devices are mainly classified into one of two basic categories, TEGs which generates electricity when it subjected to a temperature difference, and thermoelectric coolers (Peltier coolers) which generates a temperature difference when supply an electric current. Both have the same basic schematic with unicouple architecture, as shown in Figure 2.6. It consists of p- and n-type semiconductor TE materials that are connected by an electrically and thermally conducting material. The connections are developed in such a way that they are

electrically in series and thermally in parallel. A more detailed discussion of this setup is provided in a later part of this section.

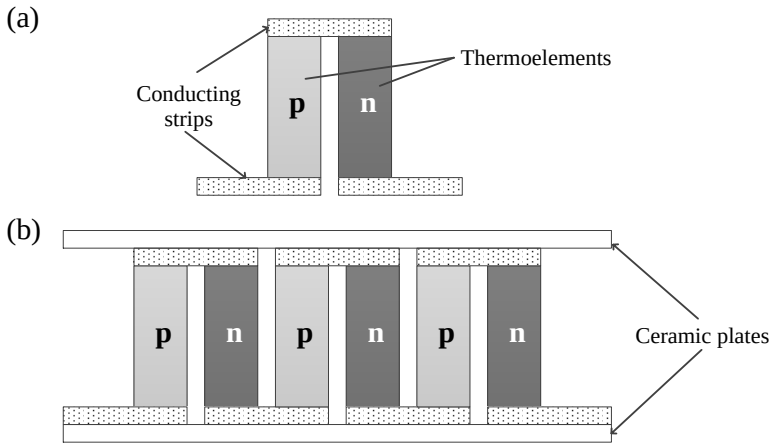

Figure 2.6: (a) Basic thermoelectric unicouple, (b) Thermoelectric module, where p is the p-leg, and n is the n-leg

The applications of TEGs range from a wristwatch powered by a TEG using body heat [3] to a spacecraft powered by a radioisotope TEG [46]. TEGs are used in a vast range of temperatures, from room temperature to more than 1000 °C. Regardless of the temperature range or the complexity of the system in which it is applied, the basic physics behind TEGs are the same. A basic schematic of a TEG is shown in Figure 2.7, with unicouple TEG architecture. As shown in Figure 2.7, the p- and n-semiconductor legs of the unicouple TEG are connected to the heat source and a heat sink in such a way to keep the thermal circuit in parallel and the electrical circuit in series with the load resistor. Here, it will generate a temperature difference across the semiconductors, when the heat source injects heat into the semiconductor and the heat sink removes heat. This temperature difference will result high energy charge carriers on the hot side (side of the heat source) of the semiconductors and low energy charge carriers on the cold side (side of the heat sink). Thus, high energy charge carriers will move from the hot side to the cold and this movement generates an electric current through the semiconductors. The majority charge carriers of p- and n-type semiconductors are holes and electrons, respectively. Therefore, as shown in Figure 2.7, this movement of charge carriers will generate an electric current in the opposite directions of the p- and n-legs, which will help maintain the series connection of the electrical circuit of the TEG [111].

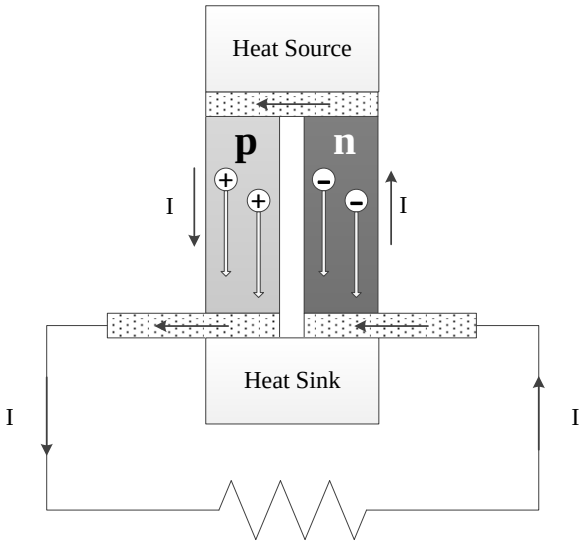

Figure 2.7: Basic schematic of thermoelectric generator, where p is the p-leg, n is the n-leg, and I is the electrical current

TEGs can be developed as bulk TEGs and thin-film TEGs and the main difference between these two types is the thickness of the thermoelements. Bulk TEGs are based on bulk TE materials with higher TE material thicknesses comparing to the thin-film TEGs. Generally, the thickness of the TE martials in the bulk TEGs are in the millimetre to centimetre range and these have been the most common type of TEGs for decades. Thicknesses of the TE materials in the thin-film TEGs are in the nanometre to micrometre range [117–121]. Theoretical predictions show that the thin-film version of a TE material could possess higher zT values compared to the bulk version of it [122] and this is one of the advantages in thin-film TE materials. However, there are a number of challenges to address when working with thin-film TEGs. Preparing and characterising of thin-film TE materials need special material development and characterization techniques compared to bulk TE materials. Chemical vapour deposition [123,124], physical vapour position [125], and electro chemical deposition [67,126] are some of the thin-film TE material development techniques. Maintaining a large temperature gradient between hot and cold side of a thin-film TEG is another important challenge [121]. One of the main challenges associated with both bulk and thin-film TEGs is the contact resistance as it negatively affects the power output of a TEG [127–129]. Thus it is important to address these challenges to increase the efficiency of TEGs. TE modelling has the ability to generate these challenges in a virtual manner in a TEG system. Thus TE modelling can be a useful tool to understand and address these challenges associated with both bulk and thin-film TE devices.

Another recent concept in the field of TEGs is the Unileg-TEG (U-TEG) concept. As the name suggests it only uses one p- or n-leg TE material [56–58,130]. This concept replaces the weaker thermoelement from p- and n-

legs of the TEG with a cheaper and more readily available metal. U-TEG could reduce the cost-per-Watt of the TEG and increase the volumetric power density of the TEG under the same operating conditions. The U-TEG has a lower number of metal/semiconductor contacts in the system compared to the TEG, and thus it could exhibit a low contact resistance compared to the TEG. One of the challenges associated with the U-TEG concept is the thermal shortening effects generating by the metal that have replaced the weaker TE material of the TEG. TE modelling could simulate these challenges virtually in a TEG system and thus TE modelling can be used as a tool to address these challenges.

2.4 Modelling Thermoelectric Generators

2.4.1 Importance of Thermoelectric Generator Modelling

TE materials have achieved significant developments with the advance of nanotechnology. Moreover, TE exhibits unique advantages as an energy converter, and, these environmentally benign devices have a huge potential as a green energy source. Though TEs have a number of advantages, they still have low conversion efficiencies compared to other available energy technologies. Vining has placed the TE in relation of other available energy technologies [131] as shown in Figure 2.8. Obviously, it is impossible to match the efficiency of a Rankine cycle using a TE, and therefore, it is unlikely that TE will be competitive in the field of large-scale electricity production. What is more likely is that niches, where a combination of the positive properties of TEs outweighs its negative features, will be identified, and TEGs will be designed to meet these demands. However, a key aspect in these uses is the minimization of the loss of material efficiency through the design of the actual module, and in the larger perspective, through the power management system.

A TEG module is a device that consists of a combined thermal circuit and an electrical circuit, and in its simplest form, consists of a single unicouple. Three types of materials are generally used to build the device: semiconductors, conductors and ceramics. Figure 2.9 shows a model of a unicouple TEG design under load conditions, giving (a) the total displacement due to thermal expansion and (b) the von Mises stress. Matching those thermal and electrical circuits using these three types of materials involves a number of physical and engineering phenomena, such as TE fundamentals, Joule heating, thermal conductivity matching, thermal and electrical contact resistances, thermal expansion differences, thermomechanical stress, mechanical bonding, non-uniformity effects, and possibly radiation effects. This confirms that developing an efficient and durable TEG is a complex process, so that modelling may be an appropriate tool, facilitating both the design and the development of a deeper understanding of the complex interactions between the transfer processes involved.

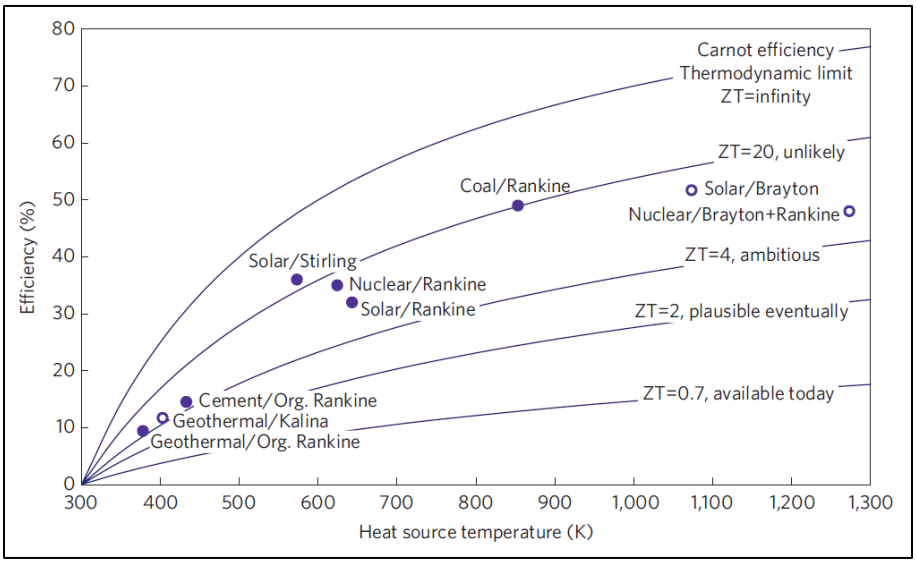

Figure 2.8: Estimates of TE efficiency in the context of other available energy sources [131].

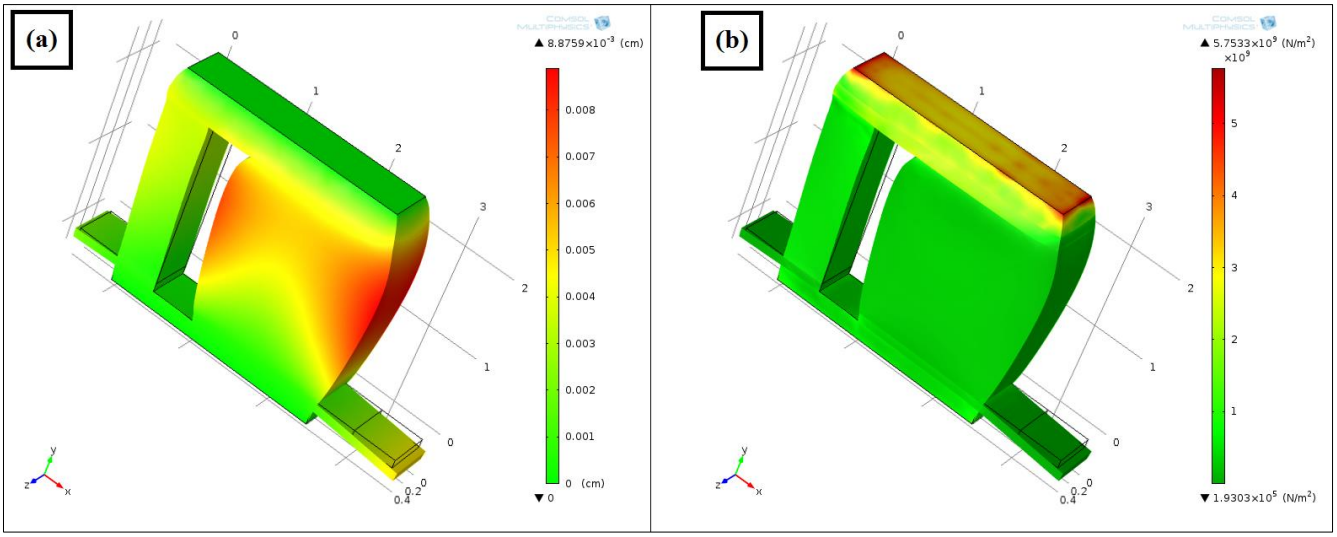

Figure 2.9: Unicouple TEG consists of semiconductors, conductors and ceramics (a) total displacement, (b) von Mises stress. Top and bottom surfaces of the TEG kept as fixed surfaces. Top surface at 1100 K and the bottom surface at 400 K.

The approach used to develop a TEG can be illustrated as in Figure 2.10. Starting with a case defining the physical boundary of the TEG (typically the temperatures), a model of the TEG is developed to provide the architecture and expected performance. Then the process could be connected to a virtual prototyping loop before it continues with a prototype. This could ultimately reduce the need for experiments for each prototype. However, in order for this to be trustworthy, the model and submodels need to be stringently formulated as well as very well validated. Additionally, they need to address the "departure from ideal conditions" that real devices experience. In here, the focus should be on 3-D modelling techniques as well as the 1-D modelling techniques, due the ability of the 3-D models to include these non-ideal effects. Thus 3-D models could closely predict the performances of a TEG closely to the real conditions. In this type of modelling, not only the predicted performance is important, but the understanding of the transfer processes and non-ideal effects in the context of the particular design are also important, guiding the design towards an optimal solution. Initial differences in the V-I curves of the real device and the ideal device are shown in Figure 2.11(a) [132]. The presence of these non-ideal effects is clearly illustrated in Figure 2.11(b). A major proportion of this PhD work considers the virtual prototyping loop in Figure 2.10, and numerical and finite element modelling techniques are used for this and it helps to include real effects from real applications as well as investigate departures from non-ideal conditions.

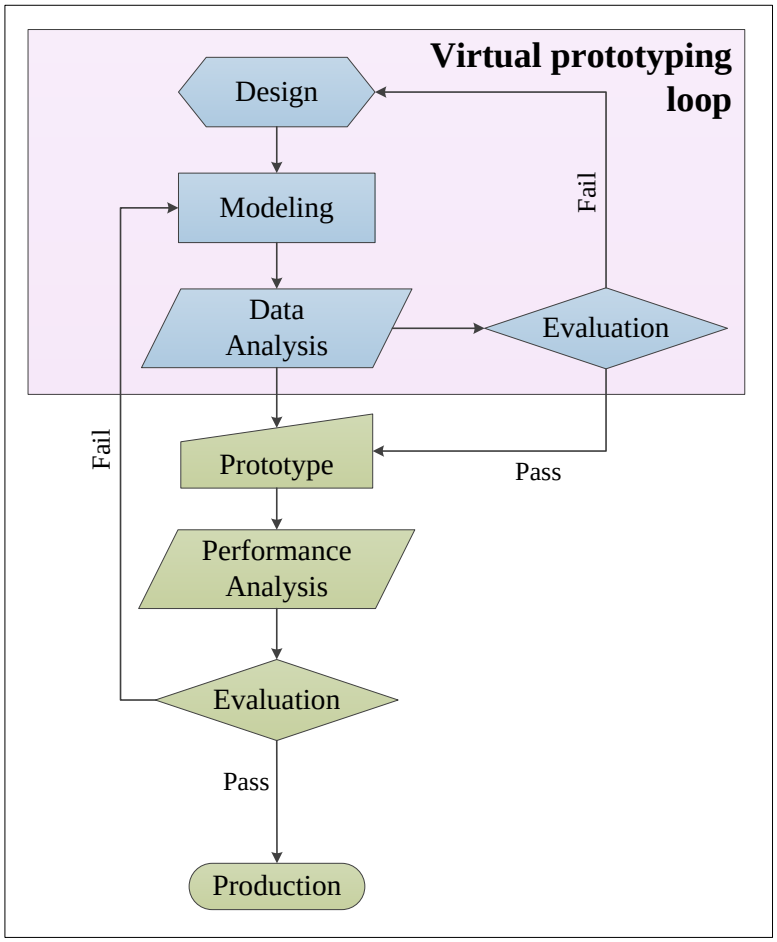

Figure 2.10: Development of a TEG

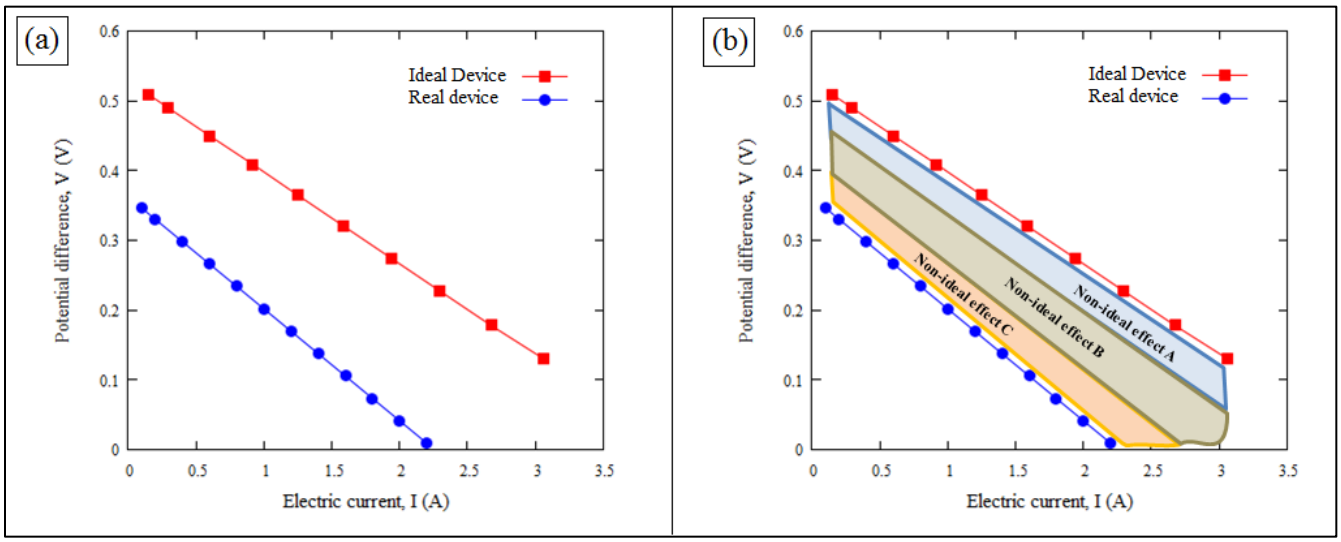

Figure 2.11: (a) Initial V-I curves from the ideal device and the real device [132], (b) presence of non-ideal effects in between ideal and real devices

2.4.2 Thermoelectric Generator Modelling Considerations

Pioneering work on the thermodynamics of thermoelectric phenomena was conducted by Onsager [133]. He considered the reciprocal relationships of irreversible processes and showed the equalities of some ratios between flows and forces in thermodynamic systems that are not in equilibrium but in which a local equilibrium exists. Some literature provide further explanations and discuss the applicability of Onsager's work, for example [134,135].

After Onsager, further optimizations and numerical models were introduced based on the fundamental theorems of thermoelectricity. The optimal cross-sectional areas of the p- and n-legs, and the length to cross-sectional area ratios were introduced by Ioffe [53]. Other work also considered the impact of the shape of the thermoelements on the final power output [136–138]. A method to define the most efficient area ratio for the p- and n-leg thermoelements and length of the thermoelectric device was introduced by Snyder *et al.* [51,52]. This is an advanced method that could be used for TE materials with either temperature-dependent or temperature-independent TE properties. Though segmented and cascade TEG designs already exist [139,140], the concept of the compatibility factor has enabled the more efficient segmented and cascade TEG designs [141].

A TEG consists of a number of metal-semiconductor contacts, and these will work as a hindrance to the flows of heat and electricity. Thus, the electrical and thermal contact resistance and interfacial heat transfer of a TEG are important concerns in the TEG design process, [55,82,142–144]. In a TEG, the surfaces of the thermoelements are open to the environment, and thus, heat could transfer from the thermoelements to the environment by convection and also by radiation, especially in high-temperature applications. Therefore, it is important to consider the effects of the surface heat losses of a TEG [145,146]. The Thomson effect is a fundamental TE effect that is neglected in most TEG modelling developments. However, some works have considered the effects of the Thomson terms on the final TEG outcome [147–149]. Joule heating or resistive heating is a basic physical

concept describing the heat generation when passing a current through a conductor. Thus, it is an important TEG design consideration [150–156]. Segmented and cascade TEG designs are important designs that could be used to increase the efficiency and the temperature difference between hot and cold sides of a TEG, compared to the unicouple TEG design [48,51]. However, this will increase the number of contact layers in a TEG device and the contact resistance could negatively affect the outputs of these designs. Therefore, the electrical and thermal contact resistance and interfacial heat transfer are important issues in segmented and cascade devices [48]. This is a major concerns of the OTE-Power project too [48]. Some of the other interesting design parameters are the transient behaviour of the TE system [157,158] and the density variation or spatial distribution [159].

2.4.3 Thermodynamics of Thermoelectric Phenomena

Simple thermodynamic expressions of TE phenomena are available in many books. The following thermodynamic explanation used is for one TE unicouple. Figure 2.12 shows a TE unicouple consisting of p- and n-type thermoelements, a metal bridge to connect thermoelements, electrical insulators, and an external load [53,160].

In Figure 2.12, $H_{total,h}$ is the heat input to the TEG, $H_{total,c}$ is the heat output from the TEG, and T_h and T_c are the hot and cold side temperatures of the TEG, respectively. The load resistance, R_L, is connected to the cold side of the TEG, and the current passing through the circuit is I. The potential difference between the p- and n-leg thermoelements on the cold side of the TEG is V.

In the following discussion, R is the electrical resistance, K is the thermal conductance, A is the cross-sectional area of thermoelement, l is the thermoelement length, ρ is the electrical resistivity, κ is the thermal conductivity, and α is the Seebeck coefficient. Moreover, the subscripts "p", "n", "h", and "c" represent the p-leg, n-leg, hot side, and cold side of the TEG, respectively. The TE properties of the materials are considered to be temperature independent in this discussion.

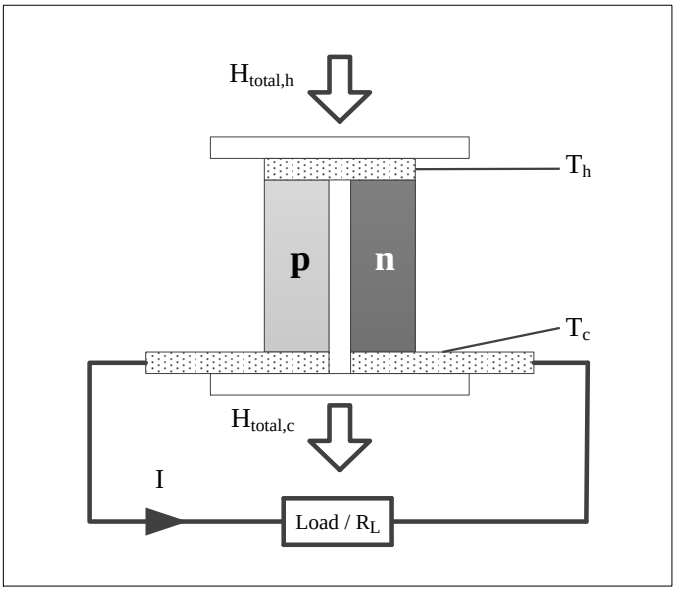

Figure 2.12: TEG

The electrical resistance of the thermoelements connected in series is

$$R = R_p + R_n = \rho_p \frac{l_p}{A_p} + \rho_n \frac{l_n}{A_n} \quad (2.11)$$

Because both the p- and n-thermoelements have the same length,

$$R = R_p + R_n = \rho_p \frac{l_p}{A_p} + \rho_n \frac{l_n}{A_n} = \left(\frac{\rho_p}{A_p} + \frac{\rho_n}{A_n}\right) l \quad (2.12)$$

The TEG is thermally parallel, and thus, the total thermal conductance of the TEG is

$$K = K_p + K_n = \kappa_p \frac{A_p}{l_p} + \kappa_n \frac{A_n}{l_n} = \left(\kappa_p A_p + \kappa_n A_n\right) \frac{1}{l} \quad (2.13)$$

The Seebeck coefficient of the TEG ($\bar{\alpha}$) can be defined as follows:

$$\bar{\alpha} = \alpha_p - \alpha_n \quad (2.14)$$

Four components are involved in the energy conservation at each of the hot and cold sides of the TEG and can be expressed as follows. A graphical explanation is shown in Figure 2.13.

The four main components involved at the hot side of the TEG for energy conservation are the heat input ($H_{total,h}$) from the heat source, the energy removal by the Peltier effect (P_{PE}), the conduction hear transfer ($H_{cond.}$) away from the hot side, and the Joule heating (H_{Joule}) input from the thermoelement [53,160].

The four main components involved at the cold side of the TEG for the energy conservation are the heat output ($H_{total,c}$) from the TEG, the energy input by the Peltier effect (P_{PE}), the conduction hear transfer ($H_{cond.}$) to the cold side, and the Joule heating (H_{Joule}) input by the thermoelement [53,160].

The energy associated with the Peltier effect at the hot and cold sides of the TEG can be defined as

$$P_{PE\_h} = \bar{\alpha} \cdot T_h \cdot I \quad (2.15(a))$$

$$P_{PE\_c} = \bar{\alpha} \cdot T_c \cdot I \quad (2.15(b))$$

The heat transferred by conduction at both thermoelements is

$$H_{cond.} = K \cdot \Delta T \quad (2.16)$$

The Joule heat generated inside the thermoelements is

$$H_{Joule} = I^2 R \quad (2.17)$$

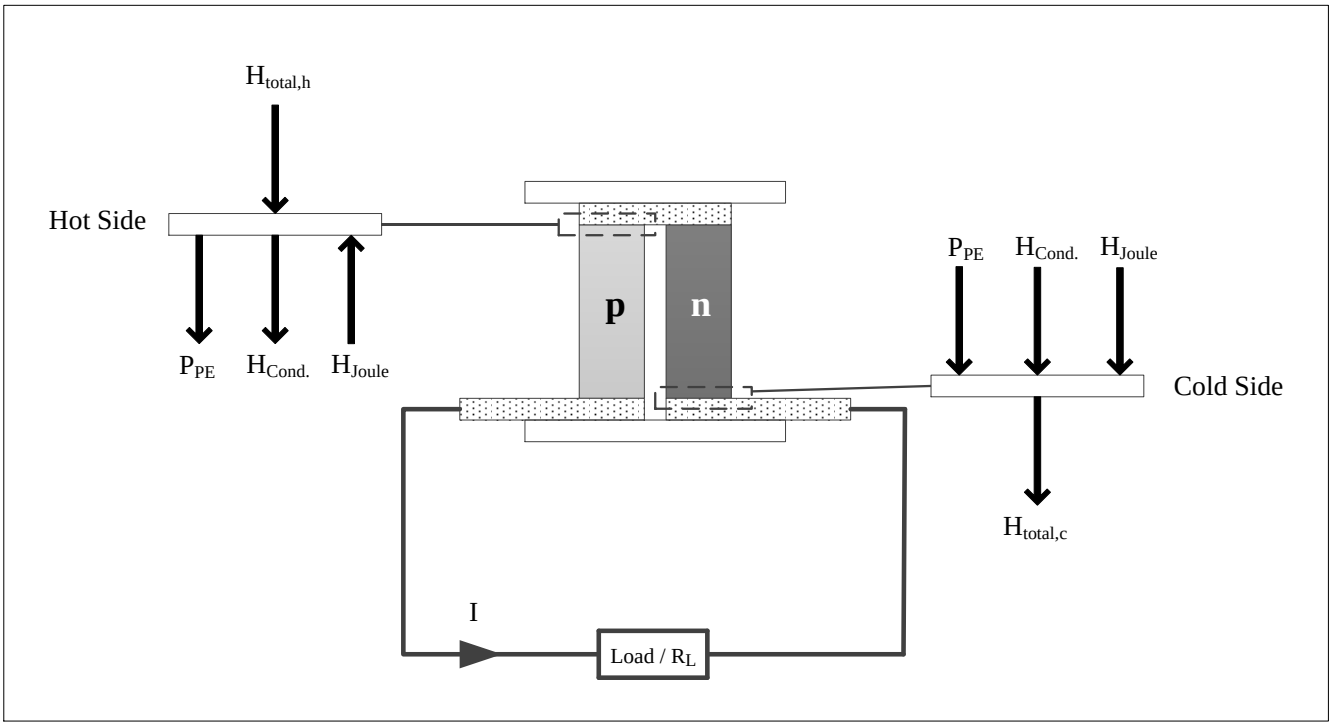

Figure 2.13: Energy balance of a TEG [160].

Nearly linear temperature profiles were obtained in both materials. One of the central assumption of the TE theorem is that an equal amount of Joule heating is generated on both the hot and cold sides, and half of the Joule heat generated by the materials is at the hot side and the other half is at the cold side of the thermoelements [160]. Thus, the heat input at the hot side (Q_h) and the heat output at the cold side (Q_c) can be defined as follows.

$$H_{total,h} = \bar{\alpha} \cdot T_h \cdot I + K \cdot \Delta T - \frac{1}{2} I^2 R \tag{2.18}$$

$$H_{total,c} = \bar{\alpha} \cdot T_c \cdot I + K \cdot \Delta T + \frac{1}{2} I^2 R \tag{2.19}$$

The electrical current (I) through the system is

$$I = \frac{\bar{\alpha} \cdot \Delta T}{R + R_L} = \frac{\bar{\alpha} \cdot \Delta T}{R\,(1+\lambda)} \; ; \; \lambda = \frac{R_L}{R} \tag{2.20}$$

When the power output by the TEG is $P = I^2 R_L$, the efficiency (η) of the TEG can be define as the ratio of the total power output by the TEG to the amount of energy consumed from the heat source:

$$\eta = \frac{P}{H_{total,h}} = \frac{I^2 R_L}{\bar{\alpha} \cdot T_h \cdot I + K \cdot \Delta T - \frac{1}{2} I^2 R} \tag{2.21}$$

$$\eta = \frac{\Delta T}{T_h} \cdot \frac{\frac{\lambda}{\lambda+1}}{1+\frac{K\cdot R}{\bar{\alpha}^2}\cdot\frac{\lambda+1}{T_h}-\frac{1}{2}\frac{(T_h-T_c)}{T_h(\lambda+1)}} \tag{2.22}$$

Thus, the efficiency of a TEG depends on three main factors [53]:

- Hot and cold side temperatures
- $\frac{K\cdot R}{\bar{\alpha}^2}$, which represents the TE properties of the materials and can be defined as $\frac{1}{Z}$
- The ratio $\lambda = \frac{R_L}{R}$

This Z is defined as the figure-of-merit of the TEG materials:

$$Z = \frac{\bar{\alpha}^2}{K\cdot R} \tag{2.23}$$

It is important to find the optimal A_p and A_n to find the maximum efficiency for the given α, ρ, κ, and λ [53]. Thus, it is necessary to find the minimum $K \cdot R$ value ($K \cdot R_{min}$). Therefore, by Equations (2.2) and (2.3),

$$K \cdot R = \left(\kappa_p A_p + \kappa_n A_n\right) \cdot \left(\frac{\rho_p}{A_p} + \frac{\rho_n}{A_n}\right) = \kappa_p \rho_p + \kappa_n \rho_n + \kappa_p \rho_n \frac{A_p}{A_n} + \kappa_n \rho_p \frac{A_n}{A_p}$$

By differentiating w.r.t. $d\left(\frac{A_p}{A_n}\right)$ and equating the derivative to zero,

$$\frac{\rho_p \kappa_n}{\kappa_p \rho_n} = \left(\frac{A_p}{A_n}\right)^2 \tag{2.24}$$

At this $\frac{A_p}{A_n}$ value, $K \cdot R_{min}$ is

$$K \cdot R_{min} = \left(\sqrt{\kappa_p \rho_p} + \sqrt{\kappa_n \rho_n}\right)^2 \tag{2.25}$$

Thus, the maximum figure of merit (Z_{max}) is given at this $\frac{A_p}{A_n}$ value

$$Z_{max} = \frac{\bar{\alpha}^2}{\left(\sqrt{\kappa_p \rho_p}+\sqrt{\kappa_n \rho_n}\right)^2} \tag{2.26}$$

Now, the $\lambda = \frac{R_L}{R}$ ratio that provides the maximum efficiency can be obtained as follows. We can set $\frac{\partial \eta}{\partial \lambda} = 0$ to obtain the condition for maximum efficiency.

$$\left(\frac{R_L}{R}\right)_{\max \eta} = \Lambda = \sqrt{1 + \frac{1}{2} Z_{max}(T_h + T_c)} \tag{2.27}$$

This provides the efficiency equation as

$$\eta = \frac{T_h - T_c}{T_h} \cdot \frac{\Lambda - 1}{\Lambda + \frac{T_c}{T_h}} \quad (2.28)$$

The Carnot efficiency of a reversible engine is given by the first factor of this equation (2.28), and the second factor explains the reduction of the efficiency due to the irreversible losses. Therefore, the efficiency reduction will decrease for higher values of Z and ($T_h + T_c$). Thus, increasing the hot side temperature (T_h) will increase the efficiency by increasing the Carnot efficiency and *B* [53].

Now, the open circuit voltage (V_{OC}) and short circuit current (I_{SC}) of the TEG can be defined as follows [160]:

$$V_{OC} = \bar{\alpha} \cdot \Delta T \quad (2.29)$$

$$I_{SC} = \frac{\bar{\alpha} \cdot \Delta T}{R} \quad (2.30)$$

At the matched load conditions ($R_L = R$), the maximum power output (P_{Max}) by the TEG occurs at the point of half of the open circuit voltage and half of the short circuit current [160].

$$P_{Max} = \frac{(\bar{\alpha} \cdot \Delta T)^2}{4 \cdot R} \quad (2.31)$$

This is a straightforward method to calculate the TEG architecture and power output. However, this does not apply for temperature-dependent TE materials.

2.4.4 Modelling Concepts

As described in above, a number of phenomena in physics and engineering should be considered when developing a model for a TEG, such as TE fundamentals, Joule heating, thermal conductivity matching, thermal and electrical contact resistances, thermo-mechanical stress, mechanical bonding, non-uniformity effects, and radiation effects. Two of the important branches of TEG modelling are: one dimensional modelling and multidimensional modelling. Several one dimensional (1-D) models have been developed to determine the different aspects of a TEG, such as the efficiency of a TEG [161], the different geometries of the leg [162], the effects of the contact resistance [163], the effects of inhomogeneity and segmentation [164–168].

A simple 1-D technique to determine the power output and conversion efficiency of a TEG was proposed by Min et al. [54,55,169,170]. This method can be further used to define the TEG architecture. Figure 2.6(b) shows the TE module considered by the method. Other than the thermoelements, the method defined a contact layer that is a combination of conducting strips and ceramic plates. Thus, it importantly accounted for the influence of the contact layers on the final outcome. Furthermore, the method only considered the temperature independent TE material properties and the same cross-sectional area for both p- and n-thermoelements. Initially, the potential difference across the TEG and the current that passes through the TEG when the TEG is operating at the matched load conditions are defined. These results are used to calculate the power output and, subsequently, the efficiency of the TEG. Plotting the power output and efficiency with the thermoelement length will provide the

appropriate length for the thermoelements. This work clearly indicates that, when the thermoelement length of a TEG is increased, the power output decreases and the efficiency increases.

Min et al. further introduced a method to calculate the cost per-kilowatt-hour of a TEG [54]. If the heat source is expensive, the TEG should be designed to obtain large conversion efficiency. However, if the heat source is inexpensive (essentially free), the TEG should be designed to obtain a higher power output. Nevertheless, some of the major drawbacks of this method are that it cannot be used for temperature dependent TE material properties and that it does not provide the optimal area ratio for the p- and n-legs.

The drawbacks of the method proposed by Min et al. can be overcome by the Reduced Current Approach (RCA) proposed by Snyder et al. [51,52] and this method is used as the main TEG design technique in this project. One of the fundamental design parameters of RCA is the reduced current density. The main focus of the RCA is to define the most efficient TEG architecture. It can be used for either temperature dependent or temperature independent TE properties. Initially, RCA defines the "reduced current density" using the current density, thermal conductivity, and temperature gradient. Then, a detailed analysis of the thermal and electrical circuits of the TEG is conducted. The RCA further used the concept of a "compatibility factor", which is essential to develop segmented and cascaded TEGs [51,52,171]. The RCA passes the same current through the p- and n-thermoelements of the unicouple TE module. However, the current densities of the p-and n-thermoelements are altered to reach the optimal values by changing the area of the thermoelements. RCA succeeded in determined the most efficient area ratio of the p- to the n-leg of the TEG. Furthermore, it can be used to define the most efficient length, potential difference, current, and power output of the TEG.

However, 1-D modelling is not fully able to overcome the multidimensional effects of a TEG, such as the effects of the boundary conditions, non-ideal effects, integration of the TEG thermal system with other systems, and TEGs with different shapes than the conventional design [80,172–177]. Therefore, multidimensional models are needed to find the optimal engineering designs that consider the multidimensional effects of a TEG. Thus, the COMSOL 4.3a Multiphysics Solver is used in this PhD project as a three-dimensional (3-D) modelling technique. From here onwards the COMSOL Multiphysics is referred to COMSOL in this thesis. The following subsections, in this section first briefly introduce the RCA and then give a description of the COMSOL model developed. Then this is extended to a description of modelling the non- uniformity effects using COMSOL.

2.4.4.1 Reduced Current Approach as a 1-D Model

The following is a brief explanation of the RCA [51,52], and it is introduced under following conditions:

- Fully temperature dependent TE material properties
- One dimensional calculation ($\nabla = d/dx$)
- No electrical or thermal contact resistance
- No heat losses

Figure 2.14 illustrate a flow diagram of different steps of RCA.

Nomenclature for Figure 2.14

T	temperature
zT	Figure-of-Merit
Max	maximum
S	compatibility factor
u	reduced current density
dT	temperature difference
A	cross-sectional area
H	Heat input

Greek symbols

α	Seebeck coefficient
ρ	resistivity
σ	electrical conductivity
κ	thermal conductivity
η	efficiency
Φ	thermoelectric potential
$\Delta\Phi$	thermoelectric potential difference

Subscripts

h	hot side
c	cold side
r	reduced value
m	m^{th} value
$m\text{-}1$	$m\text{-}1^{th}$ value
p	p-leg
n	n-leg
$total$	total value

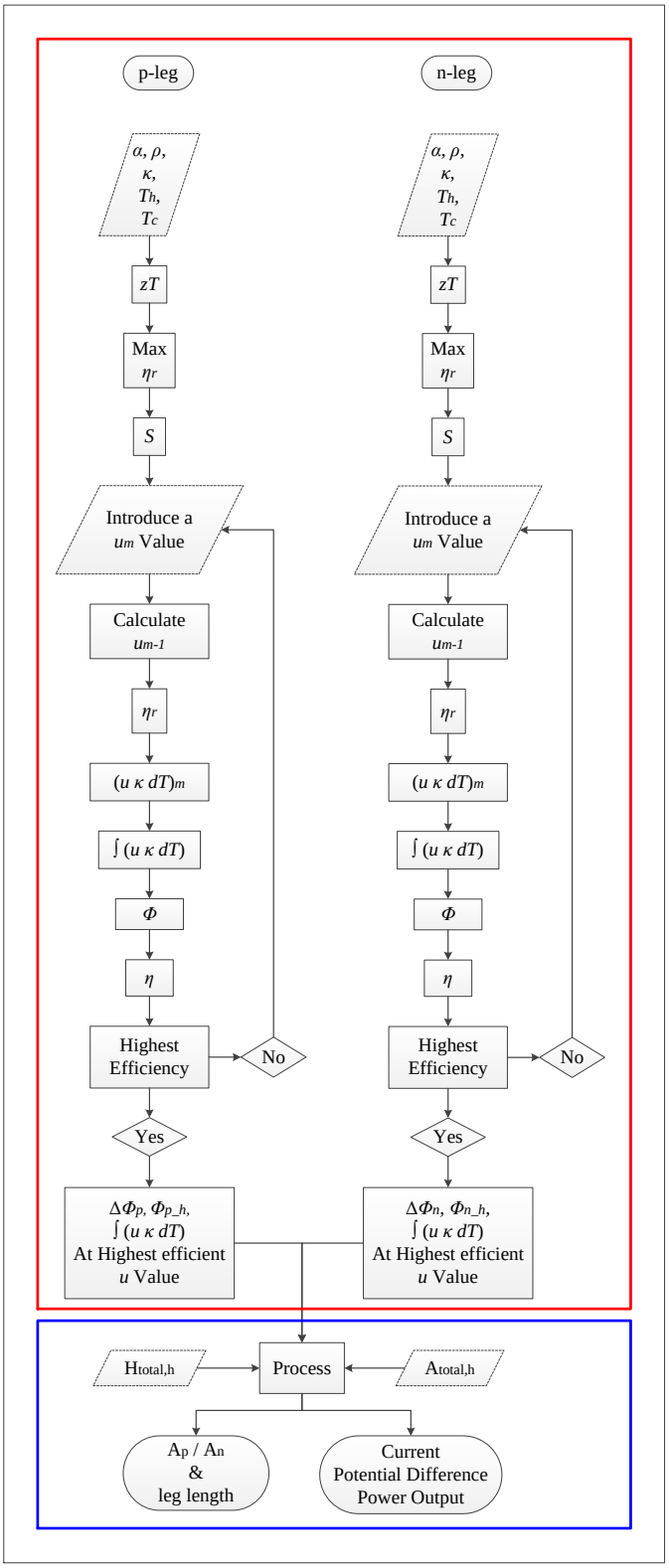

Figure 2.14: Flow diagram of the steps of the TEG design techniques of the Reduced Current Approach (RCA). Solid lined rectangles represent the steps of the method; dashed lined rhombuses represent the inputs to the method; and circular edged boxes represent the output results. The red and blue boxes represent the different sub-sections of the calculations.

2.4.4.1.1 Finding the reduced current density value that leads to the most efficient TEG architecture

The main focus of this section is to determine the u value of a thermoelement when the thermoelement is functioning at its highest efficiency for specific operating conditions. This section is represented by the red box in Figure 2.14. A single thermoelement as shown in Figure 2.15 is considered in this section.

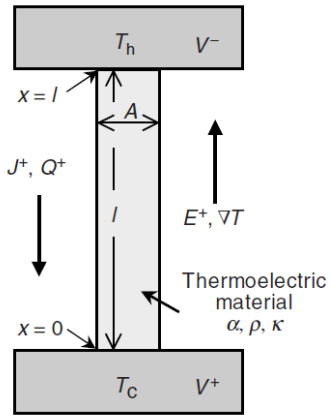

Figure 2.15: Single thermoelement under temperature gradient, where T_h is the hot side temperature, T_c is the cold side temperature, V is the potential, J is the electric current density, Q is the heat current density (heat flux), E is the electric field, ∇T is the temperature gradient, and A is the cross-sectional area [51].

When the TE material properties are given, the Figure-of-Merit (zT) of the material can be defined as in Equation (2.6). The electric field (E) can be defined using the reversible Seebeck effect and the irreversible Ohm's law.

$$E = \alpha \nabla T - \rho J \tag{2.32}$$

The heat flux (Q) can be defined using reversible heat transfer by the Peltier effect and irreversible heat transfer by Fourier's law.

$$Q = \alpha T J + \kappa \nabla T \tag{2.33}$$

The steady state heat equation for the irreversible heat flow is

$$\nabla(\kappa \nabla T) = -T \frac{d\alpha}{dT} J \nabla T - \rho J^2 \tag{2.34}$$

The current density (J) and reduced current density (u) can be defined as follows.

$$J = \frac{I}{A} \tag{2.35}$$

$$u = \frac{J}{k \nabla T} \tag{2.36}$$

where

I = current
A = cross-sectional area of the thermoelement
κ = thermal conductivity
T = absolute temperature
$\nabla = \frac{d}{dx}$ (1-D)

Thus, for the one-dimensional case for the constant cross-sectional area;

$$\nabla\left(\frac{1}{u}\right) = -T\frac{d\alpha}{dT}\nabla T - \rho J \tag{2.37}$$

For the 1-D case, $\nabla\left(\frac{1}{u}\right) = \frac{-1}{u^2}\frac{du}{dx}$, $\frac{du}{dx} = \frac{du}{dT}\nabla T$, $J = u\kappa\nabla$. Thus;

$$\frac{du}{dT} = u^2 T\frac{d\alpha}{dT} + u^3\rho\kappa \tag{2.38}$$

A zero Thomson effect approximation together with a zero resistance gives:

$$\frac{1}{u_m} = \frac{1}{u_{m-1}}\sqrt{1 - 2u_{m-1}^2\overline{\rho\kappa}\Delta T} - \bar{T}\Delta\alpha \tag{2.39}$$

Where $\Delta\alpha = \alpha(T_m) - \alpha(T_{m-1})$, $\overline{\rho\kappa}$ is the average value of $\rho\kappa$ between T_m and T_{m-1}.

Because there is a temperature gradient inside a thermoelement, the temperature along the length of the material varies. However, the TE material is temperature dependent. Thus, based on Equation (2.36), there will be different u values along the length of the material.

If consider an arbitrary segment in a leg, and if the u value at the hot side is known (u_m), the following u value (u_{m-1}) can be calculated using Equation (2.40).

$$\frac{1}{u_m} = \frac{1}{u_{m-1}}\sqrt{1 - 2u_{m-1}^2\left(\frac{\rho_m k_m + \rho_{m-1}k_{m-1}}{2}\right)(T_m - T_{m-1})} - \left(\frac{T_m + T_{m-1}}{2}\right)(\alpha_m - \alpha_{m-1}) \tag{2.40}$$

The maximum reduced efficiency (η_r) of a material can be stated as follows.

$$\max\eta_r = \frac{\sqrt{1+zT}-1}{\sqrt{1+zT}+1} \tag{2.41}$$

The compatibility factor (s) of a material can be indicated as follows.

$$s = \frac{\sqrt{1+zT}-1}{\alpha T} \tag{2.42}$$

The reduced efficiency can be further defined using the u value as follows.

$$\eta_r = \frac{u(\alpha - u\rho k)}{u\alpha + \frac{1}{T}} \tag{2.43}$$

If we consider a segment of the thermoelement between temperatures T_m and T_{m-1}, the length of that segment can be defined as $\frac{(ukdT)_m}{J}$. Moreover, the value of $(ukdT)_m$ can be expanded as follows.

$$(ukdT)_m = \frac{u_m k_m + u_{m-1} k_{m-1}}{2} (T_{m-1} - T_m) \tag{2.44}$$

The length of the thermoelement (l) can be obtained by summing up all the $(ukdT)$ values along the thermoelement length,

$$l(T) = \frac{1}{J} \int_{T_c}^{T_h} ukdT \tag{2.45}$$

The TE potential (Φ) at a point in the thermoelement can be defined as follows.

$$\Phi = \alpha T + \frac{1}{u} \tag{2.46}$$

Furthermore, the efficiency of the thermoelement (η) can be identified by using the TE potentials at the hot and cold sides of the thermoelement as follows.

$$\eta = 1 - \frac{\alpha_c T_c + \frac{1}{u_c}}{\alpha_h T_h + \frac{1}{u_h}} \tag{2.47}$$

Therefore, the above Equations (2.32) to (2.47) can be used for the initial calculations of the unicouple TEG design by RCA. The first step of RCA is to identify the u value of a thermoelement when it operating at its highest efficiency under specific operating conditions. Thus, the hot (T_h) and cold (T_c) sides temperatures are defined as the initial operating conditions of the thermoelements. When considering the p-leg, any positive real number ($\mathbb{R}_+$) value is applied as the initial u value at the hot end (when it is the n-leg, any negative real number ($\mathbb{R}_-$) value is applied), and the corresponding efficiency is calculated. Thus, the u value at the highest efficiency point for each p- and n-thermoelement can be calculated. As discussed in Paper A in this thesis, for this project, $Ca_3Co_4O_9$ and Al-doped ZnO were used as the TE materials for the p- and n-legs, respectively [49,50]. Figure 2.16 shows the TE properties of the $Ca_3Co_4O_9$ and Al-doped ZnO. Using these TE properties, the variation of the efficiency of the thermoelements of $Ca_3Co_4O_9$ and Al-doped ZnO for different u values is illustrated, as is shown in Figure 2.17. Here, operating conditions of 1073 K and 373 K are used for the hot and cold sides of the thermoelements, respectively. Thus, Tables 2.1 and 2.2 summarize the initial calculations of the RCA at the most efficient u value for the p- and n-leg thermoelements, respectively.

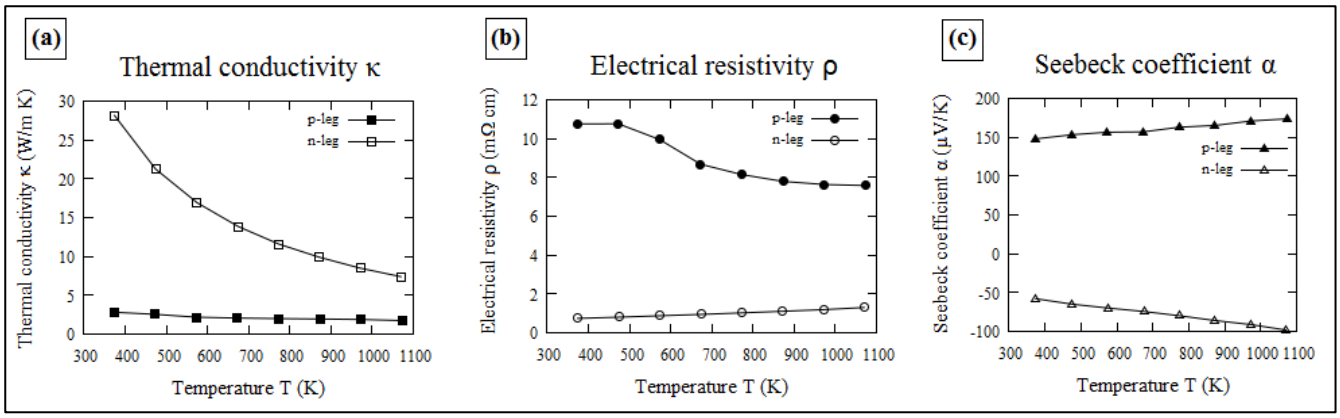

Figure 2.16: Temperature dependent TE properties of the $Ca_3Co_4O_9$ (p-leg) and Al-doped ZnO (n leg); (a) Thermal conductivity, (b) Electrical resistivity, (c) Seebeck coefficient [49,50].

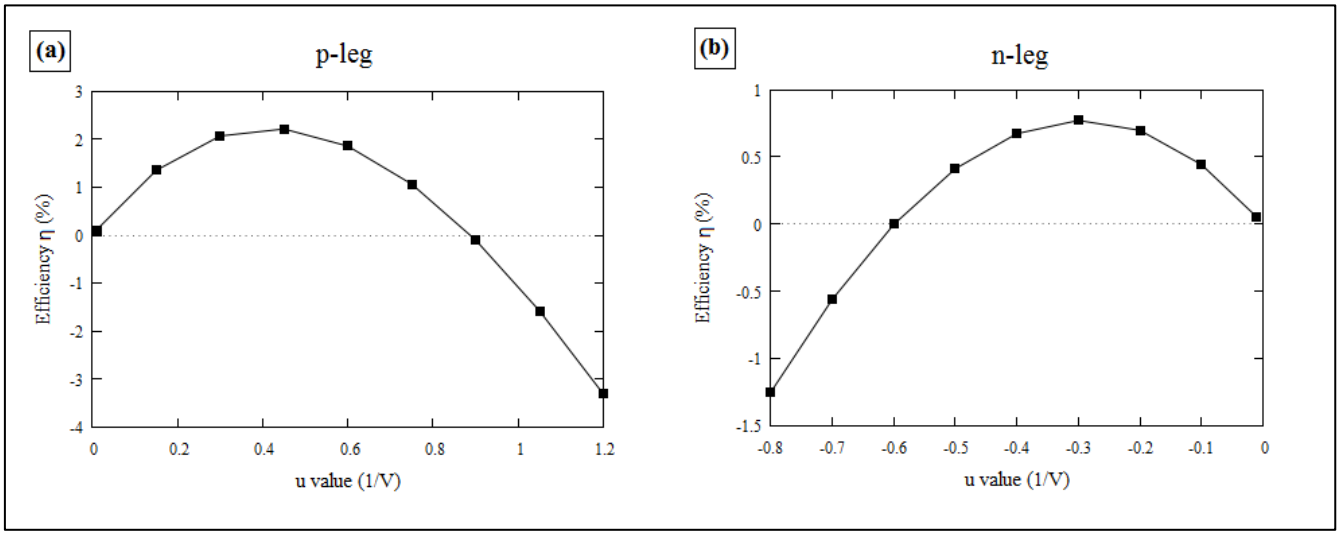

Figure 2.17: Variation of the efficiency of (a) p-type $Ca_3Co_4O_9$. (b) n-type Al-doped ZnO with u values

Table 2.1: Initial calculation of RCA for the p-type $Ca_3Co_4O_9$ at the most efficient configurations

Temperature (T)	Figure-of-Merit (zT)	Max reduced efficiency ($Max\ \eta_r$)	Compatibility factor (S)	u Value	Reduced efficiency	$uk\ dT$	Jl [running sum of $ukdT$]	TE potential (Φ)	Efficiency (η)
K		%	1/V	1/V	%	A/m	A/m	V	%
1073	0.245	5.465	0.621	0.416	4.914	0.000	0.000	2.590	
973	0.198	4.513	0.568	0.415	4.204	75.242	75.242	2.579	0.444
873	0.157	3.648	0.525	0.413	3.490	79.049	154.290	2.568	0.858
773	0.126	2.968	0.486	0.411	2.901	81.158	235.449	2.558	1.241
673	0.093	2.212	0.428	0.409	2.207	83.312	318.761	2.549	1.588
573	0.065	1.567	0.355	0.408	1.534	86.694	405.455	2.541	1.881
473	0.040	0.991	0.276	0.406	0.780	96.193	501.648	2.536	2.093
373	0.027	0.664	0.243	0.404	0.378	108.528	610.175	2.533	2.223

Table 2.2: Initial calculation of RCA for the n-type Al-doped ZnO at the most efficient configurations

Temperature (T)	Figure-of-Merit (zT)	Max reduced efficiency ($Max\ \eta_r$)	Compatibility factor (S)	u Value	Reduced efficiency	$uk\ dT$	Jl [running sum of $ukdT$]	TE potential (Φ)	Efficiency (η)
K		%	1/V	1/V	%	A/m	A/m	V	%
1070	0.107	2.547	-0.497	-0.292	2.126	0.000	0.000	-3.530	
971	0.080	1.920	-0.442	-0.291	1.701	-229.319	-229.319	-3.523	0.185
872	0.059	1.432	-0.388	-0.290	1.344	-264.672	-493.991	-3.518	0.348
774	0.042	1.017	-0.333	-0.290	1.001	-305.299	-799.290	-3.513	0.486
675	0.028	0.702	-0.282	-0.289	0.701	-364.359	-1163.649	-3.509	0.601
575	0.019	0.471	-0.236	-0.289	0.448	-444.263	-1607.912	-3.505	0.691
474	0.012	0.290	-0.189	-0.288	0.212	-555.462	-2163.373	-3.503	0.753
374	0.006	0.150	-0.139	-0.287	-0.022	-710.354	-2873.727	-3.503	0.772

2.4.4.1.2 Combining the most efficient configurations of p- and n-type thermoelements to produce the most efficient TEG setup

The main focus of this section is to combine the p- and n-leg thermoelements and define the TEG architecture, maintaining the most efficient reduced current densities (u values) through each thermoelement. This section is represented by the blue box in Figure 2.14. Tables 2.1 and 2.2 provide the following important outcomes for future calculations of the TEG. The most efficient u values are 0.416 and -0.292; the $\int_{T_c}^{T_h} ukdT$ values are 610.175 and -2873.727; the TE potentials at the hot side (Φ_h) are 2.590 and -3.530; and the potential differences ($\Delta\Phi = \Phi_h - \Phi_c$) are 0.058 and -0.027 for the p- and n-legs, respectively.

The output voltage (V) of the TEG can be calculated directly by using the above results, which is the difference between the potential differences of each thermoelement.

$$V = \Delta\Phi_p - \Delta\Phi_n \tag{2.48}$$

As in Figure 1.8(a), a unicouple TEG architecture has same length (l). Therefore, by Equation (2.45) and Equation (2.35);

$$l = \frac{1}{J_p}\int_{T_c}^{T_h} u_p k_p dT = \frac{1}{J_n}\int_{T_c}^{T_h} u_n k_n dT \tag{2.49}$$

$$I = J_p A_p = -J_n A_n \tag{2.50}$$

Here, in Equation (2.50), the negative value of the current density at the n-leg is due to the directional changes of the electric current when it is at the p-leg and n-leg (Figure 1.11(a)). Thus, the area ratio in between the p- and n-legs can be calculated by Equations (2.49) and (2.50);

$$\frac{A_p}{A_n} = \frac{-J_n}{J_p} = \frac{-\int_{T_c}^{T_h} u_n k_n\, dT}{\int_{T_c}^{T_h} u_p k_p\, dT} \tag{2.51}$$

when the total cross-sectional area of the thermoelements $\left(A_{total} = A_p + A_n\right)$ is known,

$$A_p = \frac{A_{total}}{1+\frac{A_n}{A_p}} \quad (2.52)$$

$$A_n = \frac{A_{total}}{1+\frac{A_p}{A_n}} \quad (2.53)$$

When the total heat input $(H_{total,h})$ to the hot side of the TEG is known, the total heat flux through the TEG can be expressed as follows.

$$H_{total,h} = Q_{total} A_{total} \quad (2.54)$$

Additionally, H_{total} can be defined using the electrical current as follows:

$$H_{total} = I(\Phi_{h\_p} - \Phi_{h\_n}) \quad (2.55)$$

Thus, the current density at the p-leg (J_p) can be calculated using Equations (2.50), (2.52), and (2.55):

$$J_p = \frac{H_{total,h}}{A_{total}} \times \frac{1+\frac{A_n}{A_p}}{\Phi_{p,h} - \Phi_{n,h}} \quad (2.56)$$

Therefore, the length of the thermoelements can be calculated using Equations (2.49), and (2.56). Moreover, the electric current through the TEG can be calculated using Equations (2.50), (2.52), and (2.56). Therefore, the most efficient architecture is finalized.

2.4.4.2 Designing the 3-D model using COMSOL

Finite element modelling is a powerful tool when designing TEG. It can easily combine different physical phenomena of the TEG. Some of the previous work that focuses on this can be summarized as follows.

Ebling et al. has studied TEG performance using multiphysics simulations and compares it with real TEG [178]. They further investigated the effects of contact resistance on the final module, depending on different soldering materials. They also identified the effects of convection and radiation on the real TEG. Jang et al. discussed the micro-TEG consisting of thin film TE materials, using the finite element method [179]. They also studied the effects of the geometric factors of the thermoelements to the final TEG output and the effects of the thickness of the substrate on the final device output. Yang et al. has studied solar TEG using the finite element method [180]. They identified that the contact resistance and heat loss by natural convection highly reduces the effectiveness of the solar TEG. Kim et al. has presented a mathematical model to obtain the voltage and power of a TE module and extended this model to track the maximum power point of the module [181]. Ziolkowski et al. presented a 3-D finite element model for TEGs that was developed on ANSYS, and they have compared their 3-D model with 1-D model developed in-house [182]. Then they evaluated the efficiency reduction from radiation, convection and a contact resistance compared to the ideal conditions. Wang et al. conducted a finite element analysis of a TEG [183]. A hydrogen based catalytic combustion is used as the thermal source for this study.

In this project COMSOL 4.3a has been applied as the finite element modelling tool. COMSOL is an advanced computational modelling tool that can simulate many physical phenomena. COMSOL also has the ability to

combine many physical phenomena in an efficient and accurate manner. This is a suitable tool to investigate the non-uniformity and multidimensional effects of the TEG [184,185]. However, COMSOL 4.3a does not have a standard thermoelectric model for simulating TEGs, which can be directly applied for TEGs. Thus, a simulation model was developed for TEG modelling in COMSOL 4.3a using the existing standard formulation framework for physical models in COMSOL. Using symmetrical and adiabatic boundary conditions to ensure 1-D condition, this 3-D COMSOL model was validated against 1-D RCA. After that, this 3-D model was used to develop and analyse TEG systems throughout the project. Figure 2.18 shows a flow diagram of the different steps of the COMSOL TE model.

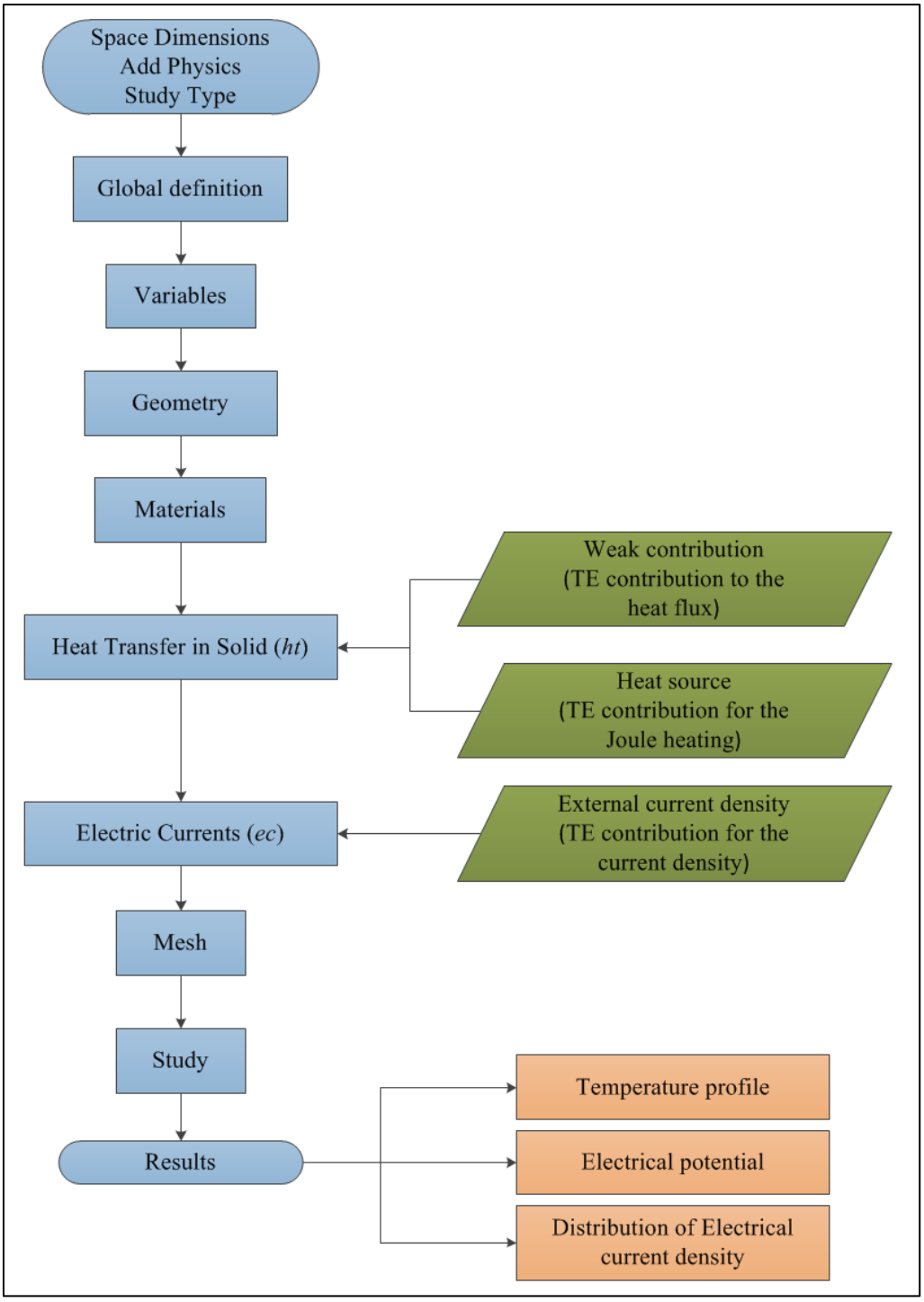

Figure 2.18: Flow diagram of the steps of the TE module of the COMSOL . The blue boxes represent the process given by the COMSOL, the green boxes represent the TE contributions to the TE module, and the red boxes represent the results.

2.4.4.2.1 TE energy conversion fundamentals for modelling

This section briefly discusses the fundamentals of TE phenomena and the integration of those phenomena with the standard models that exist in COMSOL. Basically, TE is a combination of heat transfer and electrics. Thus, "Heat Transfer in Solids" and "Electric Currents" are used as the main standard COMSOL models. However, the above two models are not able to give a full description of the TE phenomena. Thus, the additional contributions of the TE effects are combined with those standard models [186]. Following briefly discuss this implementation.

According to Equation (2.4), the Peltier effect (π) can be indicated as $\pi = \alpha T$, where α is the Seebeck coefficient, and T is the absolute temperature. The heat flux (Q) can be expressed as a combination of the irreversible heat transfer by the Fourier's law $(\kappa \nabla T)$ and the reversible heat transfer by the Peltier effect $(\alpha T J)$.

$$Q = -\kappa \nabla T + \alpha T J \tag{2.57}$$

where J is the flux of the electrical current, κ is thermal conductivity, and ∇T is the temperature gradient.

Furthermore, the flux of the electrical current (J) can be expressed as the sum of the contributions from the pure resistive element by Ohm's law and the contribution from the Seebeck effect.

$$J = -\sigma \nabla V - \sigma \alpha \nabla T \tag{2.58}$$

where σ is the electrical conductivity, and V is the electrical potential.

Furthermore, the electric field (E) and Joule heating $\left(H_{Joule}\right)$ can be expressed as follows:

$$E = -\nabla V \tag{2.59}$$

$$H_{Joule} = J \cdot E \tag{2.60}$$

Moreover, the heat energy conversion and current conversion can be written as in Equations (2.61) and (2.62), respectively:

$$dC \frac{\partial T}{\partial t} + \nabla \cdot Q = H_{Joule} \tag{2.61}$$

$$\nabla \cdot J = \frac{\partial d_c}{\partial t} \tag{2.62}$$

where d is the density, C is heat capacity, t is time, and d_c is space charge density. When it is in the steady state,

$$\nabla Q = H_{Joule} \tag{2.63}$$

$$\nabla \cdot J = 0 \tag{2.64}$$

Therefore, by Equations (2.57), (2.58), (2.59), (2.60), (2.63), and (2.64),

$$\nabla \cdot \left(-\kappa \nabla T + \pi(-\sigma \nabla V - \sigma \alpha \nabla T)\right) = (-\sigma \nabla V - \sigma \alpha \nabla T) \cdot (-\nabla V) \tag{2.65}$$

$$\nabla \cdot (-\sigma \nabla V - \sigma \alpha \nabla T) = 0 \tag{2.66}$$

Considering the left side of Equation (2.65), in COMSOL, "heat transfer in solid" domain consists of heat transfer by conduction. Thus, the additional part by the TE effect is added to the model as a "Weak contribution" domain. The Equation (2.67) states the "weak equation" that is added to the domain which written in COMSOL language is:

Thus, the TE contribution to the heat flux is $\nabla \cdot \left(\pi(-\sigma\nabla V - \sigma\alpha\nabla T)\right)$

$$\begin{aligned}\nabla \cdot (\pi(-\sigma\nabla V - \sigma S\nabla T)) &= \pi * (ec.Jx * test(Tx) + ec.Jy * test(Ty) + ec.Jz * test(Tz) - \alpha * ((ec.sigmaxx * Tx \\ &+ ec.sigmaxy * Ty + ec.sigmaxz * Tz) * test(Tx) + (ec.sigmayx * Tx + ec.sigmayy \\ &* Ty + ec.sigmayz * Tz) * test(Ty) + (ec.sigmazx * Tx + ec.sigmazy * Ty \\ &+ ec.sigmazz * Tz) * test(Tz)))\end{aligned} \tag{2.67}$$

where $ec.Jx$ ($ec.Jy$, and $ec.Jz$) is the current density x (y, and z) component, Tx (Ty, and Tz) is the temperature gradient x (y, and z) component, $ec.sigmaxx$ ($ec.sigmaxx$, $ec.sigmaxy$, $ec.sigmaxz$, $ec.sigmayx$, $ec.sigmayy$, $ec.sigmayz$, $ec.sigmazx$, $ec.sigmazy$, and $ec.sigmazz$) is the electrical conductivity xx (xy, xz, yx, yy, yz, zx, zy, and zz) component.

Now let us consider the right side of Equation (2.65). The TE contribution to the Joule heating is $[(-\sigma\alpha\nabla T) \cdot (-\nabla V)]$. Then, this contribution is added to the model as a "Heat source" domain. The Equation (2.68) states the weak equation that has been added to this domain which written in COMSOL language is:

TE contribution for the Joule heating is $(-\sigma\alpha\nabla T) \cdot (-\nabla V)$

$$(-\sigma\alpha\nabla T) \cdot (-\nabla V) = -\alpha * (ec.Jx * Tx + ec.Jy * Ty + ec.Jz * Tz) \tag{2.68}$$

Furthermore, Equation (2.66) explains the current density equation. When assigning a "Current conservation" domain to a thermoelement, the current density by the pure resistive part of the thermoelement is introduced into the domain. Therefore, the additional part by the TE effect is added to the model as an "External current density" domain. The Equation (2.69) states the "weak equations" that are added to the domain which written in COMSOL language is:

$$\begin{aligned}&\text{x component} \equiv -\alpha * (ec.sigmaxx * Tx + ec.sigmaxy * Ty + ec.sigmaxz * Tz) \\ &\text{y component} \equiv -\alpha * (ec.sigmayx * Tx + ec.sigmayy * Ty + ec.sigmayz * Tz) \\ &\text{z component} \equiv -\alpha * (ec.sigmazx * Tx + ec.sigmazy * Ty + ec.sigmazz * Tz)\end{aligned} \tag{2.69}$$

In the computation a number of different linear equations solvers are available in COMSOL. For this project, the "conjugate gradient" iterative solver was used. The linear equation preconditioner used in here is a multigrid solver with both a geometric and an algebraic multigrid solver [186].

Figure 2.19 illustrates the temperature profile of the TEG and the temperature profile of each thermoelement, based on the model developed.

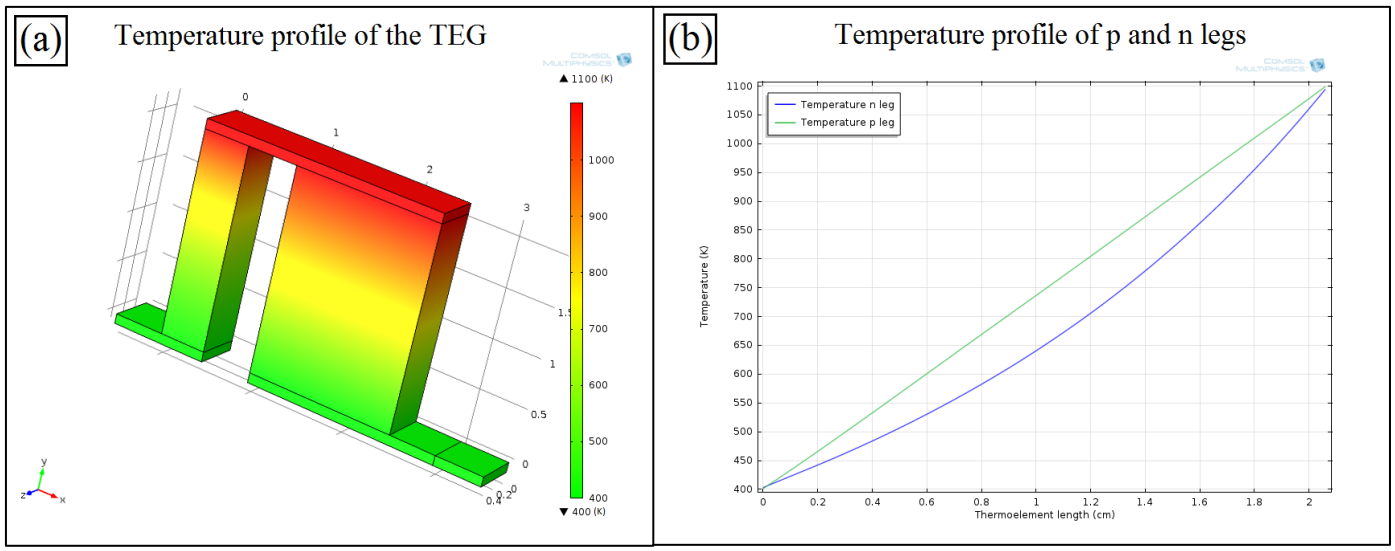

Figure 2.19: Temperature profile of unicouple TEG in COMSOL (units K): (a) surface profile and (b) profile inside each leg.

The closed circuit electrical potential throughout the TEG and external resistor is illustrated in the Figure 2.20(a), and the electrical current density is shown in Figure 2.20(b). The direction of the current is illustrated by the arrows in Figure 2.20(b), and the relative magnitude of the current density at a point is illustrated by the relative size of the arrow at that point.

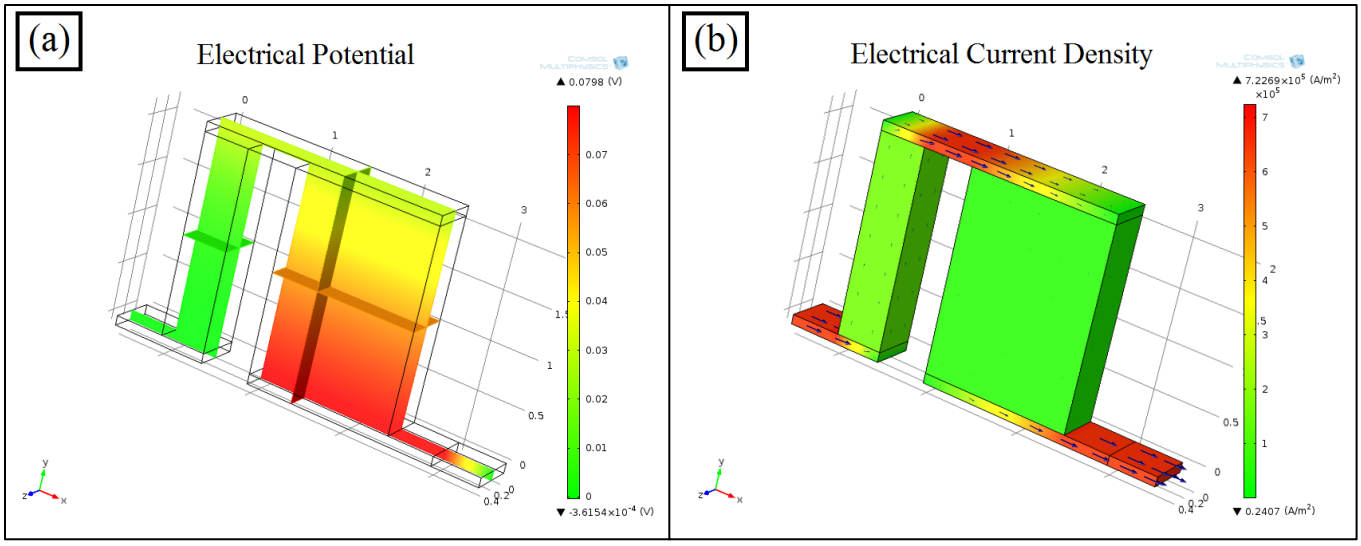

Figure 2.20: In a unicouple TEG, (a) distribution of electrical potential (units V) and (b) distribution of electrical current density (units A/m^2)

2.4.4.3 Validating the 3-D COMSOL model using the 1-D reduced current approach

The validation process of the 3-D model is performed using V-I curves for both 1-D and 3-D models, changing the current through the TEG and recording the potential differences of both the 1-D and 3-D models. For the same operating conditions, the current through the TEG can be changed by changing the external load resister of the TEG. Thus, the V-I curve for the 3-D model can be generated by changing the resistance of the external load resister in the COMSOL model, which is shown in the Figure 2.21.

For the 1-D reduced current approach, changing the current should be carried out in a systematic manner, because changing the current can result in changes to the architecture of the TEG. According to the RCA, the current through a thermoelement can be changed by changing the u value at the hot side. Based on Equations (2.35) and (2.36),

$$\frac{u}{I} = \frac{1}{A\,k\,\nabla T} \tag{2.70}$$

From the calculations for the RCA, the most efficient u values for each leg and the output current of the TEG are already known. Considering these as u_1 and I_1; if the TEG architecture and the temperature profile are fixed, then the right side of Equation (2.70) will become a constant. Therefore, when considering another situation with the same TEG architecture and a different current (I_2) compared to the most efficient configuration, the new u value (u_2) can be calculated using Equation (2.71). Then, the potential different for the new current can be calculated using RCA. Figure 2.21 indicates that the developed 3-D COMSOL model matches the 1-D RCA model, and the 3-D model is validated using this approach.

$$\frac{u_1}{I_1} = \frac{u_2}{I_2} \tag{2.71}$$

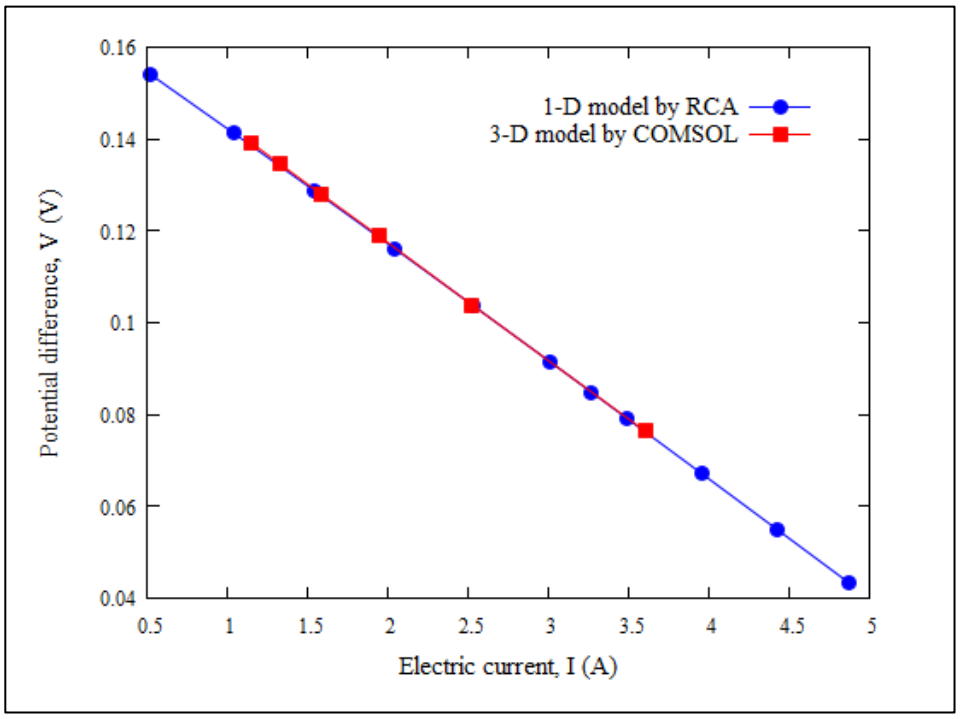

Figure 2.21: V-I Curves of 1-D model by RCA and 3-D model by COMSOL

2.4.4.4 Modelling non-uniformity effects using COMSOL

As discussed in "Section 2.4.1" and Figure 2.11: in the real TEG, "departure from the ideal conditions" will most likely arise due to the non-uniformity effects, such as uneven thermal loading, poor contact, material density variation, non-uniform segmenting *etc*. Those effects cannot be treated sufficiently by 1-D modelling, which introduces the need to use 3-D modelling. Well defined 3-D models can help identify the differences, and the causes of these, between the ideal and the real situations.

As an example of the insight provided by 3-D modelling, the influence of non-uniform coupling effects to the TEG unicouple was studied in a simple setup. Figure 2.22 illustrates the imposed non-uniformity in terms of reduced contact surface as well as spatial distribution of this. These are all applied to the p-leg, whereas the contact surface of the n-leg is kept ideal. The bottom part of Figure 2.22 shows the percentage power output obtained by each of the non-uniformity cases compared to the power output of the fully contacted TEG unicouple which is "TEG Unicouple No: 1".

The power output of the TEG unicouples are obtained at the matched load conditions. Thermoelements p and n of the TEG unicouple are built with $Ca_3Co_4O_9$ and Al-doped ZnO respectively, and those are connected using Nickel electrodes. In addition contact layers are introduced in between Nickel electrodes and oxide thermoelements. All the calculations were carried out using the thermoelectric model implemented in COMSOL.

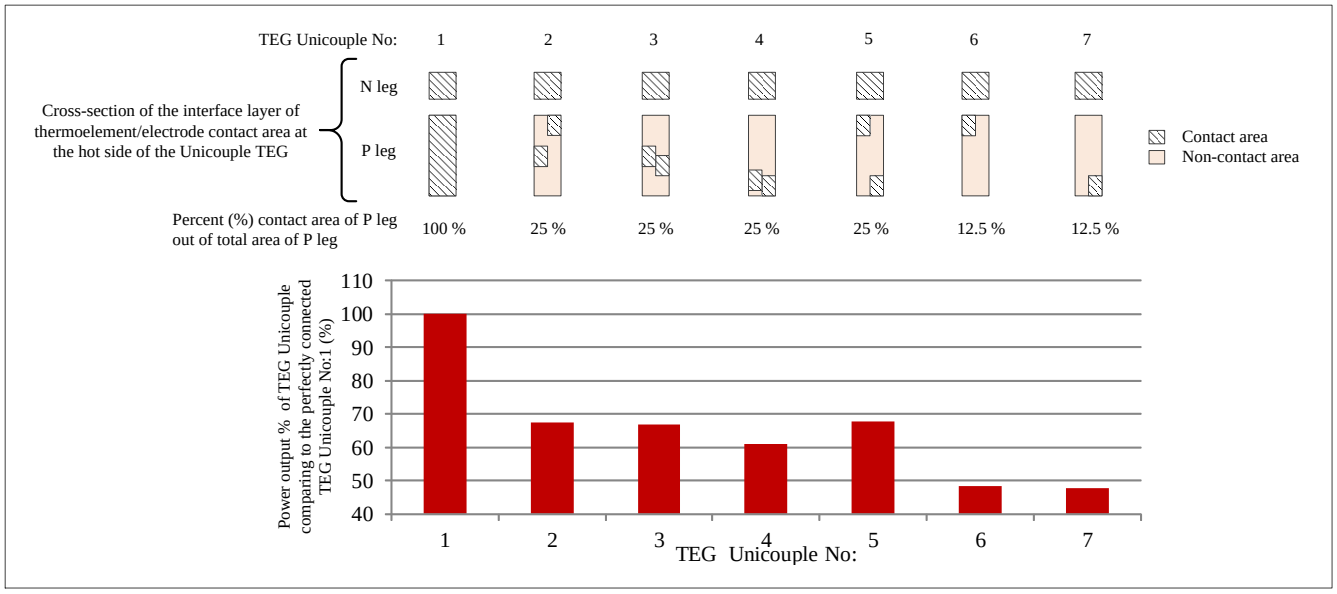

Figure 2.22: Variation of power output of a TEG unicouple with different thermoelement/electrode contact area in different places at the hot side of a TEG. Here consider about 7 different TEG unicouples. The top part of the figure illustrated the interface layer of the thermoelement/electrode contact area and the value of percent contact area of the P leg comparing to the total area of the P leg. Bottom part of the figure illustrates the percent power output of a TEG unicouple comparing to the TEG unicouple No:1, which has perfect contacts.

Figure 2.22 clearly illustrates the influence of the contact layer on the power output of the TEG. It shows that when decreasing the size of the contact layer, the power output of the TEG decreases. Furthermore it shows that

even at the same reduction of contact area (case 2, 3, 4 and 5; case 6 and 7, respectively), the spatial distribution of contact surface can play a significant role in determining the power output. Including this type of effect into the complete modelling framework is an important contribution to understanding real TEG module performance.

Figure 2.23 illustrates the temperature profile/isothermal contours of the TEG Unicouple No: 4, when 1/3 of the cold side of the P-leg is contacted to the electrode. It can be seen that temperature profile of the TEG is highly influenced by the size and place of the contact areas.

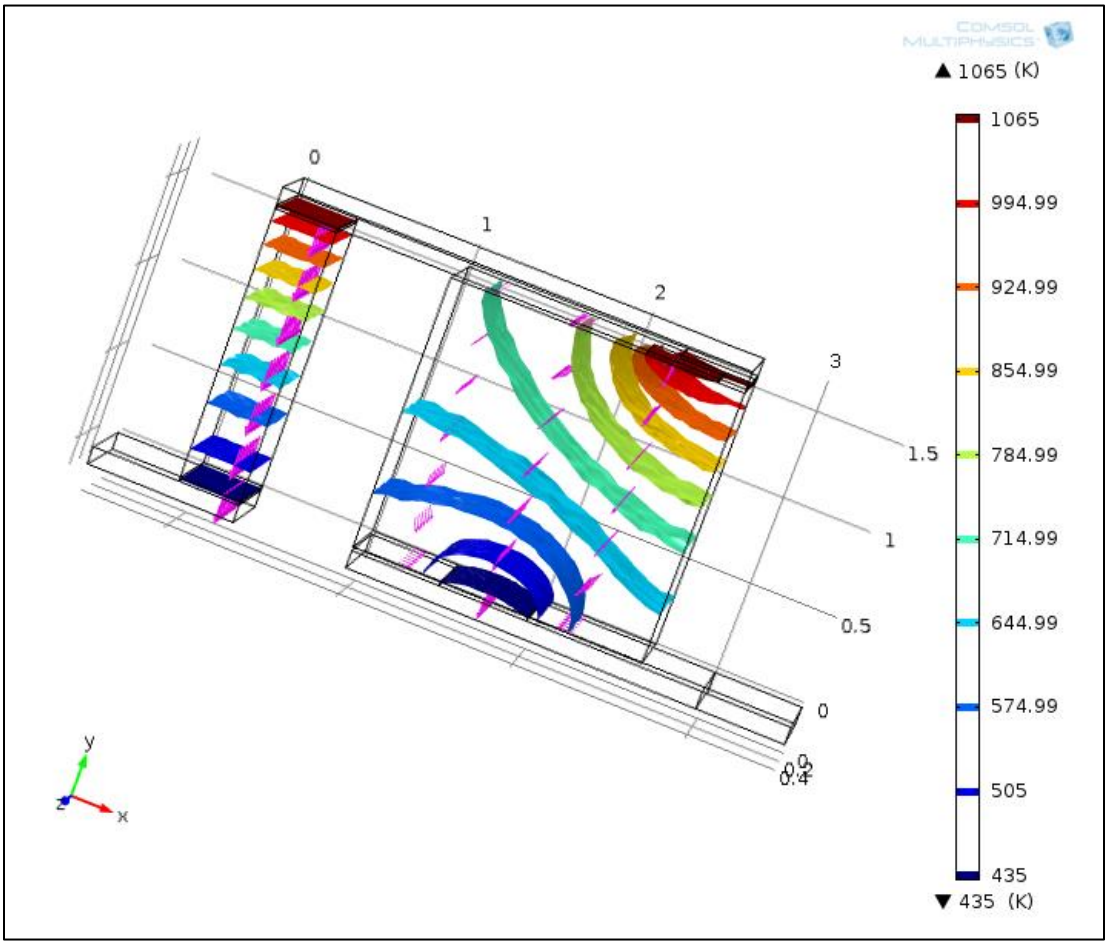

Figure 2.23: Temperature profile/isothermal contours of the TEG Unicouple No: 4. Direction of the arrow is indicating the direction of the heat flux and the size of the arrow is proportional to the relative magnitude of the heat flux at specific point.

3. Extended reduced current approach to increase the volumetric power density

This chapter focuses on minimizing the cost-per-Watt of a TEG by increasing the volumetric power density. Thus the concepts of known TEG design techniques, proposed by Snyder et al. [51,52] and by Min et al [54,55] are studied. Then these techniques are developed to introduce an alternative approach to design TEGs. This modified TEG design technique is well suited for the combinations of TE materials with mismatched zT values. For the OTE-Power project, this modified TEG design technique is able to produce TEGs with a higher volumetric power density compared to the TEG design technique proposed by Snyder et al. for high temperature applications.

One of the main arguments in TEG design is what should the main focus be when designing a TEG; should it be efficiency or power output? Some publications imply that TEG design for higher power and higher efficiency will not be the same [54,55,187,188]. However, others indicate that the TEG design for the highest efficiency will provide the highest power output [189,190]. Moreover, with regard to the system level integrations of TEG (combination of TEG, heat exchangers, thermal contact surfaces, *etc*.), some references stress that the TEG design for higher efficiency is more beneficial than the higher power output [189]. However, Yee et al. showed that this heavily relies on which cost category of the TEG system is the most dominant: volumetric module cost, cost per area of module, or heat exchanger cost [191]. Thus, these discussions about the TEG architecture for maximum power and maximum efficiency represent two extremes in terms of what constitutes the optimum design.

However, the results obtained in this work imply a new optimal design that does not belong to either extreme but is a combination of both arguments. Briefly, if the TE material properties (or zT) of the p- and n-legs of the TEG are comparable (the same or close values), the TEG architecture for the maximum efficiency will provide the maximum power density. However, if the TE material properties (or zT) of the p- and n-legs of the TEG are not comparable (not the same nor close values), TEG architecture for the maximum efficiency will not provide the maximum power density, and TEG architecture for the maximum efficiency and maximum power density should be different. Moreover, this work modified the Reduced Current Approach (RCA) TEG designing technique proposed by Snyder et al. [51,52] to design a TEG that can produce higher power densities. For simplicity, this version is named the Extended Reduced Current Approach (ERCA).

This work benefits the OTE-Power project for several reasons. The OTE-Power project is concerned with oxide TE materials, and p-type oxide materials typically have significantly higher TE properties than n-type oxide materials. In other words, TE material properties (or zT) of the p- and n-leg materials chosen to build the TEG are incomparable (not the same nor close values). Thus, the new concept (ERCA) confirms that the OTE-Project should focus on TEG designs with higher power densities.

According to Min et al. the TEG design should focus on higher power outputs when it operates at higher temperatures [54,55] due to the cost effectiveness of the TEG. This can be seen by Equation (3.1) [54].

$$c = \frac{c_m}{P\Delta t} + \frac{c_f}{\eta} \tag{3.1}$$

Where c is the cost per-kilowatt-hour, c_m is the fabrication cost, P is the power output of the TE module, Δt is the period of operation, c_f is the input thermal energy cost and η is the conversion efficiency of the TE module. Therefore, by Equation (3.1), when the input thermal energy cost is essentially zero, such as the high-temperature waste heat recovery applications targeted by the OTE-Power project, the TEG design should focus on power output to reduce the cost per-kilowatt-hour. As stated earlier, ERCA will increase the power density of the TEG fabricated in the OTE-Power project, thus increasing the cost effectiveness of the OTE-Power TEG.

3.1 RCA and ERCA

RCA is a technique that focuses on developing the most efficient TEG architecture, from the standpoint of optimizing the p- and n-legs individually, and then merging to find the optimal unicouple. The focus of ERCA is to develop a TEG with a higher volumetric power density than that predicted by the RCA. When a unicouple TEG device (shown in Figure 2.6(a)) is developed using the RCA; initially it treats p- and n-legs individually and finds the most efficient configuration/reduced current density value for each thermoelement. Then RCA combines these most efficient configurations of p- and n-legs to develop the most efficient unicouple TEG. When using the ERCA to develop a unicouple TEG device, it focuses upon the initial part of the RCA and a different optimum is identified by altering some of the calculation steps of RCA. Then ERCA combines these new optimal configurations of each p- and n-legs as in RCA to develop a unicouple TEG with a higher volumetric power density.

Following explanations about RCA and ERCA are based on the following conditions:

- Fully temperature dependent TE material properties
- One dimensional calculation ($\nabla = d/dx$)
- No electrical or thermal contact resistance
- No heat losses

Considering the concept of ERCA, some of the key equations of RCA that have used to develop the concept of ERCA can be stated as follows (a detailed discussion of RCA is included in Chapter 2):

Current density (J)

$$J = \frac{I}{A} \tag{2.35}$$

Reduced current density (u)

$$u = \frac{J}{k\,\nabla T} \tag{2.36}$$

TE potential

$$\Phi = \alpha T + \frac{1}{u} \tag{2.46}$$

Length of the thermoelement

$$l = \frac{1}{J_p}\int_{T_c}^{T_h} u_p k_p dT = \frac{1}{J_n}\int_{T_c}^{T_h} u_n k_n dT \quad (2.49)$$

The relationship between the area ratio of the p- and n-legs

$$\frac{A_p}{A_n} = \frac{-J_n}{J_p} = \frac{-\int_{T_c}^{T_h} u_n k_n \, dT}{\int_{T_c}^{T_h} u_p k_p \, dT} \quad (2.51)$$

Current density of a leg

$$J_p = \frac{H_{total,h}}{A_{total}} \times \frac{1+\frac{A_n}{A_p}}{\Phi_{p,h}-\Phi_{n,h}} \quad ; \quad J_n = \frac{H_{total,h}}{A_{total}} \times \frac{1+\frac{A_p}{A_n}}{\Phi_{p,h}-\Phi_{n,h}} \quad (2.56)$$

Where

I	= current
A	= cross-section area of the thermoelement
κ	= thermal conductivity
T	= absolute temperature
∇	= d/dx
u_p	= reduced current density of p-leg
u_n	= reduced current density of n-leg
κ_p	= thermal conductivity of p-leg
κ_n	= thermal conductivity of n-leg
T_h	= hot side temperature
T_c	= cold side temperature
α	= Seebeck coefficient
Φ	= thermoelectric potential
J_p	= current density of p-leg
J_n	= current density of n-leg
$\Phi_{p,h}$	= TE potential at hot end (h) of p-leg
$\Phi_{n,h}$	= TE potential at hot end (h) of n-leg
$\frac{H_{total,h}}{A_{total}}$	= total constant external heat flux supplied to hot side of TEG
l	= length of the thermoelement

For the same operating conditions, the efficiency of a TEG increases when increasing the thermoelement length, whilst the power density decreases [54,55]. Therefore reducing the thermoelement length, from the optimum predicted by RCA, will increase the power density of the TEG.

Based on Equation (2.49), the length is highly dependent on the u value. Thus, changing the length could change the u value. The influence of changes of u value to the TEG design parameters can be summarized as follows. According to Equations (2.46) and (2.51); the TE potential, area ratio, and current density are highly affected by the changes in the u values. The αT in Equation (2.46) is always of the order of 10^{-3} to 10^{-2} (V) in realistic real-world situations. Power generation applications (TEG) prefer small u values in the range of $0 \leq u \leq (z/\alpha)$ [51]. Therefore the u values are in the range of 10^{0} ($1/V$) or less, and thus $1/u$ values are in the range of 10^{-1} (V) or higher. Hence, for a TEG application, u values could influence the TE potential more than the αT in Equation (2.46). According to Equation (2.56), the current density of each thermoelement is influenced by the area ratio and TE potential.

By considering the above factors, changing the most efficient area ratio given by RCA is the main approach of ERCA, in order to change the u value of each thermoelement and to reduce the length of the thermoelements. Now, a TE material combination for p- and n-leg TE materials of a TEG is needed. The TE material combination used for the OTE-Power project is used here. Hence the TE materials used for these calculations are $Ca_3Co_4O_9$ and Al doped ZnO as p- and n-leg materials respectively [49,50]. TE properties of these materials are given in Figure 2.16. Thus the chosen p-leg thermoelement has higher TE properties or zT than the n-leg TE material. Therefore it could be beneficial to dominate the TEG design with the material that has higher TE properties (superior TE material) to achieve a higher conversion of thermal energy to electrical energy. Then in this case;

$A_p > A_n$

And thus

$\frac{A_p}{A_n} > \frac{A_n}{A_p}$, and $u_n k_n dT > u_p k_p dT$,

Due to the same current passing through both thermoelements, and by Equation (2.35),

$J_n > J_p$

The cross sectional areas of the p- and n-legs given by RCA are A_{p1} and A_{n1} , respectively, and the cross sectional areas of the p- and n-legs given by ERCA are A_{p2} and A_{n2} , respectively. The subscripts "1" and "2" represent the RCA and ERCA, respectively.

The total area of the thermoelements and external heat flux supplied to the hot side of the TEG in both RCA and ERCA is constant. Thus, the new condition to increase the performance of the superior TE materials in the TEG design is:

$A_{p2} > A_{p1}$

According to the Equation (2.51), this result is achievable by decreasing the u_p whilst increasing the $|u_n|$ values, which means

$J_{n1} < J_{n2}$ and $J_{p1} > J_{p2}$

These changes to the u value will affect equations (2.46) and (2.56). Thus, new u_{p2} and u_{n2} values should satisfy the following conditions to achieve a shorter thermoelement length by ERCA.

$$\left|\left(\frac{J_{n2}-J_{n1}}{J_{n1}}\right)\right| > \left|\left(\frac{\int u_{n2}\times\kappa_{n2}\times dT - \int u_{n1}\times\kappa_{n1}\times dT}{\int u_{n1}\times\kappa_{n1}\times dT}\right)\right|$$

and

$$\left|\left(\frac{J_{p2}-J_{p1}}{J_{p1}}\right)\right| < \left|\left(\frac{\int u_{p2}\times\kappa_{p2}\times dT - \int u_{p1}\times\kappa_{p1}\times dT}{\int u_{p1}\times\kappa_{p1}\times dT}\right)\right|$$

These results indicate that the TE potential in Equation (2.46) is a significant factor in the design of a TEG. Thus ERCA considers the product of "efficiency (η)" and "TE potential difference ($\Delta\Phi$)" to find the optimum u value.

Now the focus is to plot the "efficiency (η)" against the u value, as in RCA, and plot the "TE potential difference × Efficiency ($\Delta\Phi \times \eta$)" against the u value, as in ERCA. For both RCA and ERCA, hot (T_h) and cold (T_c) side temperatures are set as 1073 K and 373 K, respectively as the initial operating conditions.

The first focus is on the RCA calculations. Different u values are applied as the initial u value at the hot side of the TE material and the corresponding efficiency (η) is calculated. Then this efficiency is plotted against the u value, as in Figure 3.1, for both p- and n-legs. This will give the u value at the highest efficiency for both p- and n-legs. Then considering the ERCA calculations, different u values are applied as the initial u value at the hot side of the TE material and the corresponding efficiency (η) is calculated. Then the "product of TE potential difference and efficiency ($\Delta\Phi \times \eta$)" is plotted against the u value as in Figure 3.1 for both p- and n-legs. According to the Figure 3.1, the ERCA provides a maximum and minimum point to find the optimal u value for the TEG design for both the p- and n-legs.

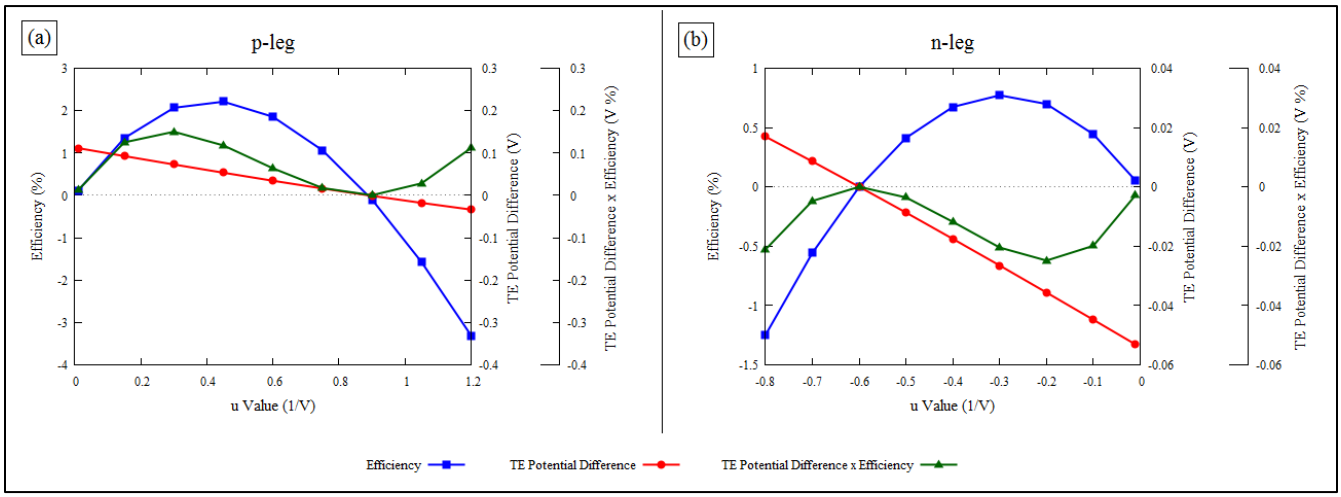

Figure 3.1: The variation of the "efficiency (η)", "TE potential difference ($\Delta\Phi$)", and "TE potential difference × Efficiency ($\Delta\Phi \times \eta$)" versus u values for the p- and n-legs.

Interestingly, the u values of these maximum and minimum points given by ERCA lie on either side of the u value of the maximum efficiency point given by the RCA. This can be explained using Figure 3.1. Focusing on Figure 3.1(a) for the p-leg, the x-axis region from zero u value up to the u value for the maximum efficiency, the efficiency is increasing whilst the TE potential difference is decreasing when the u value is increased. Thus, when calculating the product of TE potential difference and efficiency, the maximum is obtained at a u value in between the zero u value and the u value for the maximum efficiency. Considering the x-axis region with higher u values than the u value for the maximum efficiency, both the efficiency and TE potential difference is

decreasing when the u value is increased. Moreover, both efficiency and TE potential difference are decreasing to zero at the same u value when the u value is increased. At this u value, the product of TE potential difference and efficiency reaches its minimum. After this u value both the efficiency and TE potential difference are decreasing with negative values, when the u value is increased. Thus the product of TE potential difference and efficiency is again increasing with positive values, when the u value is increased. The same behaviour illustrated by the n-leg according to the Figure 3.1(b) and the "TE potential difference × efficiency" curve with negative values is obtained due to the initial negative TE potential differences given by the n-leg. By this figure of "TE potential difference × Efficiency ($\Delta\Phi \times \eta$)" against the u value, ERCA finds the new optimal configuration/reduced current density value for each p- and n-leg.

Now the focus is on the attainment of a new optimal configuration for ERCA using the figure of "TE potential difference × Efficiency ($\Delta\Phi \times \eta$)" against the u value. The target is to obtain larger thermoelement area for the superior TE material than in RCA $\left(A_{p2} > A_{p1} \right)$. Decreasing the u_p while increasing the $|u_n|$ values is required to achieve $A_{p2} > A_{p1}$ according to the equation (2.51). Therefore, a higher $|u_n|$ value and lower u_p value than the most efficient $|u_n|$ value and u_p value, are chosen from the maximum and minimum points of the "TE potential difference × Efficiency ($\Delta\Phi \times \eta$)" plot, which will increase the area of the p-leg of the ERCA over that of the RCA. After obtaining these new optimal configurations for p- and n-legs, the remainder of the procedure is carried out as in the original RCA, where these new configurations are matched to define the TEG architecture.

A summary of calculations, of the RCA for both p- and n-legs is given in Table 3.1 and 3.2 respectively. Table 3.3 and 3.4 represent the summery of the calculations of the ERCA for both p- and n-legs respectively. Thus according to the Table 3.1 and 3.2, the most efficient u_p and u_n values for these oxide TE materials are 0.416V^{-1} and -0.292 V^{-1}, respectively at these operating conditions. To fulfil the requirements, ERCA needs a higher $|u_n|$ value and lower u_p values, compared to the most efficient $|u_n|$ and u_p values obtained from the RCA. Therefore, according to the Figure 3.1 and, Table 3.3 and 3.4; u_p and u_n values for the ERCA should be 0.274 V^{-1} and -0.6 V^{-1} respectively at these operating conditions.

Table 3.1: Summary of the calculations to find the efficiency of p type TE material for a specific u value [51]. TE material properties for the p-leg from the reference [49].

Temperature (T)	Thermal Conductivity (κ)	Resistivity (ρ)	Seebeck Coefficient (α)	Figure of Merit (zT)	Reduced Current Density (u)	$ukdT$	Jl or $\int u\kappa dT$	TE potential (Φ)	Efficiency (η)
K	W/(m K)	mΩ cm	μV/K		1/V	A/m	A/m	V	%
1073	1.744	7.583	173.638	0.245	0.416	0	0	2.590	
973	1.880	7.637	170.936	0.198	0.415	75.242	75.242	2.579	0.444
873	1.943	7.798	165.160	0.157	0.413	79.049	154.290	2.568	0.858
773	1.998	8.145	162.918	0.126	0.411	81.158	235.449	2.558	1.241
673	2.064	8.680	156.929	0.093	0.409	83.312	318.761	2.549	1.588
573	2.180	9.953	156.517	0.065	0.408	86.694	405.455	2.541	1.881
473	2.549	10.761	153.146	0.040	0.406	96.193	501.648	2.536	2.093
373	2.814	10.757	147.832	0.027	0.404	108.528	610.175	2.533	2.223

Table 3.2: Summary of the calculations to find the efficiency of n type TE material for a specific u value [51]. TE material properties for the n-leg are from the reference [50].

Temperature (T)	Thermal Conductivity (κ)	Resistivity (ρ)	Seebeck Coefficient (α)	Figure of Merit (zT)	Reduced Current Density (u)	$ukdT$	Jl or $\int u\kappa dT$	TE potential (Φ)	Efficiency (η)
K	W/(m K)	mΩ cm	μV/K		1/V	A/m	A/m	V	%
1070	7.397	1.302	-98.239	0.107	-0.292	0	0	-3.530	
971	8.493	1.189	-91.134	0.080	-0.291	-229.319	-229.319	-3.523	0.185
872	9.894	1.105	-85.971	0.059	-0.290	-264.672	-493.991	-3.518	0.348
774	11.582	1.026	-79.859	0.042	-0.290	-305.299	-799.290	-3.513	0.486
675	13.849	0.946	-74.342	0.028	-0.289	-364.359	-1163.649	-3.509	0.601
575	16.913	0.874	-69.945	0.019	-0.289	-444.263	-1607.912	-3.505	0.691
474	21.246	0.804	-64.867	0.012	-0.288	-555.462	-2163.373	-3.503	0.753
374	28.156	0.741	-57.905	0.006	-0.287	-710.354	-2873.727	-3.503	0.772

Table 3.3: Summery of the calculations of ERCA for the p-leg. TE material properties for the p-leg from the reference [49].

Temperature (T)	Thermal Conductivity (κ)	Resistivity (ρ)	Seebeck Coefficient (α)	Figure of Merit (zT)	Reduced Current Density (u)	$ukdT$	Jl or $\int u\kappa dT$	TE potential (Φ)	Efficiency (η)
K	W/(m K)	mΩ cm	μV/K		1/V	A/m	A/m	V	%
1073	1.744	7.583	173.638	0.245	0.274	0	0	3.836	
973	1.880	7.637	170.936	0.198	0.274	49.603	49.603	3.822	0.351
873	1.943	7.798	165.160	0.157	0.273	52.214	101.816	3.810	0.684
773	1.998	8.145	162.918	0.126	0.272	53.712	155.528	3.798	1.000
673	2.064	8.680	156.929	0.093	0.272	55.247	210.775	3.786	1.296
573	2.180	9.953	156.517	0.065	0.271	57.608	268.383	3.776	1.564
473	2.549	10.761	153.146	0.040	0.271	64.065	332.448	3.767	1.794
373	2.814	10.757	147.832	0.027	0.270	72.474	404.922	3.760	1.983

Table 3.4: Summery of the calculations of ERCA for the n-leg. TE material properties for the n-leg are from the reference [50].

Temperature (T)	Thermal Conductivity (κ)	Resistivity (ρ)	Seebeck Coefficient (α)	Figure of Merit (zT)	Reduced Current Density (u)	$ukdT$	Jl or $\int u\kappa dT$	TE potential (Φ)	Efficiency (η)
K	W/(m K)	mΩ cm	μV/K		1/V	A/m	A/m	V	%
1070	7.397	1.302	-98.239	0.107	-0.600	0	0	-1.772	
971	8.493	1.189	-91.134	0.080	-0.595	-469.982	-469.982	-1.768	0.200
872	9.894	1.105	-85.971	0.059	-0.591	-539.978	-1009.960	-1.766	0.347
774	11.582	1.026	-79.859	0.042	-0.587	-620.164	-1630.124	-1.764	0.434
675	13.849	0.946	-74.342	0.028	-0.584	-736.861	-2366.985	-1.764	0.457
575	16.913	0.874	-69.945	0.019	-0.580	-894.516	-3261.501	-1.765	0.406
474	21.246	0.804	-64.867	0.012	-0.576	-1113.241	-4374.741	-1.767	0.266
374	28.156	0.741	-57.905	0.006	-0.571	-1416.188	-5790.929	-1.772	-0.001

Therefore $\frac{A_{p1}}{A_{n1}} < \frac{A_{p2}}{A_{n2}}$ is achieved and one requirement to achieve $J_{n1} < J_{n2}$ is fulfilled according to the Equation (2.56). However, $J_{n1} < J_{n2}$ depends on the TE potential difference ($\Phi_{p,h} - \Phi_{n,h}$). The new TE potentials show the following relationship with the old TE potentials based on equation (2.46) and according to the Table 3.1 – 3.4.

$\left|\Phi_{n,h\,1}\right| > \left|\Phi_{n,h\,2}\right|$, and $\Phi_{p,h\,1} < \Phi_{p,h\,2}$

The changes in the TE potential difference highly depend on the amount that the u value has changed. Moreover, these variations of u values depend on the TE material properties of the p- and n-leg materials. Therefore the TE properties (or zT) of the p- and n-leg TE materials will define the effectiveness and the limitations of the ERCA over RCA.

The discussion of the TEG architectures according to the RCA and ERCA is concluded. The heat flux through the hot side of the unicouple TEG and the total area of the thermoelements ($A_{total} = A_p + A_n$) are kept constant at 20 W/cm^2 and 1 cm^2, respectively for both RCA and ERCA. TEG architecture and outputs are presented in Table 3.5 by both RCA and ERCA. Table 3.5 also shows the percentage difference between the results of ERCA and RCA compared to RCA.

Table 3.5: Comparison of the architecture and the output results by RCA and ERCA

	RCA	ERCA	$\left[\frac{ERCA - RCA}{RCA}\right]\%$
Area of n-leg, An (cm^2)	0.175	0.065	-62.685
Area of p-leg, Ap (cm^2)	0.825	0.935	13.310
Length of TE (cm)	1.540	1.061	-31.099
Output potential (V)	0.085	0.076	-10.348
Output current (A)	3.268	3.567	9.134
Power output (W)	0.277	0.271	-2.160
VPD (W/cm^3)	0.180	0.256	42.002

According to the Table 3.5, ERCA has increased the area of p-leg by 13% and reduced the area of the n-leg by 63% comparing to RCA. Thus, ERCA gave a higher priority to the superior TE material in the TEG unicouple. Furthermore, ERCA has reduced the length of the thermoelements by 31% compared to RCA, which helps to increase the power density. Moreover, ERCA reduces the power output by 2% compared to the RCA. Thus ERCA has improved the volumetric power density $\left(VPD = \frac{Power\ output}{total\ TE\ volume}\right)$ by 42% compared to RCA.

As shown in Table 3.5, ERCA significantly changes the TEG architecture proposed by RCA. Therefore these changes affect the rate of conduction heat transfer ($Q_{cond.}$), heat conduction resistance (thermal resistance) ($R_{cond.}$), efficiency, and power given by each p- and n-leg of the TEG. These results are shown in Table 3.6. Conduction heat transfer and heat conduction resistance are stated as in Equations (3.2) and (3.3) respectively [192]. The efficiency of each thermoelement for both RCA and ERCA can be determined using Table 3.1 – 3.4. Power output (P) can be calculated using Equation (2.21) [53,189].

$$Q_{cond.} = \kappa A \frac{T_h - T_c}{l} \tag{3.2}$$

$$R_{cond.} = \frac{l}{\kappa A} \tag{3.3}$$

$$P = \eta\, H_{total,h} \tag{2.21}$$

where, $H_{total,h}$ is the amount of heat transfer to the hot side.

To simplify the calculations, two assumptions have been made. Firstly, the average thermal conductivity of thermoelement is taken as the thermal conductivity of thermoelement. Secondly, the heat transfer by Peltier effect is negligible and therefore $H_{total,h} \cong Q_{cond.}$. As an example: considering the p-leg by RCA, the heat transfer by conduction is 8.047 W, but heat transfer by Peltier effect is 0.38 W.

Table 3.6: Rate of heat conduction, heat conduction resistance (thermal resistance), efficiency (by Table 3.1 – 3.4) and power produced by the TEG according to both RCA and ERCA for p- and n-legs using the average thermal conductivity of thermoelements

		RCA	ERCA
Rate of conduction heat transfer, $Q_{cond.}$ (W)	p-leg	8.047	13.234
	n-leg	11.695	6.334
Heat conduction resistance (thermal resistance), $R_{cond.}$ (K/W)	p-leg	86.984	52.893
	n-leg	59.855	110.521
Efficiency, η	p-leg	0.022	0.020
	n-leg	0.008	0.000
Power produced by the TEG, P (W)	p-leg	0.179	0.262
	n-leg	0.090	0.000
	Total	0.269	0.262

As shown in Table 3.5, ERCA has increased the area of p-leg (superior TE material) by 13% and reduced the area of the n-leg (weaker TE material) by 63% compared to RCA. Therefore this will help to change the thermal resistance of each p- and n-leg, as shown in Table 3.6; the thermal resistance of the p-leg by RCA is 86.984 K/W, and ERCA reduces the thermal resistance of the p-leg down to 52.893 K/W. On the other hand, ERCA increases the thermal resistance of n-leg up to 110.521 K/W (it was 59.855 K/W in RCA). Therefore, this will allow the p-leg of ERCA to conduct more heat than the p-leg of RCA. From Table 3.6, the rate of conduction heat transfer of the p-leg by ERCA is 13.234 W and by RCA is 8.047 W. On the other hand, the rate of conduction heat transfer of the n-leg by ERCA is 6.334 W and by RCA it is 11.695 W. Therefore ERCA lets more heat passes through the superior TE material and reduces the amount of heat transfer by the weaker TE material compared to RCA.

The total power output given by RCA and ERCA in Table 3.5 and 3.6 are almost the same. The small difference could occur due to the two assumptions that have been made in the calculation of Table 3.6. For this example, Table 3.6 shows that no considerable power was generated by the n-leg when using the ERCA. However, for this example, both methods produce almost the same power. According to the Table 3.5, ERCA produce TEG with shorter thermoelement length than RCA. Thus, ERCA generates a higher VPD than RCA.

Therefore ERCA is able to increase the volumetric power density of oxide TE materials used by the OTE-Power project ($Ca_3Co_4O_9$ and Al doped ZnO) by 42%, compared to the RCA at high temperature operating conditions. This will help to reduce the cost-per-Watt of the OTE-Power TEG.

3.2 Limitations of ERCA

As explained earlier, the applicability of ERCA depends on the zT of the TE materials used to develop the TEG. Therefore, to identify the limitations of ERCA, TE materials with different zT values are combined to generate a series of TEGs that have different zT ratios $\left(\frac{zT\ of\ n\ leg}{zT\ of\ p\ leg}\right)$. Then the TEG architecture and the power output are calculated according to the RCA and the ERCA.

The development of pseudo-TEG unicouples are shown in Figure 3.2. The n-type Al-doped ZnO and the p-type $Ca_3Co_4O_9$ used in Section 3.1 are used as the starting TE materials for the pseudo-TEG unicouples. The average zT ratio $\left(\frac{Average\ zT\ of\ n\ leg}{Average\ zT\ of\ p\ leg}\right)$ of these TE materials is 0.37 for the specific operating conditions stated in Section 3.1. Temperature dependent TE properties are used for all the calculations of this section. However, the average zT ratios of the pseudo-TEG unicouples are used to plot the data to obtain a clear illustration in Figure 3.3 and 3.4. When developing the pseudo-TEG unicouples, as shown in Figure 3.2, the zT of the n-type material is changed by only changing the thermal conductivity whilst keeping the TE properties of the p-type material constant. The thermal conductivity variation of those n-leg TE materials with temperature for the different pseudo-TEG unicouples are shown in Figure 3.3.

Now applying the RCA and ERCA for each pseudo-TEG unicouple. As the initial operating conditions, the hot and cold side temperatures are set to 1073 K and 373 K respectively, for all the pseudo-TEG unicouples. The heat flux throughout the hot side of the unicouple and the total area of the thermoelements are kept constant at 20 W/cm^2 and 1 cm^2, respectively for all the pseudo-TEG unicouples. Figure 3.4 shows the VPD given by RCA and ERCA. Moreover Figure 3.4 illustrates the percent change of the VPD given by ERCA compared to the RCA; $\left\{\frac{[(VPD\ by\ ERCA)-(VPD\ by\ RCA)]}{(VPD\ by\ RCA)}\%\right\}$. According to the Figure 3.4, ERCA can produce TEGs with significantly higher VPD, when the zT of p- and n-leg of a TEG are not close to the same values. Thus the limitation of ERCA depends on the zT of p- and n-leg materials of a TEG.

The initial question of this chapter: "does the TEG design concept focus on efficiency or power output"; can answered by Figure 3.4. According to Figure 3.4 at particular operating conditions, if the TE material properties (or zT) of the p- and n-legs of the TEG are comparable (the same or close values), the TEG architecture for the maximum efficiency will provide the maximum power density. However, at particular operating conditions, if the TE material properties (or zT) of the p- and n-legs of the TEG are not comparable (not the same nor close values), the TEG architectures for the maximum efficiency and maximum power density should be different.

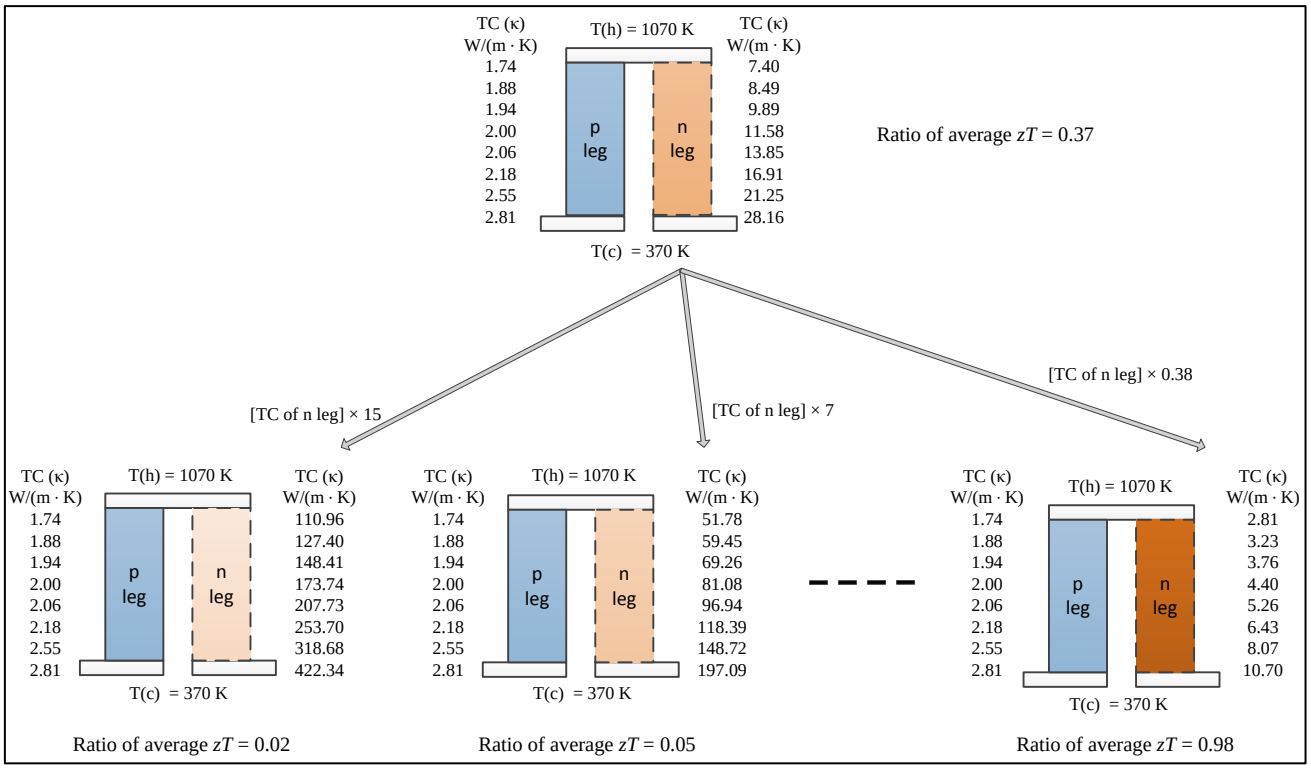

Figure 3.2: Process of developing predicted TEG unicouples with different zT ratios. TC = Thermal Conductivity; T(h) = Hot side temperature; T(c) = Cold side temperature [204].

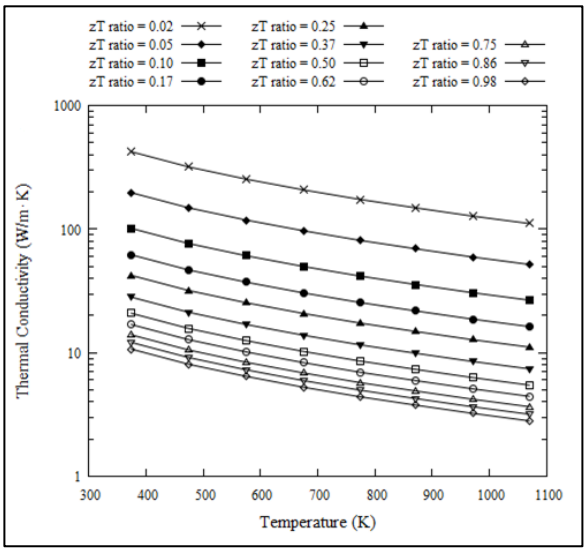

Figure 3.3: Thermal conductivity variation of predicted n leg TE material with temperature for the different pseudo-TEG unicouples [204].

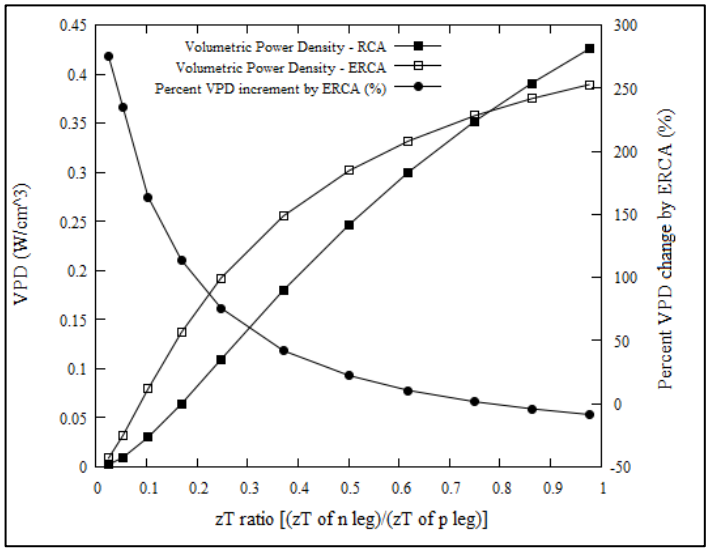

Figure 3.4: Variation of volumetric power density (VPD) and Percent VPD change by ERCA versus zT ratio. [204].

4. Removing the Weaker Material as a means to performance enhancement

This chapter focuses on the minimization of the cost-per-Watt of a TEG by removing the weaker TE material from the TEG system. Here the concept of Unileg-TEG (U-TEG) for the oxide TE materials is introduced. The U-TEG is able to increase the volumetric power density and decrease the cost-per-Watt of the OTE-Power TEG. In the latter part of the chapter the U-TEG system is generalized by using an idealized metal.

As shown in Figure 4.1(a) [130], the conventional unicouple TEG designs consists of two p- and n-type thermoelements, and the electrical connections are in series. However, as shown in Figure 4.1(b) [130], the U-TEG design consists of p- or n-type TE material serially connected with a conductor [56–58]. Moreover, the U-TEG design can be further improved, as shown in the Figure 4.1(c) [130].

The choice of p- and n-leg TE materials for a TEG depends on many factors. Due to the physical properties, such as melting point, different TE materials are stable in different temperature ranges. For instance, due to the low melting point of intermetallic alloy TE materials, they are stable at low temperature ranges. In contrast, oxide TE materials have higher melting points and thus they are stable at even elevated temperatures. Therefore, when choosing TE materials for a TEG device, not only the TE properties, but also the physical properties of the TE materials play an important role. Therefore, in real applications, the p- and n-type materials chosen for a TEG may not have the same zT values. Hence if one material has considerably weaker TE properties, it could hinder the performances of the stronger material. In the worst case, the weaker material could act like another resistor and have a negative impact on the TEG. Therefore, the weaker TE material could reduce the power generated by the stronger TE material. Since the weaker TE material also claimed a considerable volume out of the total thermoelement volume in TEG, it will affect the volumetric power density (VPD) of the TEG.

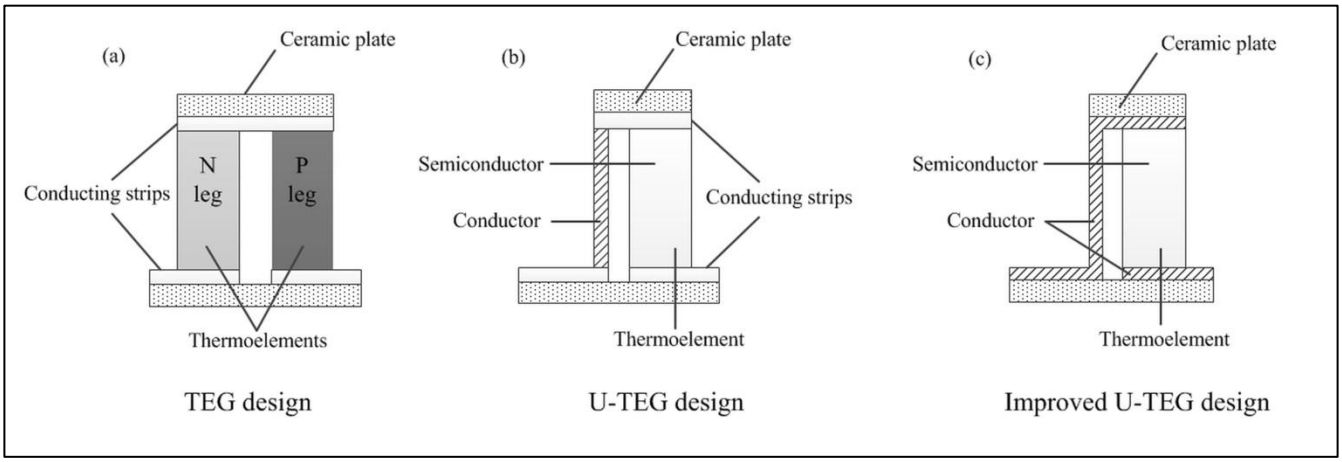

Figure 4.1: Design of the (a) unicouple TEG, (b) U-TEG, and (c) improved U-TEG [130]

At the U-TEG design shown in Figure 4.1(b), the stronger TE material is kept in the system and the weaker TE material is replaced by a conductor. Moreover, it will increase the volumetric fraction of the stronger TE materials in the system and thus potentially increase the VPD.

When comparing Figures 4.1(a) and 4.1(b), the number of metal/semiconductor contacts in the U-TEG design is equal to the half of the number of metal/semiconductor contacts in the conventional unicouple TEG design. This will result in great advantages by reducing the contact resistance of the U-TEG. Furthermore, the total number of contacts in the improved U-TEG design shown in Figure 4.1(c) is equal to the half of the total number of contacts in the conventional unicouple TEG design. Thus, the improved U-TEG design could further reduce the contact resistance of a TEG. Contact resistance is one of the challenges when developing a real TEG device, as this can considerably reduce the power output of a TEG [55,82]. Thus U-TEG design solves this problem by reducing the number of metal/semiconductor contacts in a TEG system. Obviously, reducing the contact resistance will increase the power output of the system, further improving the VPD of the device. Another advantage of the U-TEG is that it can vastly reduce the cost of the TEG by replacing one thermoelement by a well-known, less expensive metal, thereby removing the production cost associated with the weaker TE material. Therefore the U-TEG will reduce the cost-per-Watt of a TEG system.

Even though U-TEG improves the performances of the electrical circuit in a TEG, it will cause some problems in the thermal circuits of the device, because, in general, highly electrical conducting metals are high thermal conductors. Thus, this behaviour could cause a thermal shortening between the hot and cold side of a TEG. However, this problem can be answered by optimising the area ratio of the metal and semiconductor of the U-TEG. The RCA can be used to find this optimal area ratio of the TEG and control the heat passing through metal by reducing the area of the metal.

The discussion above is similar to the situation in the TEG of OTE-Power project, which has a strong p-type $Ca_3Co_4O_9$ and weaker n-type Al-doped ZnO [49,50]. Thus, it is important to find an appropriate solution to this issue, and one promising solution is to introduce the U-TEG concept for the oxide TE materials. Therefore it could be possible to remove the Al-doped ZnO from the TEG and replace it with a conductor which is inexpensive and readily available. Then the thermal conductivity of the conductor will be considerably higher than the thermal conductivity of the Al-doped ZnO. Thus, when obtaining the optimal area ratio by RCA; the cross-sectional area of the conductor in the U-TEG will be considerably smaller compared to the cross-sectional area of the Al-doped ZnO in the unicouple TEG. Thus the amount/volume of $Ca_3Co_4O_9$ in the U-TEG will be higher than the unicouple TEG and it could possibly increase the VPD of the U-TEG compared to the unicouple TEG. Since U-TEG removes the production cost of Al-doped ZnO and replaces Al-doped ZnO with a cheaper option, U-TEG could help to reduce the cost-per-Watt of the device. Therefore the U-TEG is a promising concept for the OTE-Power project for increasing the VPD and decrease the cost-per-Watt of the TEG.

4.1 TEG and U-TEG

In the following, a TEG and a U-TEG are developed based on oxide TE materials. The device architecture and the power outputs of TEG and U-TEG are compared when operating under the same conditions.

The TEG is developed based on the TE materials from the OTE-Power project; p-type $Ca_3Co_4O_9$ and n-type Al-doped ZnO. Then the U-TEG device is developed by using p-type $Ca_3Co_4O_9$ and Constantan instead of the n-type material. Constantan is an alloy made by Nickel and Copper (45Ni55Cu) [193]. It has low electrical resistivity which is constant over a wide temperature range. Constantan has a high melting point of over 1500 K [194], and is thus suitable for high temperature applications. However, Constantan undergoes oxidation at above

600 K, but this can be controlled by coating a NiCr layer on Constantan [195]. Moreover, Constantan has a negative Seebeck value and thus it can act as an n-type semiconductor, and thus it helps by generating additional power when it is subjected to a temperature gradient.

The TE material properties of above materials used to develop the TEG and U-TEG are shown in Figure 4.2. Hot and cold side temperatures of the TEG and U-TEG are kept at 1070 K and 370 K, respectively. The heat flux at the hot side of the device and total thermoelement area are kept constant at 20W/cm^2 and 1 cm^2, respectively for both TEG and U-TEG. The RCA is used to develop both TEG and U-TEG. The most efficient device architecture and the outputs obtained for both TEG and U-TEG by RCA are shown in Table 4.1. The V-I curves for both TEG and U-TEG are then obtained by using COMSOL and those are shown in Figure 4.3. The heat flux through the TEG and U-TEG are obtained by using COMSOL and the results are shown in Figure 4.4.

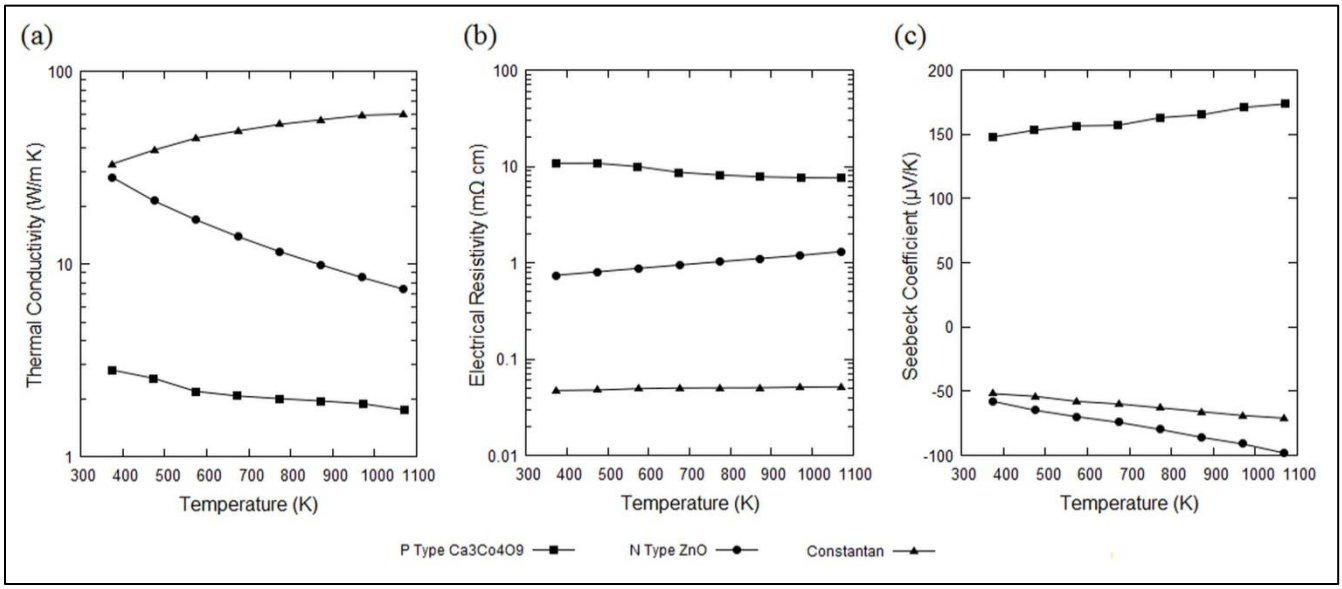

Figure 4.2: (a) Thermal conductivity, (b) Electrical resistivity, and (c) Seebeck coefficient of $Ca_3Co_4O_9$, Al-doped ZnO and Constantan [49,50,193]

According to Table 4.1, U-TEG increases the area of p-type $Ca_3Co_4O_9$ and increases the area dominancy of the superior TE material. The area ratio (A_p / A_n) of U-TEG is 14 times higher than the TEG design and Constantan claims only 1% of the total thermoelement area of the U-TEG and this will maintain the thermal circuit of the U-TEG and control the thermal shortening effects between hot and cold side of the U-TEG. The rate of conduction heat transfer ($Q_{cond.}$) through a material can be stated as Equation (3.2). According to the Figure 4.2, Constantan has a high thermal conductivity (κ). When the temperature difference between hot and cold side ($T_h - T_c$), thermal conductivity, and the length (l) of the material are fixed, the amount of heat transfer from hot side to cold side of the material is controlled by the cross-sectional area (A) of the material. Therefore in a TEG, the material with the higher thermal conductivity the area ratio should be less dominant, compared to the material with the lower thermal conductivity.

$$Q_{cond.} = \kappa A \frac{T_h - T_c}{l} \quad (3.2)$$

Table 4.1: Most efficient reduced current density, device architecture and the outputs obtained for both TEG and U-TEG by RCA

	Thermoelements length (cm)	*p-leg* area A_p (cm^2)	*n-leg* area A_n (cm^2)	Area ratio A_p / A_n	Voltage (V)	Current (A)	Power Output (W)	VPD (W/cm^3)
TEG	1.54	0.825	0.175	4.710	0.0848	3.2680	0.2772	0.18
U-TEG	1.04	0.986	0.014	68.652	0.0796	5.7594	0.4585	0.44

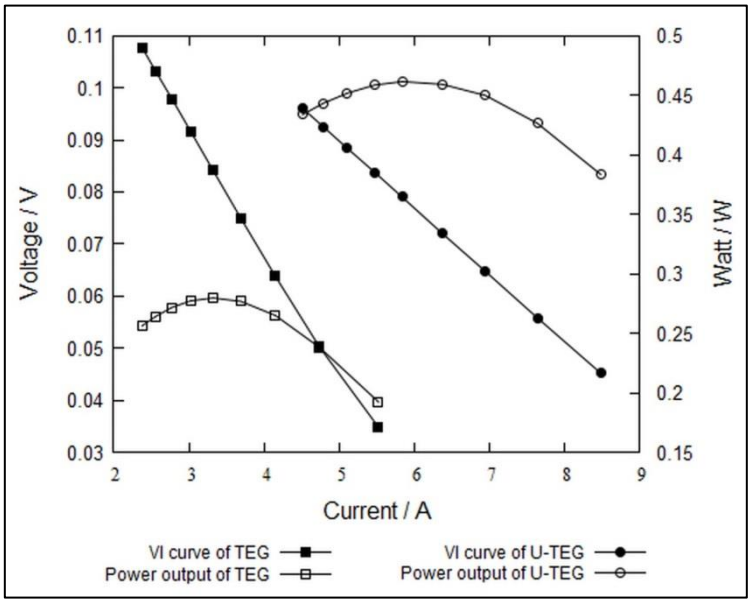

Figure 4.3: V–I and power output curves obtained using the COMSOL software for both the TEG and U-TEG architectures. The heat flux through both the unicouple TEG and U-TEG was 20 W/cm^2 [130]

According to Table 4.1, the U-TEG can generate 65% higher power output than the TEG design studied in OTE-Power project. Furthermore, the VPD given by U-TEG is 145% higher than the TEG design studied in OTE-Power project. Therefore for the OTE-Power project, the U-TEG design with $Ca_3Co_4O_9$ and Constantan is highly beneficial in terms of power output and VPD compared to the TEG with $Ca_3Co_4O_9$ and Al-doped ZnO.

According to the Table 4.1, the voltage given by both TEG and U-TEG are almost the same. This is mainly due to the Al-doped ZnO and Constantan which possess similar Seebeck coefficients, as shown in Figure 4.2. From the V-I curve of the Figure 4.3, the U-TEG has a low total electrical resistance compared to the TEG. This is due

to two main reasons: one is the low electrical resistivity of Constantan compared to Al-doped ZnO, the other reason is that the higher cross sectional area and lower length of the $Ca_3Co_4O_9$ leg gives lower electrical resistance in the U-TEG compared to the TEG. According to Table 4.1, electrical current given by the U-TEG is higher than the TEG.

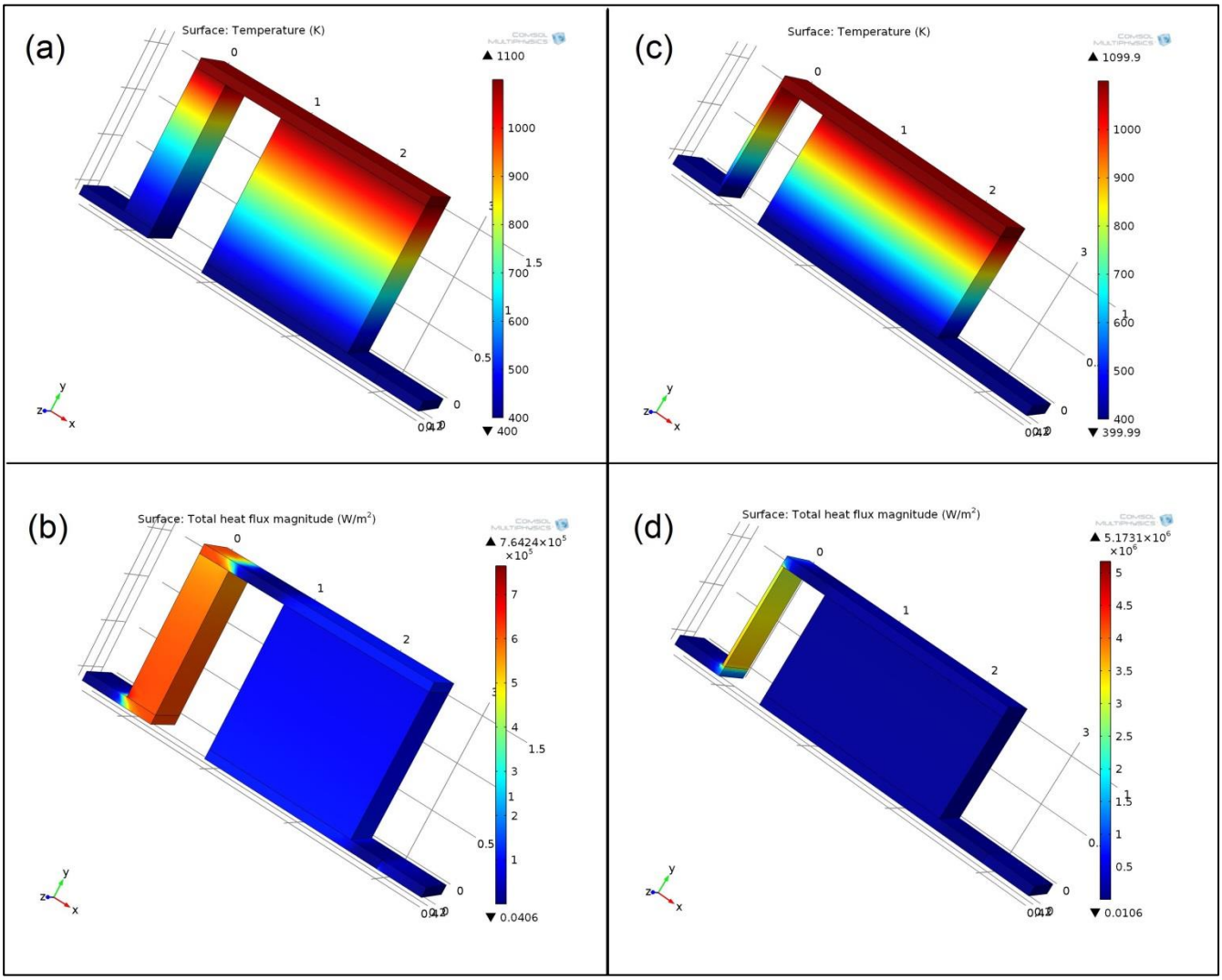

Figure 4.4 (a) and (b) Temperature profile and heat flux of TEG respectively. (c) and (d) Temperature profile and heat flux of U-TEG respectively.

The length of the thermoelement (l) is stated in Equation (2.49) according to the RCA. Since the same p-leg is used under the same operating conditions for both TEG and U-TEG designs, the value of the most efficient $\int_{T_c}^{T_h} u_P \kappa_P dT$ is the same for both designs. The area of p-leg in the U-TEG is 19% higher than the TEG and the electrical current (I) in the U-TEG is 76% higher than the TEG. Therefore, the current density of the p-

leg ($J_P = {}^{I}/_{A_p}$) in U-TEG is higher than the TEG. Thus, according to Equation (2.49), U-TEG has a shorter thermoelement length than TEG.

$$l = \frac{1}{J_P}\int_{T_c}^{T_h} u_P \kappa_P dT \tag{2.49}$$

Therefore, the low electrical resistivity of Constantan makes it a better material than the Al-doped ZnO when developing a TEG with $Ca_3Co_4O_9$. However, the high thermal conductivity of Constantan could make negative impacts to the thermal circuit of the TEG and create thermal shortening effects. This problem is addressed in RCA by considerably reducing the cross-sectional area of Constantan. Figure 4.4 shows the temperature profiles and the heat flux magnitudes for both TEG and U-TEG designs. Both designs possess similar temperature profiles, as shown in Figure 4.4(a) and (c), and similar heat flux profiles, as shown in Figure 4.4(b) and (d). Therefore no thermal shortening effects acting in the U-TEG design.

By considering the above facts it can be claimed that the U-TEG is a promising concept for the OTE-Power project to increase the VPD and decrease the cost-per-Watt of the TEG.

4.2 Generalization of U-TEG using an idealized metal

This section discusses the device architecture and the VPD of a U-TEG when using an idealized metal as the conductor of the U-TEG. Thus the p-type $Ca_3Co_4O_9$ and an idealized metal are used as the semiconductor and the conductor of the U-TEG design respectively.

Constantan is used as the conductor of the U-TEG in Section 4.1. Due to the non-zero Seebeck coefficient, Constantan generates power in the U-TEG system though it used as a conductor. Thus the power output of the U-TEG not solely dependent on the semiconductor. However, when generalizing the U-TEG design, the conductor should not contribute to the power output of the system. Thus an idealized metal is used as the conductor in this section and the Seebeck coefficient of the idealized metal is taken as zero. Therefore the conducting leg does not contribute to power production for the U-TEG device and it only helps to maintain the thermal and electrical circuits of the U-TEG system. Hence the TE material is responsible for all the power that is generated by the U-TEG. However, the electrical resistivity and the thermal conductivity of the idealized metal are taken to be temperature dependent.

Generating the electrical resistivity data for an idealized metal is the first step. A common assumption is that the electrical resistivity of a metal is linearly dependent on the temperature, as shown in Equation (4.1) [196]. Additionally, two other assumptions have been made for the temperature dependencies of the electrical resistivity: one is a quadratic relationship (upper extreme) and one is a constant relationship (lower extreme). The quadratic dependency of electrical resistivity on temperature (quadratic relationship) is shown in Equation (4.2) and the non-temperature dependency of electrical resistivity (constant relationship) is shown in Equation (4.3).

$$\rho = \rho_0 \left(\frac{T}{T_0}\right) \tag{4.1}$$

$$\rho = \rho_0 \left(\frac{T}{T_0}\right)^2 \quad (4.2)$$

$$\rho = \rho_0 \quad (4.3)$$

where, ρ is electrical resistivity, ρ_0 is electrical resistivity at room temperature (initial resistivity), T is temperature and T_0 is the ambient temperature.

Due to the resultant electrical resistivity dependency on the initial resistivity, three different initial resistivities are studied for each temperature dependency of electrical resistivity. Thus nine different idealized metals are generated, based on three different temperature dependencies and three different initial electrical resistivities.

Silver is one of the commonly used highly electrical conducting materials And thus the electrical resistivity of silver (0.0015 mΩ cm [197]) has been used as a one initial electrical resistivity. Another initial electrical resistivity considered here is a hypothetical electrical resistivity 0.001 mΩ cm, which is lower than the electrical resistivity of silver. Finally, the average electrical resistivity of Constantan (0.05 mΩ cm [193]) is used as another electrical resistivity. Thus these three resistivities provide a better spectrum to demonstrate the effect of the initial resistivity for the final VPD. Figure 4.5 shows the temperature dependent electrical resistivities of six different idealized metals (according to the Equation (4.3) the electrical resistivities not depend on the temperature and thus the electrical resistivities of those three idealized metal are not plotted in Figure 4.5).

As shown in Figure 2.2, insulators and metals have low and high carrier concentrations respectively. Moreover, the electronic contribution for the thermal conductivity increases exponentially, when the carrier concentration is increased [1,2]. Idealized metals have high carrier concentrations. Therefore, it is assumed that, the thermal conductivity of the idealized metals only depends on the electronic thermal conductivity and that the lattice thermal conductivity is negligible. Equation (2.10) shows the electronic contribution of the thermal conductivity, according to the Wiedemann–Franz law [1]. Therefore the thermal conductivity of the idealized metal only depends on the electrical resistivity and the temperature. Figure 4.5 shows the temperature dependent thermal conductivity of nine different idealized metals.

$$\kappa_e = \frac{LT}{\rho} \quad (2.10)$$

Nine different idealized metals, shown in Figure 4.5, are numerically combined with p-type $Ca_3Co_4O_9$ used in Section 4.1, to develop nine different pseudo U-TEG devices. The operating temperature, heat input at the hot side, and the total thermoelement area are kept the same as that in Section 4.1 for all the pseudo U-TEG devices:1070-370 K, 20W/cm^2 and 1 cm^2, respectively. The architecture and the output for these nine different pseudo U-TEG devices are shown in Table 4.2.

Due to the zero Seebeck coefficients, the idealized metal will not contribute to the power output of the U-TEG device. Thus, according to the Table 4.2, all the U-TEG devices possesss the same TE potential, current and power output; though they have different starting electrical resistivity and different temperature dependency for the resistivity.

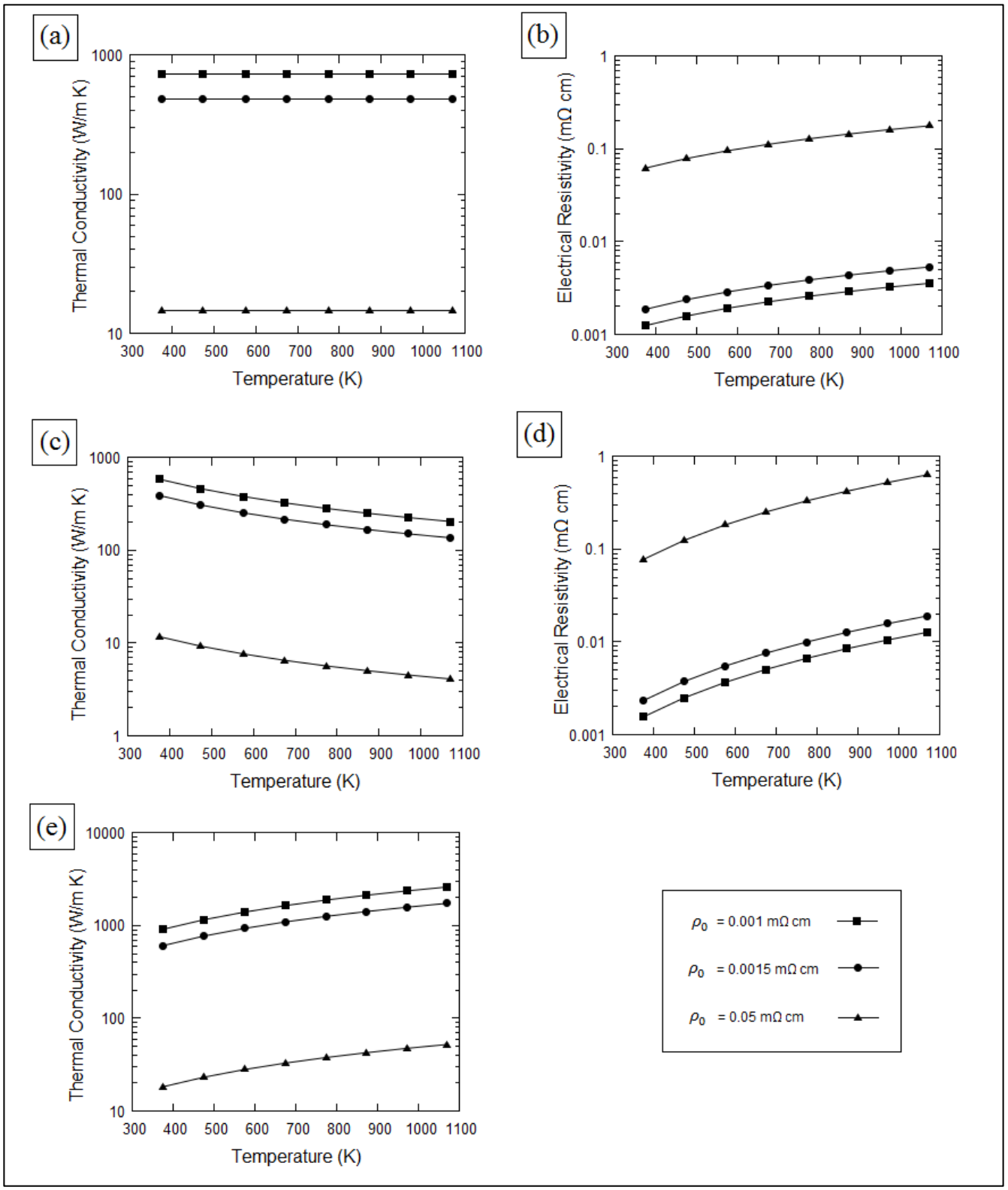

Figure 4.5 (a) Thermal conductivity, and (b) Electrical resistivity variation with temperature of an idealized metal for linear temperature dependent electrical resistivity for different initial resistivities at room temperature; (c) Thermal conductivity, and (d) Electrical resistivity variation with temperature of idealized metal when the electrical resistivities quadratically depend on the temperature for different initial resistivities at room temperature; (e) Thermal conductivity variation with temperature of idealized metal when the electrical resistivities are independent of the temperature for different initial resistivities at room temperature.

According to Table 4.2, the TE length has increased and the area of the idealized metal has decreased, when decreasing the initial resistivity at room temperature. All three temperature dependencies show this same behavior. This behavior will control the thermal shortening effects in U-TEG. According to the Equation (2.10), the thermal conductivity will increase when the electrical resistivity is decreased. Therefore, to reduce the thermal shortening effects, the TE length should increase and the area of idealized metal should decrease, according to Equation (3.2).

TEG and U-TEGs in Section 4.1 and 4.2 operate under the same operating temperature, heat input at the hot side, and the total thermoelement area. Therefore, the outputs of those TEG and U-TEGs can be compared. Thus according to the Table 4.1 and 4.2, U-TEGs with $Ca_3Co_4O_9$ and idealized metal could produce higher VPD compared to the TEG from OTE-Power project with $Ca_3Co_4O_9$ and Al-doped ZnO.

This confirms that the U-TEG design is a promising concept for the OTE-Power project. Because it increases and the VPD and decreases the cost-per-Watt of the TEG.

Table 4.2: Architectures and outputs of U-TEGs with $Ca_3Co_4O_9$ and idealized metal for different starting electrical resistivities for different temperature dependencies of the resistivity

Temperature dependency of resistivity	ρ_0 (mΩ cm)	TE length (cm)	Idealized metal area (cm^2)	$Ca_3Co_4O_9$ area (cm^2)	TE potential (V)	Current (A)	Power Output (W)	Volumetric power density W/cm3
	0.001	1.09	0.0012	0.9988	0.045	5.610	0.253	0.232
Linear	0.0015	1.09	0.0018	0.9982	0.045	5.610	0.253	0.232
	0.05	1.03	0.0555	0.9445	0.045	5.610	0.253	0.246
	0.001	1.09	0.0026	0.9974	0.045	5.571	0.253	0.232
Quadratic	0.0015	1.08	0.0039	0.9961	0.045	5.610	0.253	0.234
	0.05	0.96	0.1145	0.8855	0.045	5.610	0.253	0.263
	0.001	1.09	0.0005	0.9995	0.045	5.610	0.253	0.232
Non	0.0015	1.09	0.0007	0.9993	0.045	5.610	0.253	0.232
	0.05	1.06	0.0238	0.9762	0.045	5.610	0.253	0.239

5. Increase the cost effectiveness of a TEG using an appropriate TEG design technique

This chapter focuses on the minimization of the cost-per-Watt of a TEG by choosing the appropriate TEG design technique. TEG design techniques proposed by Ioffe [53] and Snyder et al. [51,52] are compared using the same boundary conditions and power requirements. Then the cost-per-Watt of the TEGs produced by the two different methods is calculated using real TE material costs and the results are compared.

5.1 Ioffe's Method vs RCA

This section discusses the relationship between two of the most established TEG design techniques for temperature independent TE properties. Ioffe proposed in 1957 one of the first TEG design techniques that can be used for temperature independent TE properties [53]. This pioneering work still serves as a design tool and a number of modern day TEG designs follow the concepts of the above work. In the early 2000s' Snyder et al. has introduce a comprehensive TEG design technique RCA, which can be used for temperature dependent and independent TE properties [51,198].

A detail explanation about the method proposed by Ioffe (Ioffe's method) is included in Chapter 2 in this thesis. Moreover, a detail explanation about the method proposed by Snyder et al. (RCA) is also included in Chapter 2.

Both methods can be used to design a unicouple TEG device. Unicouple TEG devices consist of p- and n-leg thermoelements, which are connected thermally in parallel and electrically in series, as shown in Figure 2.6(a).

One important similarity between Ioffe's method and RCA is that, both methods focus on the most efficient TEG architecture and more importantly both methods predict the most efficient area ratio for p- and n-legs of the TEG. However, they use different strategies to obtain the most efficient area ratio.

Ioffe's method considers the p- and n-legs of the unicouple TEG as a single unit. Then it matches the thermal conductivity (κ) and the electrical resistivity (ρ) of both legs to obtain the most efficient area ratio for p- and n-legs. Therefore the area ratio between the p- and n-legs can be stated as Equation (2.24) [53].

$$\frac{\rho_p \kappa_n}{\kappa_p \rho_n} = \left(\frac{A_p}{A_n}\right)^2 \tag{2.24}$$

Where A_p and A_n are the cross-sectional area of the p- and n-legs respectively; ρ_p and ρ_n are the electrical resistivity of the p- and n-legs respectively; κ_p and κ_n are the thermal conductivity of the p- and n-legs respectively.

According to Equation (2.24), it is clear that the material, with a comparatively low thermal conductivity and high electrical resistivity, will result in a higher cross-sectional area for p- and n-legs. This is a correct definition when considering the electrical circuit and the thermal circuit of a TEG, and can be explained as follows.

When considering the electrical circuit of a TEG, the attainment of a high power output is a primary target. According to the Ohm's law ($V = IR$) and $P = VI$, for a constant potential difference (V), a lower resistance lets

more electrical current (I) to pass and increases the power output (P). The relationship between the electrical resistivity (ρ) and the electrical resistance (R) can be stated as in Equation (5.1), where l is the length of the material and the A is the cross-sectional area. Thus according to the Equation (5.1), to reduce the electrical resistance at a constant length, the cross-sectional area should be increased. Therefore, in terms of the electrical circuit of the TEG, Equation (2.24) provides the correct definition for the p- and n-leg area ratio by increasing the cross-sectional area of the material with higher electrical resistivity.

$$R = \rho \frac{l}{A} \tag{5.1}$$

When considering the thermal circuit of the TEG, the prevention of thermal shortening between the hot and cold side of the TEG is important. According to the Equation (3.2) the rate of heat transferred by conduction ($Q_{cond.}$) will increase with the thermal conductivity and cross-sectional area of the material, at a constant length and temperature difference ($T_h - T_c$) [192]. Hence to remove the thermal shortening effects, the material with the higher thermal conductivity should result in a lower cross-sectional area in TEG. Therefore, in terms of the thermal circuit of the TEG, Equation (2.24) provides the correct definition for the p- and n-leg area ratio by decreasing the cross-sectional area of the material with the higher thermal conductivity.

$$Q_{cond.} = \kappa A \frac{T_h - T_c}{l} \tag{3.2}$$

In contrast to the Ioffe's method, the RCA considers individual p- and n-legs of the unicouple TEG initially, and find the most efficient configuration/reduced current density values for each p- and n-leg. Then RCA match these most efficient individual configurations to obtain the most efficient p- and n-leg area ratio of the TEG. Therefore the area ratio between the p- and n-legs can be stated as Equation (2.51) [51].

$$\frac{A_p}{A_n} = \frac{-J_n}{J_p} = \frac{-\int_{T_c}^{T_h} u_n k_n \, dT}{\int_{T_c}^{T_h} u_p k_p \, dT} \tag{2.51}$$

where, J is the current density, T is the temperature, u is the reduced current density, and subscripts h, c, p, and n represent the hot side, cold side, p-type and n-type respectively.

Here, the definition of the current density is $J = \frac{I}{A}$. The same current passes through the p- and n-legs of the unicouple TEG, but the current density depends on the cross sectional area of the leg. Thus a comparatively higher current density is obtained from the material with the smaller cross-sectional area from p- and n-legs. Moreover according to the Equation (2.51), the material with the comparatively low thermal conductivity and low reduced current density will result in a higher cross-sectional area. According to the Equation (3.2), the material with the higher thermal conductivity should result in a lower cross-sectional area in the TEG to remove the thermal shortening effects. Thus, in terms of the thermal circuit of the TEG, Equation (2.51) provides the correct definition for p- and n-leg area ratio by decreasing the cross-sectional area of the material with higher thermal conductivity. The definition of the reduced current density is $u = \frac{J}{k \nabla T} = \frac{I}{A\, k \nabla T}$, and thus the variation of u value highly depends on all three TE properties of the material and on the operating conditions. However, it can shown that the RCA has given higher cross-sectional area for the material with higher electrical resistivity for p- and n-leg as in Ioffe's method, and a later part of this section this behavior is also shown.

As discussed above, Ioffe's method and RCA using different approaches to obtain the most efficient area ratio for p- and n-legs. Therefore the question arises: are these methods predicting the same most efficient area ratios and power outputs at the same operating conditions? To answer this question, a number of different hypothetical TE materials are formulated and used with the calculations using both Ioffe's method and RCA, under the same operating conditions.

The calculation process is divided into two sections. The first section creates hypothetical p- and n-leg TE materials by varying the TE properties of the materials and combines those materials to generate TEG unicouples. Then the most efficient area ratios are calculated for each TEG unicouple using both Ioffe's method and RCA under the same operating conditions. Later in this section the variations of the most efficient area ratio with the p- and n-leg zT ratios $\left(\frac{zT_p}{zT_n}\right)$ are obtained.

The second section of the calculations develops TEG unicouples in COMSOL, using the most efficient area ratios given by both Ioffe's method and RCA, in the first section of the calculations. These TEG unicouples have the same thermoelement length, the same total thermoelement area, and operate under the same operating conditions. Then the power output and the efficiency for these different TEG unicouples are obtained using COMSOL.

5.1.1 Calculation Section 1

Here, 18 different n-type TE materials are created that have different TE properties under three different sets as shown in Figure 5.1. In each set, only one TE material property has changed whilst keeping the other two TE material properties constant. The only TE material parameter that has changed in Set 1, Set 2, and Set 3 is the thermal conductivity, the electrical resistivity, and the Seebeck coefficient respectively. Under each set, six different n-type TE materials are generated. Temperature independent TE material properties are considered in here for all the calculations.

Then these 18 different n-type TE martials are combined with the same p-type TE material and the generated 18 different TEG unicouples as shown in Figure 5.1. Thus these TEG unicouples possess different p- and n-leg zT ratios $\left(\frac{zT_p}{zT_n}\right)$. Then the most efficient area ratios are calculated for each TEG unicouple using both Ioffe's method and RCA under the same operating conditions and the results are shown in Table 5.1, 5.2, and 5.3 for Set 1, Set 2, and Set 3 respectively. As the initial operating conditions, the hot (T_h) and cold (T_c) side temperatures of 600_K and 300 K are used for all TEG unicouples.

Considering the p- and n-leg TE properties of TEG unicouples TC_4, ER_0.4, and SC_-200, it's clear that these are the same TEG unicouples under three different sets with different names. Thus this similarity gives the opportunity to compare the results of the different sets.

According to Table 5.1, 5.2 and 5.3, the most efficient area ratios given by Ioffe's method and RCA are the same when the both p- and n-leg material have the same TE properties. However, when the p- and n-leg material have different TE properties, the most efficient area ratio given by Ioffe's method and RCA are different. Moreover this difference increases when the difference of the zT value between the p- and n-leg materials increase.

As described above and according to Table 5.1, both Ioffe's method and RCA give a lower cross-sectional area for the material with a higher thermal conductivity for p- and n-legs in a TEG unicouple. As an example, the n-leg of the TE_14 has a higher thermal conductivity than the p-leg. Taking the total cross sectional area of the thermoelements as 1 cm^2 for both Ioffe's method and RCA, then the cross sectional areas given by Ioffe's method for the p- and n-legs are 0.65 cm^2 and 0.35 cm^2 respectively, and the cross sectional areas given by RCA for the p- and n-legs are 0.53 cm^2 and 0.47 cm^2 respectively. Moreover, it can be seen that the material with the higher thermal conductivity (here the n-leg) gives a comparatively high cross-sectional area by the RCA than the Ioffe's method.

As described above and according to Table 5.2, both Ioffe's method and RCA give higher cross-sectional areas for the material with higher electrical resistivity for the p- and n-legs in a TEG unicouple. As an example, the n-leg of the ER_1.4 has higher electrical resistivity than the p-leg. Taking the total cross sectional area of the thermoelements as 1 cm^2 for both Ioffe's method and RCA, then the cross sectional areas given by Ioffe's method for the p- and n-legs are 0.35 cm^2 and 0.65 cm^2 respectively, and the cross sectional areas given by RCA for the p- and n-legs are 0.25 cm^2 and 0.75 cm^2 respectively. Moreover, it can be seen that the material with the higher electrical resistivity (here the n-leg) gives a comparatively high cross-sectional area by the RCA than the Ioffe's method.

According to the Table 5.3, when the thermal conductivity and the electrical resistivity of p- and n-leg TE materials are the same, Ioffe's method gives the same cross-sectional area for both p- and n-legs and does not depend on the Seebeck coefficient of the materials. However, the most efficient area ratio given by RCA is dependent on the Seebeck coefficient, though the thermal conductivity and the electrical resistivity of p- and n-leg TE materials are the same.

According to Table 5.1, 5.2 and 5.3, when comparing the cross-sectional areas of the weaker TE material given by both Ioffe's method and RCA, the RCA gives a comparatively higher cross-sectional area for the weaker TE material than the Ioffe's method. Thus in a TEG architecture, the weaker TE material gets comparatively higher priority in RCA than in Ioffe's method.

Here the work done in the Chapter 3 for temperature dependent TE properties is put in to the context of above behaviour of both the RCA and Ioffe's method. One of the main focuses of ERCA in Chapter 3 is to reduce the priority given by RCA to the weaker TE material in TEG architecture. This is done by reducing the cross-section area of the weaker TE material given by RCA. As described above, the Ioffe's method provides a smaller cross-section area for the weaker TE material than the RCA for temperature independent TE properties. Similarly the concept of the ERCA provides a smaller cross-section area for the weaker TE material than the RCA for temperature dependent TE properties.

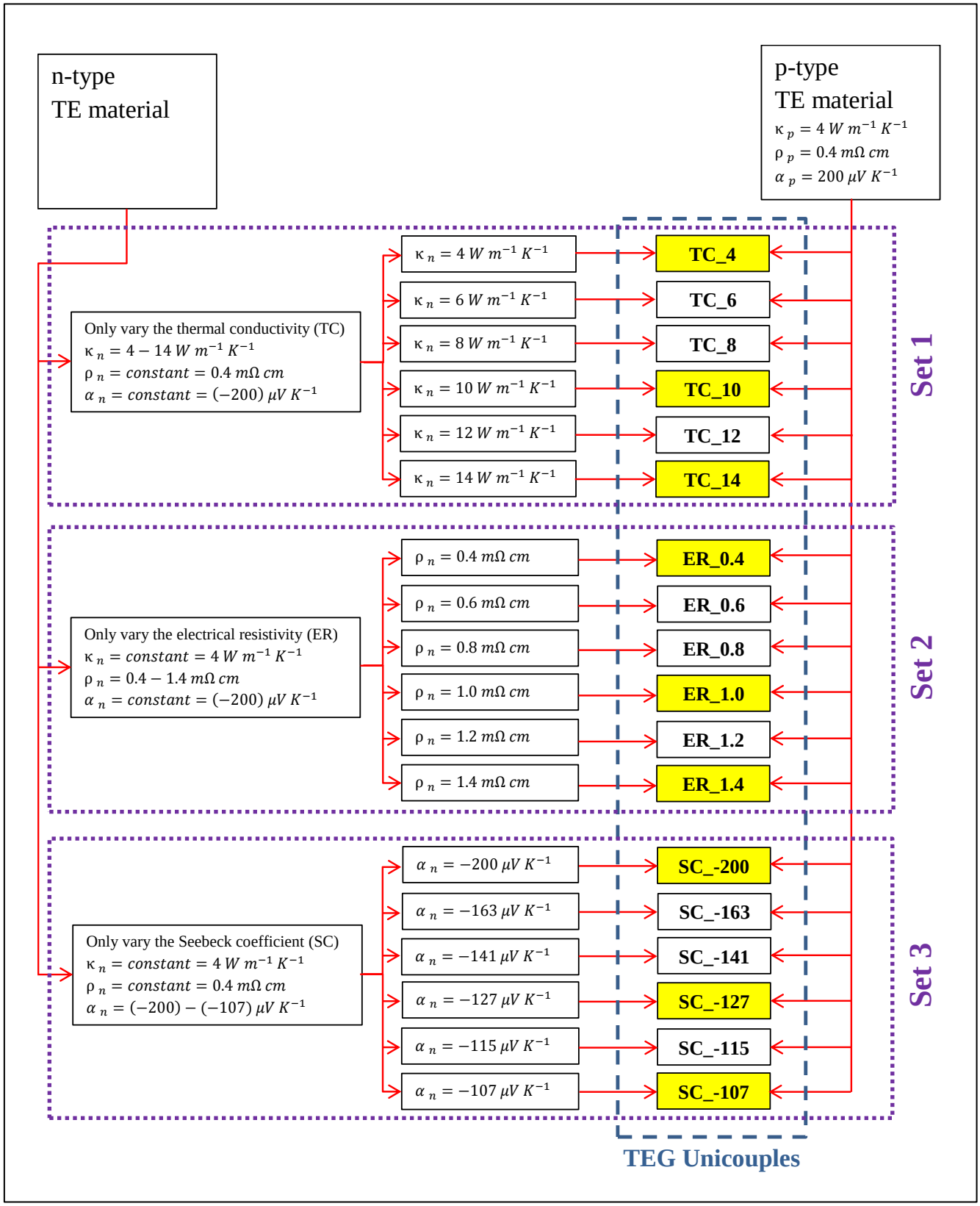

Figure 5.1: Creating different TEG unicouples by combining different n-type TE materials with the same p –type TE material. In "Set 1", only the thermal conductivity (TC) of the n-leg materials is varying and the electrical resistivity (ER) and the Seebeck coefficient (SC) of the n-leg materials are constant at 0.4 mΩ cm and -200 µV/K respectively. In "Set 2", only the ER of the n-leg materials is varying and the TC and the SC of the n-leg materials are constant at 4 W/m·K and -200 µV/K respectively. In "Set 3", only the SC of the n-leg materials is varying and the TC and the ER of the n-leg materials are constant at 4 W/m·K and 0.4 mΩ cm respectively. TEG unicouples are highlighted in yellow colour are used in the section two of the calculations for COMSOL

Table 5.1: variation of the most efficient area ratio of the TEG unicouples in Set 1

Name	Thermal Conductivity (W/m*K)		Electrical Resistivity (mΩ cm)		Seebeck coefficient (μV/K)		zT (at hot side Th=600 K)		zT Ratio $\frac{zT_p}{zT_n}$	Most efficient area ratio $\frac{A_p}{A_n}$		% most efficient $\frac{A_p}{A_n}$ Difference $\frac{(Ioffe-RCA)\%}{RCA}$	Area of the legs (cm^2) when the total area = 1 cm^2			
													Ioffe		RCA	
	p-leg	n-leg	p-leg	n-leg	p-leg	n-leg	p-leg	n-leg		Ioffe	RCA		p-leg	n-leg	p-leg	n-leg
TC_4	4	4	0.4	0.4	200	-200	1.5	1.50	1.0	1.00	1.00	0	0.50	0.50	0.50	0.50
TC_6	4	6	0.4	0.4	200	-200	1.5	1.00	1.5	1.22	1.06	16	0.55	0.45	0.51	0.49
TC_8	4	8	0.4	0.4	200	-200	1.5	0.75	2.0	1.41	1.09	30	0.59	0.41	0.52	0.48
TC_10	4	10	0.4	0.4	200	-200	1.5	0.60	2.5	1.58	1.11	42	0.61	0.39	0.53	0.47
TC_12	4	12	0.4	0.4	200	-200	1.5	0.50	3.0	1.73	1.13	54	0.63	0.37	0.53	0.47
TC_14	4	14	0.4	0.4	200	-200	1.5	0.43	3.5	1.87	1.14	64	0.65	0.35	0.53	0.47

Table 5.2: variation of the most efficient area ratio of the TEG unicouples in Set 2

Name	Thermal Conductivity (W/m*K)		Electrical Resistivity (mΩ cm)		Seebeck coefficient (μV/K)		zT (at hot side Th=600 K)		zT Ratio $\frac{zT_p}{zT_n}$	Most efficient area ratio $\frac{A_p}{A_n}$		% most efficient $\frac{A_p}{A_n}$ Difference $\frac{(Ioffe-RCA)\%}{RCA}$	Area of the legs (cm^2) when the total area = 1 cm^2			
													Ioffe		RCA	
	p-leg	n-leg	p-leg	n-leg	p-leg	n-leg	p-leg	n-leg		Ioffe	RCA		p-leg	n-leg	p-leg	n-leg
ER_0.4	4	4	0.4	0.4	200	-200	1.5	1.50	1.0	1.00	1.00	0	0.50	0.50	0.50	0.50
ER_0.6	4	4	0.4	0.6	200	-200	1.5	1.00	1.5	0.82	0.70	16	0.45	0.55	0.41	0.59
ER_0.8	4	4	0.4	0.8	200	-200	1.5	0.75	2.0	0.71	0.54	30	0.41	0.59	0.35	0.65
ER_1.0	4	4	0.4	1.0	200	-200	1.5	0.60	2.5	0.63	0.44	42	0.39	0.61	0.31	0.69
ER_1.2	4	4	0.4	1.2	200	-200	1.5	0.50	3.0	0.58	0.38	54	0.37	0.63	0.27	0.73
ER_1.4	4	4	0.4	1.4	200	-200	1.5	0.43	3.5	0.53	0.33	64	0.35	0.65	0.25	0.75

Table 5.3: variation of the most efficient area ratio of the TEG unicouples in Set 3

Name	Thermal Conductivity (W/m*K)		Electrical Resistivity (mΩ cm)		Seebeck coefficient (μV/K)		zT (at hot side Th=600 K)		zT Ratio $\frac{zT_p}{zT_n}$	Most efficient area ratio $\frac{A_p}{A_n}$		% most efficient $\frac{A_p}{A_n}$ Difference $\frac{(Ioffe-RCA)\%}{RCA}$	Area of the legs (cm^2) when the total area = 1 cm^2			
													Ioffe		RCA	
	p-leg	n-leg	p-leg	n-leg	p-leg	n-leg	p-leg	n-leg		Ioffe	RCA		p-leg	n-leg	p-leg	n-leg
SC_-200	4	4	0.4	0.4	200	-200	1.5	1.50	1.0	1.00	1.00	0	0.50	0.50	0.50	0.50
SC_-163	4	4	0.4	0.4	200	-163	1.5	1.00	1.5	1.00	0.86	16	0.50	0.50	0.46	0.54
SC_-141	4	4	0.4	0.4	200	-141	1.5	0.75	2.0	1.00	0.77	30	0.50	0.50	0.43	0.57
SC_-127	4	4	0.4	0.4	200	-127	1.5	0.60	2.5	1.00	0.71	42	0.50	0.50	0.41	0.59
SC_-115	4	4	0.4	0.4	200	-115	1.5	0.50	3.0	1.00	0.65	54	0.50	0.50	0.39	0.61
SC_-107	4	4	0.4	0.4	200	-107	1.5	0.43	3.5	1.00	0.61	64	0.50	0.50	0.38	0.62

5.1.2 Calculation Section 2

The second section of the calculations used 9 different TEG unicouples out of the 18 different TEG unicouples that were generated in the first section of the calculations. These selected 9 different TEG unicouples are highlighted in yellow in Figure 5.1.

The criterion for selecting these TEG unicouples is as follows: Three TEG unicouples are selected from each Set; the first TEG unicouple selected has identical p- and n-leg TE properties and the other two have highly different p- and n-leg TE properties. Those selected TEG unicouples are TC_4, TC_10, TC_14 from Set 1; ER_0.4, ER_1.0, ER_1.4 from Set 2; and SC_-200, SC_-127, and SC_-107 from Set 3. However, as stated earlier, TC_4, ER_0.4, and SC_-200 are the same TEG unicouple under three different sets with different names. Therefore in this section, these 3 TEG unicouples are named as B_1 (B_1 ≡ TC_4 ≡ ER_0.4 ≡ SC_-200). Thus 7 different TEG unicouples are considered in this section and those are B_1, TC_10, TC_14, ER_1.0, ER_1.4, SC_-127, and SC_-107.

Then depending on the most efficient area ratios given by Ioffe's method and RCA for these 7 different TEG unicouples, 14 different TEG unicouples are created using COMSOL. The thermoelement length, total thermoelement area, hot side temperature, and cold side temperature of all these 14 different TEG unicouples are kept constant at 2 cm, 1 cm^2, 600 K, and 300 K respectively. Then the internal resistance, power output, heat input at the hot side and the efficiency for these 14 different TEG unicouples are obtained using COMSOL and the results are shown in Figure 5.2.

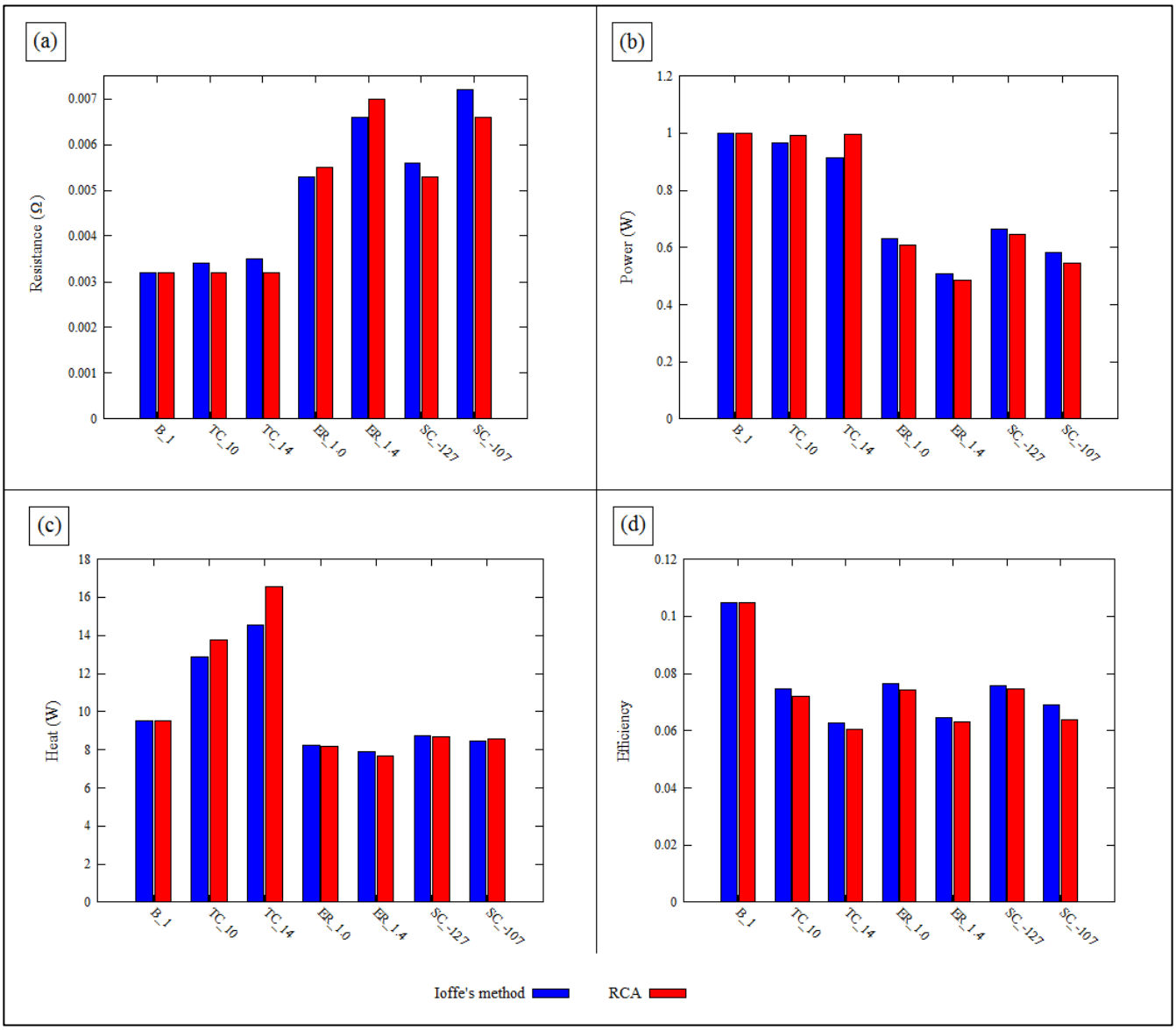

Figure 5.2: The (a) internal resistance, (b) power output, (c) heat input at the hot side, and (d) efficiency of the TEG unicouples B_1, TC_10, TC_14, ER_1.0, ER_1.4, SC_-127, and SC_-107.
(B_1 ≡ TC_4 ≡ ER_0.4 ≡ SC_-200)

According to Figure 5.2, the internal resistance, power output, heat input at the hot side, and efficiency given by Ioffe's method and RCA are almost the same for all the different TEG unicouples, though the heat input at the hot side given by Ioffe's method is a little lower than the RCA for the TEG unicouples TC_10 and TC_14

Therefore, according to Table 5.1 – 5.3 and Figure 5.2, it can concluded that both Ioffe's method and RCA generate TEG unicouples with almost the same power output and efficiency for any p- and n-leg TE material

combination at the same operating conditions; though these two methods do predict different most efficient area ratios for the p- and n-leg depending on the TE material properties. This behaviour is summarized in Figure 5.3.

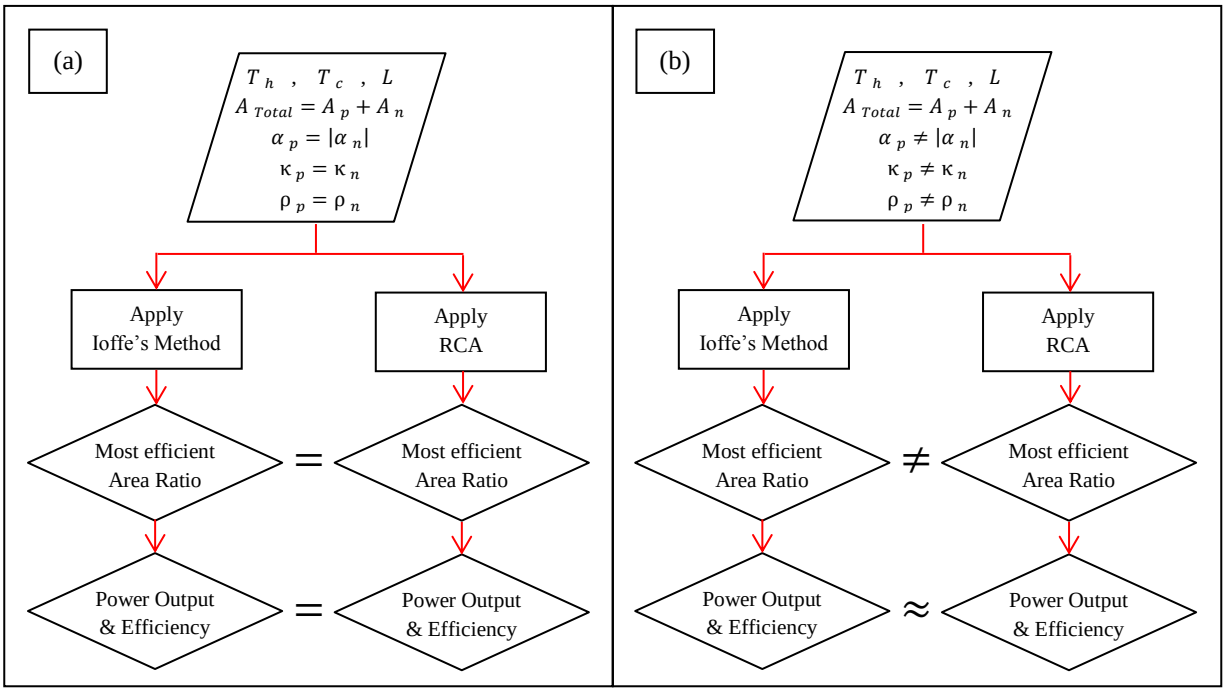

Figure 5.3: Relation between most efficient area ratio, efficiency and power output given by Ioffe's method and RCA for the same material combination and given operating conditions: (a) when the TE properties of the p- and n-legs are the same, (b) when the TE properties of the p- and n-legs are different.

5.1.3 The maximum efficiency of a TEG at different area ratios

The following discusses about the relation between the maximum efficiency predicted by Ioffe's method and RCA for different area ratios of a TEG unicouple. Figure 5.4 represents the value of the maximum efficiency given by Ioffe's method (blue dots) and RCA (red dots) for different p- and n-leg area ratios (A_p/A_n) of a TEG unicouple. P- and n-leg TE materials of TE_14 are used for this TEG unicouple. Thermoelement length, total thermoelement area, hot side temperature and cold side temperature of the TEG unicouple are kept constant at 2 cm, 1cm^2, 600 K and 300 K respectively, for all the cases studied.

According to Figure 5.4, the maximum efficiency predicted by both methods for any p- and n-leg area ratio is almost the same. However, when defining the optimum configuration (the most efficient area ratio and the corresponding efficiency) for a TEG unicouple, Ioffe's method and RCA define different most efficient area ratios, although reaching almost the same efficiency. These optimum configurations for Ioffe's method and RCA are shown in Figure 5.4 as grey and green circles respectively.

According to Figure 5.4, the maximum efficiency curve does not show a sharp peak at any specific A_p/A_n value for both Ioffe's method and RCA; and a range of A_p/A_n values are able to generate almost the same maximum

efficiency of a TEG. The most efficient A_p/A_n values given by Ioffe's method and RCA are at either end of this range of A_p/A_n values. Thus, for this study, when the p-leg has a higher zT value than the n-leg; the RCA and the Ioffe's methods predict the lower and upper limits of this range of A_p/A_n values, that could generate a TEG with the maximum efficiency.

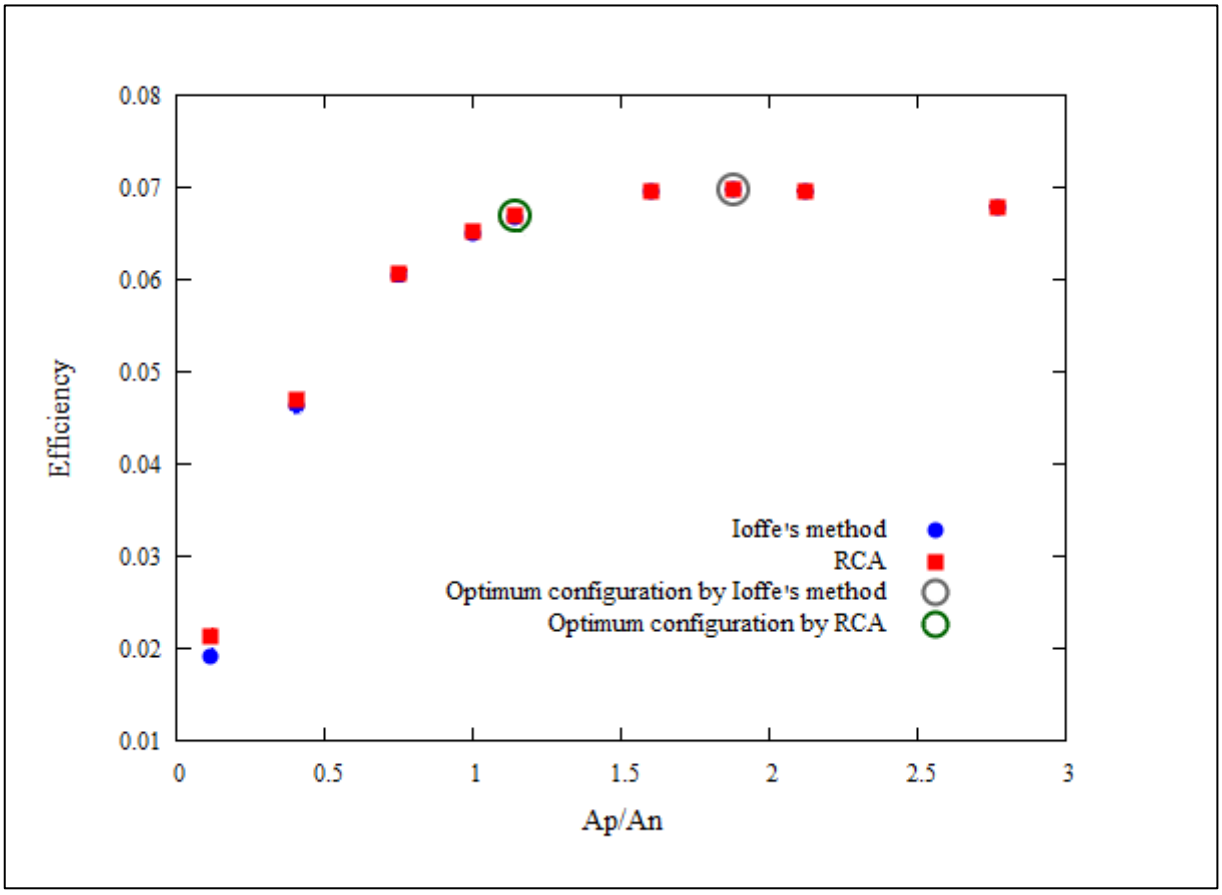

Figure 5.4: The value of maximum efficiency given by the Ioffe's method (blue dots) and RCA (red dots) for different p- and n-leg area ratios (A_p/A_n) of a TEG unicouple. The TEG unicouple is based on the TE materials that used for the TE_14. Thermoelement length, total thermoelement area, hot side temperature and cold side temperature are kept constant for all the cases at 2 cm, 1cm^2, 600 K and 300 K respectively.
The most efficient area ratio and the corresponding efficiency predicted by Ioffe's method (grey circle) and RCA (green circle) for the above TE materials and operating conditions are shown.

Another important consideration is the relation between the maximum efficiency predicted by Ioffe's method and RCA for different area ratios of a TEG, when the zT values of two thermoelements are highly different. The highest zT ratio between two thermoelements of a TEG can be observed in a U-TEG device, when the U-TEG develops by combining a TE material and an idealized metal. A detailed discussion about the U-TEG concept is

included in Chapter 4 of the thesis. Following obtained the relation between the highest efficiency predicted by Ioffe's method and RCA for different area ratios of a U-TEG device with an idealized metal.

Figure 5.5 represents the value of the maximum efficiency given by Ioffe's method (blue dots) and RCA (red dots) for different p-leg and idealized metal area ratios (A_p/A_{idz}) of a U-TEG. TE properties of the p-leg and idealized metal of the U-TEG are shown in Table 5.4. For the idealized metal, the resistivity is taken as 0.002 mΩ cm (this resistivity value is closer to the resistivity of the silver). Due to the high electrical conductivity of the idealized metal, it can be considered that the thermal conductivity of the idealized metal is only depending on the electronic contribution of the thermal conductivity and the lattice contribution of the thermal conductivity is negligible. Thus using the Equation (2.10) [1], the thermal conductivity of the idealized metal is calculated. The Seebeck coefficient of the idealized metal is taken as zero. Thus zero power is generated by the idealized metal. Thermoelement length, total thermoelement area, hot side temperature and cold side temperature of the U-TEG are kept constant at 2 cm, 1cm^2, 600 K and 300 K respectively, for all the cases studied. Under the above operating conditions, the most efficient area ratios given by Ioffe's method and RCA are shown in Table 5.4.

According to Figure 5.5, the maximum efficiency predicted by both methods for any p-leg and idealized metal area ratio is the same. However, when defining the optimum configuration for the U-TEG, Ioffe's method and RCA are defining different most efficient area ratios, although reaching almost the same efficiency. These optimum configurations for Ioffe's method and RCA are shown in Figure 5.5 as grey and green circles respectively.

According to Figure 5.5, the maximum efficiency curve does not show a sharp peak at any specific A_p/A_{idz} value for both Ioffe's method and RCA; and a range of A_p/A_{idz} values are able to generate almost the same maximum efficiency of a U-TEG. The most efficient A_p/A_{idz} values given by Ioffe's method and RCA are at either end of this range of A_p/A_{idz} values. Thus, for this study, the RCA and the Ioffe's methods predict the lower and upper limits of this range of A_p/A_{idz} values, that could generate a U-TEG with maximum efficiency.

Table 5.4: TE properties of the p-leg and idealized metal used to develop the U-TEG in Figure 5.5 and the most efficient area ratios predicted by Ioffe's method and RCA

Name	Thermal Conductivity (W/m*K)		Electrical Resistivity (mΩ cm)		Seebeck coefficient (μV/K)		zT (at hot side Th=600 K)		Most efficient area ratio $\frac{A_p}{A_{idz}}$	
	p leg	Idealized metal	p leg	Idealized metal	p leg	Idealized metal	p leg	Idealized metal	Ioffe	RCA
U-TEG_1	4	732	0.4	0.002	200	0	1.5	0	191	103

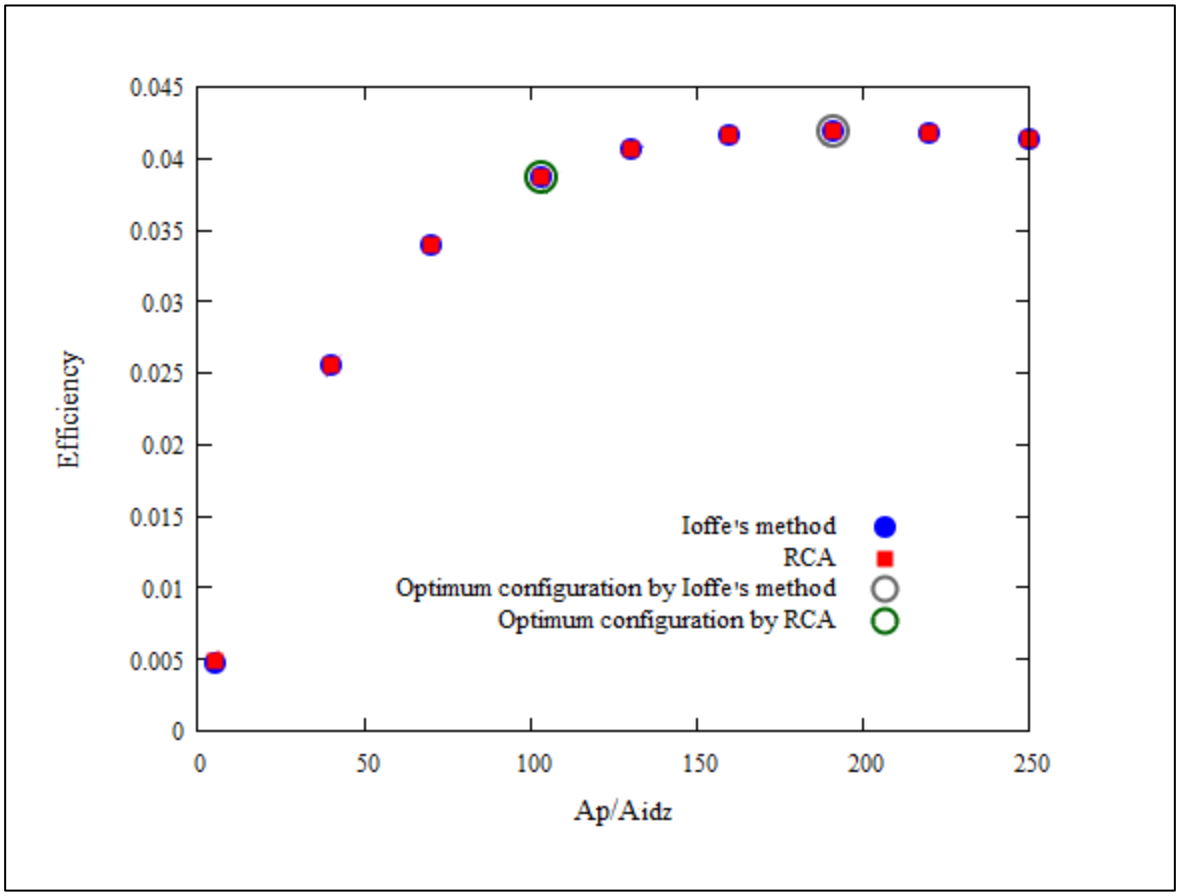

Figure 5.5: The value of maximum efficiency given by the Ioffe's method (blue dots) and RCA (red dots) for different p-leg and idealized metal area ratios (A_p/A_{idz}) of a U-TEG. The TE properties of the U-TEG materials are shown in Table 5.4. Thermoelement length, total thermoelement area, hot side temperature and cold side temperature are kept constant for all the cases at 2 cm, 1cm^2, 600 K and 300 K respectively.
The most efficient area ratio and the corresponding efficiency predicted by Ioffe's method (grey circle) and RCA (green circle) for the above TE materials and operating conditions are shown.

5.2 Cost of a TEG by different TEG design techniques

As explained in the previous section and Figure 5.3, both Ioffe's method and RCA generate TEG unicouples with almost the same power output and efficiency for any TE material combination, for the p- and n-legs at the same operating conditions. However, the most efficient area ratio given by these two methods could be different and it depends on the TE properties of both the p- and n-legs.

Therefore when the length of the p- and n-legs of a TEG unicouple is constant, the amount of a particular TE material used by Ioffe's method is different than the amount of the same TE material used by RCA. Moreover this could be significantly different, as shown in Table 5.1 – 5.3. Thus the above behaviour of these two methods

opens up a great opportunity to reduce the cost-per-Watt of a TEG, by just choosing the appropriate TEG design technique. Generally, the production cost of a p-leg chosen is different to the cost of the n-leg [47]. Therefore the cost-per-Watt of a TEG can be reduced if we could reduce the use of expensive TE material by choosing the appropriate TEG design technique.

Table 5.5 shows the cost-per-Watt for three different TEG unicouple developed from real TE materials [47]. The TEG_1 in Table 5.5 is based on p-type $NaCo_2O_4$ and n-type $Ba_8Ga_{16}Ge_{30}$[199,200]. The TEG_2 in Table 5.5 is based on p-type PbTe with Tl and n-type $Ca_{0.18}Ni_{0.03}Co_{3.97}Sb_{12.4}$ [76,201–203]. The TEG_3 in Table 5.5 is based on p-type $Ca_3Co_4O_9$ and n-type Al-doped ZnO from the OTE-Power project [49,50]. The thermoelement length, total thermoelement area, hot side temperature, and cold side temperature are kept constant for all the TEG unicouples at 0.5 cm, 1 cm^2, 900 K, and 600 K respectively.

Table 5.5: Cost-per-Watt for three different real TEG unicouple by Ioffe's method and RCA

Name	zT (at hot side Th=900 K)		Most efficient area ratio $\frac{A_p}{A_n}$		Area of the legs (cm^2) when the total area = 1 cm^2				Total cost per unicouple ($)		Power output (W)		Efficiency		Cost-per-Watt ($/W)	
					Ioffe		RCA									
	p-leg	n-leg	Ioffe	RCA	p-leg	n-leg	p-leg	n-leg	Ioffe	RCA	Ioffe	RCA	Ioffe	RCA	Ioffe	RCA
TEG_1	0.44	1.35	1.13	1.75	0.53	0.47	0.64	0.36	8.36	6.64	0.54	0.53	0.05	0.05	15.42	12.47
TEG_2	1.54	1.13	5.48	4.92	0.85	0.15	0.83	0.17	1.12	1.11	0.96	0.99	0.07	0.07	1.16	1.12
TEG_3	0.13	0.04	7.47	4.31	0.88	0.12	0.81	0.19	0.76	0.71	0.14	0.16	0.01	0.01	5.44	4.44

According to Table 5.5, using RCA is cheaper for the TEG_1 and RCA saves $ 1.72 per unicouple compared to Ioffe's method. Moreover cost-per-Watt given by RCA is $ 3 cheaper than Ioffe's method. For the TEG_2, the cost per unicouple and the cost-per-Watt given by both RCA and Ioffe's method are almost the same, though RCA is little cheaper. Finally for the TEG_3 which is the TEG developed in the OTE-Power project, cost-per-Watt given by RCA is $ 1 cheaper than Ioffe's method. Therefore it can be concluded that the use of appropriate TEG design technique could reduce the cost-per-Watt of a TEG.

6. A Simple TEG Design Procedure based on RCA

As explained in the previous chapter, RCA [51,52] is an important TEG design technique even for the temperature independent TE properties as well as Ioffe's method [53]. However, RCA is a complex process compared to the Ioffe's method. Due to these difficulties, a broad knowledge about RCA is needed to work with it. Thus a simple engineering design technique is introduced in this chapter for a comprehensive TEG design technique RCA. The proposed method uses an appropriate and straightforward prediction process for the important design parameters and reduces the number of complex and time consuming calculation steps.

A number of design techniques are available to design an optimal TEG [51–55,160]. These techniques could be used to design TEGs with either temperature-dependent TE properties, temperature-independent TE properties or both. In general, comprehensive TEG design techniques provide reliable design parameters, depending on the operational conditions. However, these techniques are complex and time consuming. Therefore, the TEG designer should have a high level of knowledge to work with the technique. Simpler and more reliable versions of these complex techniques would be beneficial to engineers, allowing them to perform their initial predictions about the TEG architecture without performing long and time consuming calculations. Because the majority of TEG applications are focused on implementing TEGs using existing systems, the volume constraint is always a design consideration. To match the TE material properties with the heat input, many detailed, time consuming, and complex calculations are needed. Therefore, a simple version of these complicated designing techniques is needed.

The focus of a TE material scientist is the development of a material with a higher zT, which is a deciding factor in the efficiency of a TEG. However, when that material is at the device stage, some other material properties, such as thermal conductivity matching, thermal expansion, mechanical stress, contact resistance, *etc.*, receive high priority. If material scientists have a fundamental knowledge of TEG design, they may be able to overcome these TEG design considerations in the material stage, which will significantly benefit the final device. Therefore, a simple technique is mutually beneficial to both TEG designers and material scientists.

The RCA is a technique that can be used to define the most efficient TEG architecture for a TEG with either temperature dependent or independent TE material properties [51,52]. However, the calculation process of the RCA consists of a number of time consuming steps, as discussed in Chapter 2. Moreover, the complexity and the extent do not provide a general idea of the TEG architecture in a simple manner. This work has developed a simplified version of the Reduced Current Approach (RCA) proposed by Snyder et al. for the temperature independent TE material properties. There are simple TEG design techniques that focus on temperature independent TE material properties [53,160]. However, when designing a real TEG system, there are a number of engineering constraints that should be considered. Thus, a complete TEG design technique which can accommodate those engineering constraints is needed in the field of TEG design. Moreover, this complete TEG design technique should be a simple technique which is accessible to, not only TEG designers, but also people who do not have a wide knowledge of TEG design. TE material scientists could use this knowledge about TEG system when they design TE materials. Thus they can focus on TEG system requirements, as well as the zT of the material and this will ease the job of the TEG designer.

Thus a simplified version of the RCA to addresses this need is introduced. Moreover it gives direct methods to calculate following important parameters of a TEG system.

- Heat input to the TEG from hot side reservoir and heat output from the TEG to the cold side reservoir
- Cross-sectional areas of each thermoelements
- Length of the thermoelements
- Amount of heat passing through each thermoelement
- Current and voltage generated by the TEG
- When the length of the TEG given as a design constraint, the total heat flux which is needed to operate the TEG at its highest efficiency.

6.1 Approximating the most efficient reduced current density using compatibility factor

This section focuses on obtaining a relationship between the compatibility factor and the most efficient reduced current density of a TE material at particular operating conditions using RCA. A detailed description of RCA is included in Chapter 2. Temperature independent TE material properties are considered in here for all the calculations.

The current density (J) and the reduced current density (u) of a thermoelement can be stated as in Equation (2.35) and (2.36) respectively, when the current passing across a thermoelement is I, and the area of the thermoelement is A.

$$J = \frac{I}{A} \tag{2.35}$$

$$u = \frac{J}{\kappa \nabla T} = \frac{I}{A\,\kappa \nabla T} \tag{2.36}$$

Where $\nabla = \frac{d}{dx}$

The efficiency (η) of a device is shown in Equation (2.21), when the power produced by the system (power output) is P and the amount of heat transfer to the hot side is $H_{total,h}$.

$$\eta = \frac{P}{H_{total,h}} \tag{2.21}$$

Furthermore, the efficiency of a TEG can be explained as a combination of Carnot efficiency (η_{carnot}) and the reduced efficiency (η_r),

$$\eta = \eta_{carnot}\ \eta_r \tag{6.1}$$

$$\eta = \frac{dT}{T}\ \frac{u(\alpha - u\rho\kappa)}{u\alpha + \frac{1}{T}} \tag{6.2}$$

where $\eta_{carnot} = \frac{dT}{T}$, and $\eta_r = \frac{u(\alpha - u\rho\kappa)}{u\alpha + \frac{1}{T}}$.

The changes of the η_r with the u value is analogous to the variation of the power output of a TEG with the current. Thus the reduced efficiency will increase with the u value and reach a maximum and then it will decrease. Therefore the maximum reduced efficiency ($Max\ \eta_r$) can be stated, as in Equation (2.41). Moreover the u value that gives the $Max\ \eta_r$ is define as the compatibility factor (S) and it can be stated as in Equation (2.42) [51].

$$Max\ \eta_r = \frac{\sqrt{1+zT}-1}{\sqrt{1+zT}+1} \tag{2.41}$$

$$s = \frac{\sqrt{1+zT}-1}{\alpha T} \tag{2.42}$$

According to Equation (2.36) and (2.42), both u and S values depend on the temperature. Thus the u values at the hot (u_h) and cold (u_c) sides of a thermoelement are different. Moreover the S values at the hot (S_h) and cold (S_c) sides of a thermoelement are also different. Therefore, the focus here is to find a relationship between the most efficient u value and the compatibility factor of a thermoelement, and this gives rise to the following five different studies; Study A, B, C, D, and E.

A. "Study A" the hot side temperature of a TEG is increased step by step up to 1000 K whilst keeping the cold side at room temperature (300 K) in order to change the temperature difference between the hot and cold sides. TE properties of the p- and n-legs of the TEG are shown in Table 6.1. Then for each individual step the S versus u relationships is obtained.

B. "Study B" the cold side temperature of a TEG is increased step by step from 300 K to 900 K whilst keeping the hot side at 1000 K in order to change temperature difference between the hot and cold sides. The TE properties of the p- and n-legs of the TEG are shown in Table 6.1. Then for each individual step the S versus u relationships is obtained.

C. "Study C" considers the high temperature range and the hot side temperature of a TEG is increased step by step up to 1700 K whilst keeping the cold side at 1000 K in order to change the temperature difference between the hot and cold sides. The TE properties of the p- and n-legs of the TEG are shown in Table 6.1. Then for each individual step the S versus u relationship is obtained.

D. "Study D" the hot side temperature of a TEG is increased step by step from 1000 K to 1700 K whilst keeping a 700 K constant temperature difference between the hot and cold sides. The TE properties of the p- and n-legs of the TEG are shown in Table 6.1. Then for each individual step the S versus u relationships is obtained.

E. "Study E" focuses on the zT variation of a TEG and the TE properties of the materials are changed to obtain a gradual variation of the material zT. The TE properties of the p- and n-legs of the TEG and the corresponding zT at the hot side of the thermoelements are shown in Table 6.2. The hot and cold sides temperatures of the TEG are kept constant at1000 K and 300 K, respectively.

Study A, B and C considers the low, medium, and high temperature applications respectively. The focus of Study D is on the TEGs with high temperature gradients. Study E focuses on the most accessible of zT values of the present-day TEG applications. Thus the above studies represent the most of the possible temperature and zT ranges of present-day TEG applications.

Figure 6.1 shows details of the Study A. Figure 6.1(a) and (b) plot the most efficient reduced current densities at hot (u_{η_h}) and cold (u_{η_c}) sides; and the compatibility factor at the hot (S_h) and cold (S_c) sides for both the p- and n-legs. Moreover, Figure 6.1(c) and (d) plot the relative difference between S_c and u_{η_h}, and the relative difference between S_h and u_{η_c} for the both p- and n-legs. Thus, according to Figure 6.1, S_c is close to u_{η_h} for both p- and n-legs. Moreover, the maximum relative difference between S_c and u_{η_h} is about 1.5% and 0.5% for p- and n-legs respectively and it occurs at 700 K; that is the maximum temperature difference considered between hot and cold sides. Thus it can concluded that, for the Study A, $u_{\eta\_h} \approx S_c$.

Furthermore, according to Figure 6.1, S_h is close to u_{η_c} for both p- and n-legs. Moreover the maximum relative difference between S_h and u_{η_c} is about 2.5% and 1.5% for p- and n-legs respectively and it occurs at 700 K; that is the maximum temperature difference considered between the hot and cold sides. Thus it can concluded that, for the Study A, $u_{\eta\_c} \approx S_h$.

Table 1: Material properties for the Study A, B, C, and D for both p- and n-legs

	Seebeck coefficient (α)	Electrical resistivity (ρ)	Thermal conductivity (κ)
	μV/K	mΩ.cm	W/m.K
p-leg	295.83	0.4	9.92
n-leg	-191.25	1.09	2.74

Table 2: TE material properties used for each step, and the corresponding zT at the hot side of the thermoelement for the Study E

Step	Seebeck coefficient (α) μV/K		Electrical resistivity (ρ) mΩ cm		Thermal conductivity (κ) W/m K		zT at the hot side (T_h = 1000 K)	
	p-leg	n-leg	p-leg	n-leg	p-leg	n-leg	p-leg	n-leg
1	160	-160	6.2	4.0	1.1	2.0	0.38	0.32
2	180	-180	6.6	4.4	1.0	1.9	0.49	0.39
3	200	-200	7.0	4.8	0.9	1.8	0.63	0.46
4	220	-220	7.4	5.2	0.8	1.7	0.82	0.55
5	240	-240	7.8	5.6	0.7	1.6	1.05	0.64
6	260	-260	8.2	6.0	0.6	1.5	1.37	0.75
7	280	-280	8.6	6.4	0.5	1.4	1.82	0.88
8	300	-300	9.0	6.8	0.4	1.3	2.50	1.02

Figure 6.2 shows the relative difference between S_c and u_{η_h}, and the relative difference between S_h and u_{η_c} for the studies B, C, D, and E for both p- and n-legs. According to Figure 6.2(a) and for the Study B, the maximum relative difference between S_c and u_{η_h} is about 1.5% and 0.5% for the p- and n-legs respectively and the difference decreases when the cold side temperature is increased. Furthermore, the maximum relative difference between S_h and u_{η_c} is about 2.5% and 1.5% for the p- and n-legs respectively and the difference decreases when the cold side temperature is increased.

According to the Figure 6.2(b) and for the Study C, the maximum relative difference between S_c and u_{η_h} is about 2% and 1% for the p- and n-legs respectively and the difference increases with the temperature difference. Furthermore, the maximum relative difference between S_h and u_{η_c} is about 2.5% and 1.5% for the p- and n-legs respectively and the difference increases with the temperature difference.

According to the Figure 6.2(c) and for the Study D, the maximum relative difference between S_c and u_{η_h} is about 2% and 1% for the p- and n-legs respectively and it is constant for all the cold side temperatures. Furthermore, the maximum relative difference between S_h and u_{η_c} is about 2.5% and 1.5% for the p- and n-legs respectively and it is constant for all the cold side temperatures.

According to the Figure 6.2(d) and for the Study E, the maximum relative difference between S_c and u_{η_h} is about 1.5% and 0.4% for the p- and n-legs respectively and it occurs at the highest zT value considered. Furthermore, the maximum relative difference between S_h and u_{η_c} is about 3% and 1% for the p- and n-legs respectively and it occurs at the highest zT value considered.

Thus, from Figures 6.1 and 6.2 and the studies A, B, C, D, and E, it can concluded that $u_{\eta\_h} \approx S_c$ and $u_{\eta\_c} \approx S_h$ for most of the possible temperature and zT ranges of present day TEG applications.

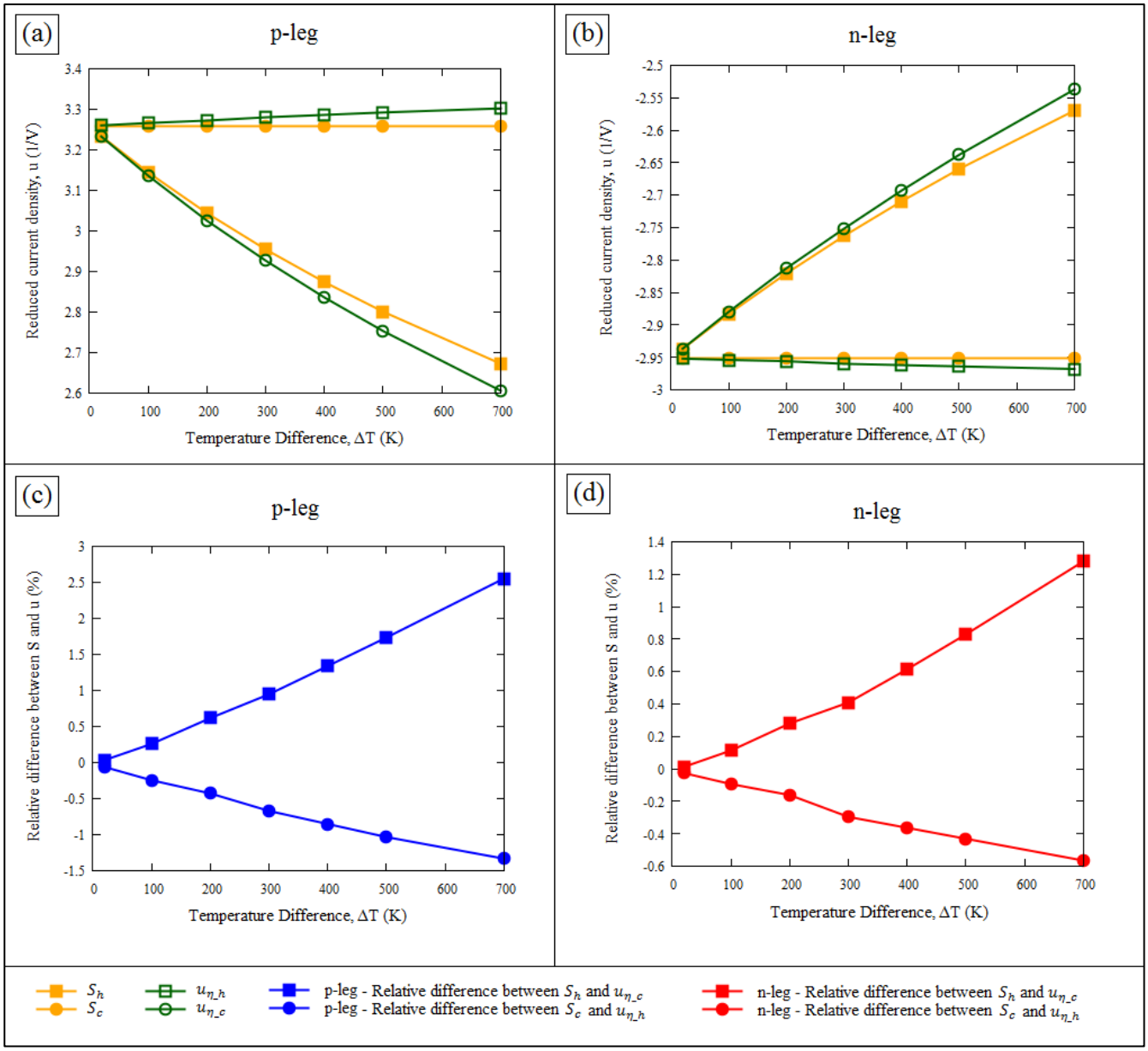

Figurer 6.1: Study A, variation of the temperature different for constant $T_c = 300\ K$: variation of the S_h, S_c, u_{η_h}, and u_{η_c} with temperature different for (a) p-leg, and (b) n-leg. Variation of relative difference between S_c and u_{η_h}, and relative difference between S_h and u_{η_c} with temperature different for (c) p-leg, and (d) n-leg.

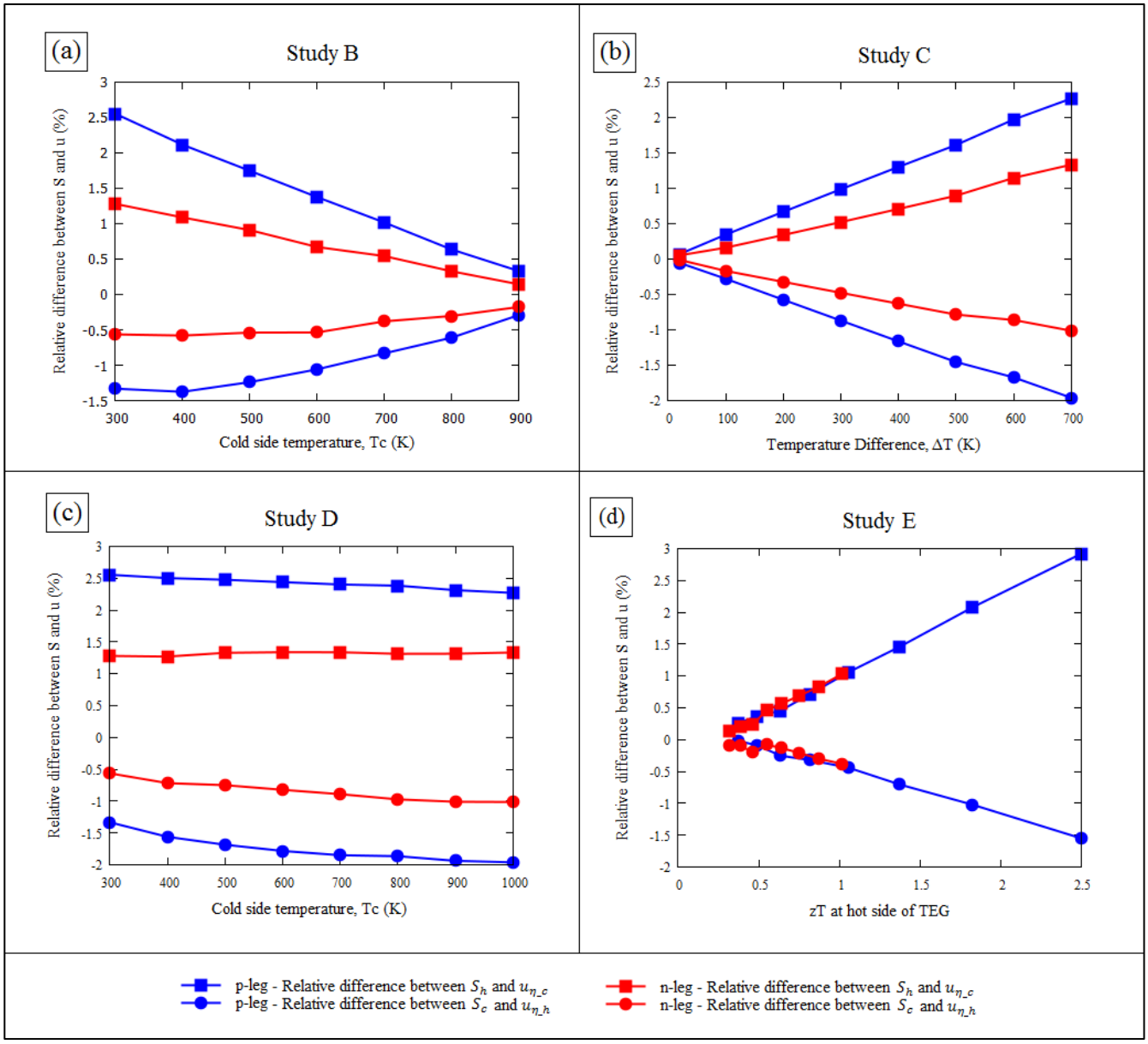

Figurer 6.2: For p- and n-legs; variation of relative difference between S_c and u_{η_h}, and relative difference between S_h and u_{η_c} (a) with cold side temperature for Study B, (b) with temperature different for Study C, (c) with cold side temperature for Study D, (d) with hot side zT for Study E

6.2 Proposed simple TEG design procedure

The proposed TEG design procedure is divided into two subsections. The first subsection of the TEG design procedure is to find the TEG architecture and the outputs, when the α_p, α_n, ρ_p, ρ_n, κ_p, κ_n, T_h, T_c, H_{total}, and A_{total} given as the initial conditions. When the length of the TEG is provided as a design constraint and the α_p, α_n, ρ_p, ρ_n, κ_p, κ_n, T_h, T_c, and A_{total} are given, the second subsection of the method finds the p- and n-leg area ratio and the required heat flux to maintain the TEG at its highest efficiency.

When considering a practical TEG application, T_h, T_c, and H_{total} are not necessarily provided as the input parameters. Most common available parameters are the temperatures of the hot (T_H) and cold (T_C) side reservoirs and the thermal resistance of the hot (Θ_H) and cold (Θ_C) side heat exchangers. Thus T_h, T_c, and H_{total} can be defined as follows.

Here the concept of the thermal resistance matching to the TEG system can be used. Therefore, to obtain the maximum power output, the thermal resistance of the TEG (Θ_{TEG}) should be equal to the total thermal resistance of the heat exchanges (Θ_{EX}) as stated in Equation (6.3) [189,190]. Thus the temperature difference across the TEG (ΔT_{TEG}) should be equal to half of the temperature difference across the heat reservoirs.

$$\Theta_{TEG} = \Theta_{EX} \tag{6.3}$$

$$\Delta T_{TEG} = T_h - T_c = \frac{(T_H - T_C)}{2} \tag{6.4}$$

When the heat rate at the hot and cold side of the TEG are H_H and H_C respectively;

$$T_H - T_h = H_H \Theta_H \tag{6.5}$$

$$T_c - T_C = H_C \Theta_C \tag{6.6}$$

Thus depending on the H_H and H_C, the TEG designer has the freedom to choose the T_h, and T_c.

The first subsection of the TEG design procedure is considered in here. As stated earlier, α_p, α_n, ρ_p, ρ_n, κ_p, κ_n, T_h, T_c, H_{total}, and A_{total} are given as the initial conditions.

As described in the previous section the most efficient reduced current density at the hot and cold side of a thermoelement are as stated as Equations (6.7) and (6.8).

$$u_{\eta\_h} \approx S_c = \frac{\sqrt{1+zT_c}-1}{\alpha T_c} \tag{6.7}$$

$$u_{\eta\_c} \approx S_h = \frac{\sqrt{1+zT_h}-1}{\alpha T_h} \tag{6.8}$$

According to the Equation (2.35) and the same current through the p- and n-legs of the TEG it as stated by Equation (2.50)

$$I = J_p A_p = -J_n A_n, \tag{2.50}$$

By Equation (2.36) (6.7), and (2.50) for both p- and n-legs:

$$I = A_p\, u_{\eta\_h\_p}\, \kappa_p \frac{dT}{dx} = -A_n\, u_{\eta\_h\_n}\, \kappa_n \frac{dT}{dx}\,. \tag{6.9}$$

Thus:

$$\frac{A_p}{A_n} = \frac{-\,u_{\eta\_h\_n}\, \kappa_n \frac{dT}{dx}}{u_{\eta\_h\_p}\, \kappa_p \frac{dT}{dx}}\,.$$

Since both legs are under the same temperature gradient and both the p- and n-legs have same length;

$$\frac{A_p}{A_n} = \frac{-\,u_{\eta\_h\_n}\, \kappa_n}{u_{\eta\_h\_p}\, \kappa_p}\,. \tag{6.10}$$

where the total area of the unicouple is $A_{total} = A_p + A_n$ and

$$A_p = \frac{A_{total}}{1+\frac{A_n}{A_p}}, \tag{2.52}$$

$$A_n = \frac{A_{total}}{1+\frac{A_p}{A_n}}. \tag{2.53}$$

The thermoelectric potential is defined as [51]:

$$\Phi = \alpha T + \frac{1}{u}\,. \tag{2.46}$$

By combining Equation (2.36) and (2.46) we have:

$$\Phi = \alpha T + \frac{\kappa \nabla T}{J}\,. \tag{6.11}$$

The heat flux, Q, through the thermoelement can be defined as the combination of the heat fluxes by conduction and Peltier effect as follows [51]:

$$Q = \alpha T J + \kappa \nabla T. \tag{2.33}$$

By combining Equation (6.11) and (2.33) we have:

$$Q = J\left(\alpha T + \frac{\kappa \nabla T}{J}\right) = J\,\Phi. \tag{6.12}$$

Thus, heat flux at the hot side of the p- and n-legs of the TEG can be stated as follows:

$$Q_p = J_p\, \Phi_{\eta\_h\_p}, \tag{6.13}$$

$$Q_n = J_n\, \Phi_{\eta\_h\_n}. \tag{6.14}$$

By Equation (6.13) and (6.14) we have:

$$\frac{Q_p}{Q_n} = \frac{J_p\,\Phi_{\eta\_h\_p}}{J_n\,\Phi_{\eta\_h\_n}}. \tag{6.15}$$

If the amount of heat which enters the hot side of the TEG is $H_{total,h}$,

$$Q = \frac{H_{total,h}}{A_{total}}. \tag{6.16}$$

Thus, by Equation (2.50), (6.15) and (6.16),

$$\frac{H_p}{H_n} = \frac{-\Phi_{\eta\_h\_p}}{\Phi_{\eta\_h\_n}}. \tag{6.17}$$

When $H_{total,h} = H_p + H_n$

$$H_p = \frac{H_{total,h}}{1+\frac{H_n}{H_p}}, \tag{6.18}$$

$$H_n = \frac{H_{total,h}}{1+\frac{H_p}{H_n}}. \tag{6.19}$$

Therefore, by Equation (2.52), (2.53), (6.11), (6.18) and (6.19) we have:

$$J_p = \frac{H_p}{A_p\,\Phi_{\eta\_h\_p}} \tag{6.20}$$

$$J_n = \frac{H_n}{A_n\,\Phi_{\eta\_h\_n}} \tag{6.21}$$

For a uniform cross-sectional area, the thermoelement length can be calculated as [51]:

$$l = \frac{1}{J_p}\int_{T_c}^{T_h} u_p k_p dT = \frac{1}{J_n}\int_{T_c}^{T_h} u_n k_n dT \tag{2.49}$$

Thus, since the both p- and n-legs have the same length, the length of the thermoelements can be stated as [51]:

$$l = \frac{\left(u_{\eta\_h\_p}+u_{\eta\_c\_p}\right)}{2}\,\frac{\kappa_p\,dT}{J_p}. \tag{6.22}$$

The current through the TEG can be calculated using Equation (2.50), (2.52) and (6.20).

The TE potential difference is given by:

$$\Delta\Phi = \left[(\alpha T)_h + \frac{1}{u_{\eta\_h}}\right] - \left[(\alpha T)_c + \frac{1}{u_{\eta\_c}}\right]. \tag{6.23}$$

Thus the output voltage is;

$$\Delta V = \Delta\Phi_p - \Delta\Phi_n. \tag{6.24}$$

The second subsection of the TEG design procedure is as follows. As stated earlier, l, α_p, α_n, ρ_p, ρ_n, κ_p, κ_n, T_h, T_c, and $A_{total}$are given as the initial conditions.

According to Equation (6.10), (2.52), and (2.53), the most efficient p- and n-leg area ratios can be calculated. Thus, by using Equation (6.22), the current densities of p- and n-legs can be calculated as follows.

$$J_p = \frac{(u_{\eta\_h\_p} + u_{\eta\_c\_p})}{2} \frac{\kappa_p \, dT}{l}, \tag{6.25}$$

$$J_n = \frac{(u_{\eta\_h\_n} + u_{\eta\_c\_n})}{2} \frac{\kappa_n \, dT}{l}. \tag{6.26}$$

Thus $H_{total,h}$ can be calculated using Equation (6.20), (6.21), (6.25), (6.26) and $H_{total} = H_p + H_n$.

Therefore the total heat flux that is needed to operate the TEG at its highest efficiency is:

$$Q_{total} = \frac{H_{total,h}}{A_{total}}. \tag{6.27}$$

6.3 Predictability of the proposed TEG design procedure

This section discusses the accuracy of the predictions of the proposed method compared to RCA. In here, the word "predictability" is used to illustrate the degree of agreement of the proposed method with the RCA. Figure 6.3 illustrates the predictability of the TEG architecture given by the proposed method compared to the RCA for the studies A, B, C, D, and E. Thus the proposed method could predict the thermoelement length of the TEG with more than 98% predictability and the area of the thermoelements with more than 97% predictability.

When considering the studies A, B, and C in the Figure 6.3(a), 6.3(b), and 6.3(c), the predictability of the TEG architecture is reduced, when the temperature difference between hot and cold side is increased. This can be explained as follows. When it was assumed that the value of the compatibility factor is approximately equal to the value of most efficient reduced current density in Section 6.1, the contributions of the Carnot term to the total efficiency was simply omitted. As in Equation (6.2), at large temperature gradients, the Carnot term has a greater contribution to the total efficiency. Thus the predictability of the above assumption decreases at large temperature differences. Therefore, as in Figure 6.3(a), 6.3(b), and 6.3(c), the predictability of the TEG architecture is decreased, when the temperature difference between hot and cold sides is increased.

For the Study D, as shown in the Figure 6.3(d), the predictability of the TEG architecture increases when increasing the cold side temperature at a constant temperature difference. As explained above, this is also due to the Carnot efficiency. According to Equation (6.2) the contribution of the Carnot efficiency to the total efficiency decreases, when increasing the cold side temperature at a constant temperature difference. According to the Figure 6.3(e), the predictability of the TEG architecture given by the proposed method decreases with the average zT of the TEG. However, it is more than 97% predictable for the present day TEG applications.

Therefore for all the possible temperature and zT ranges pertaining in present day thermoelectrics, the proposed method can predict the TEG architecture with a high predictability.

Figure 6.4 shows the predictability of the current, TE potential difference, and power output for the studies A, B, C, D, and E given by the proposed method compared to RCA. For all the studies the current can be predicted with more than 99% predictability. However, the maximum predictability given by the TE potential difference is 96% and the predictability of the TE potential difference is in the range of 88–96%. This is due to the difference between the approximate most efficient u value (S) and the real most efficient u value (u_η). When calculating the final TE potential difference using Equation (6.23) and (6.24), the difference between u_η and S values at both hot and cold side of the p- and n-legs are summed. Thus the predictability of the TE potential given by the proposed method it reduced.

Power output also shows the same behavior as the TE potential difference, due to the power output is obtained by multiplying the TE potential difference by the current, and the current is almost 100% predictable compared to RCA. Thus this behavior of the power output is solely attributable to the TE potential difference.

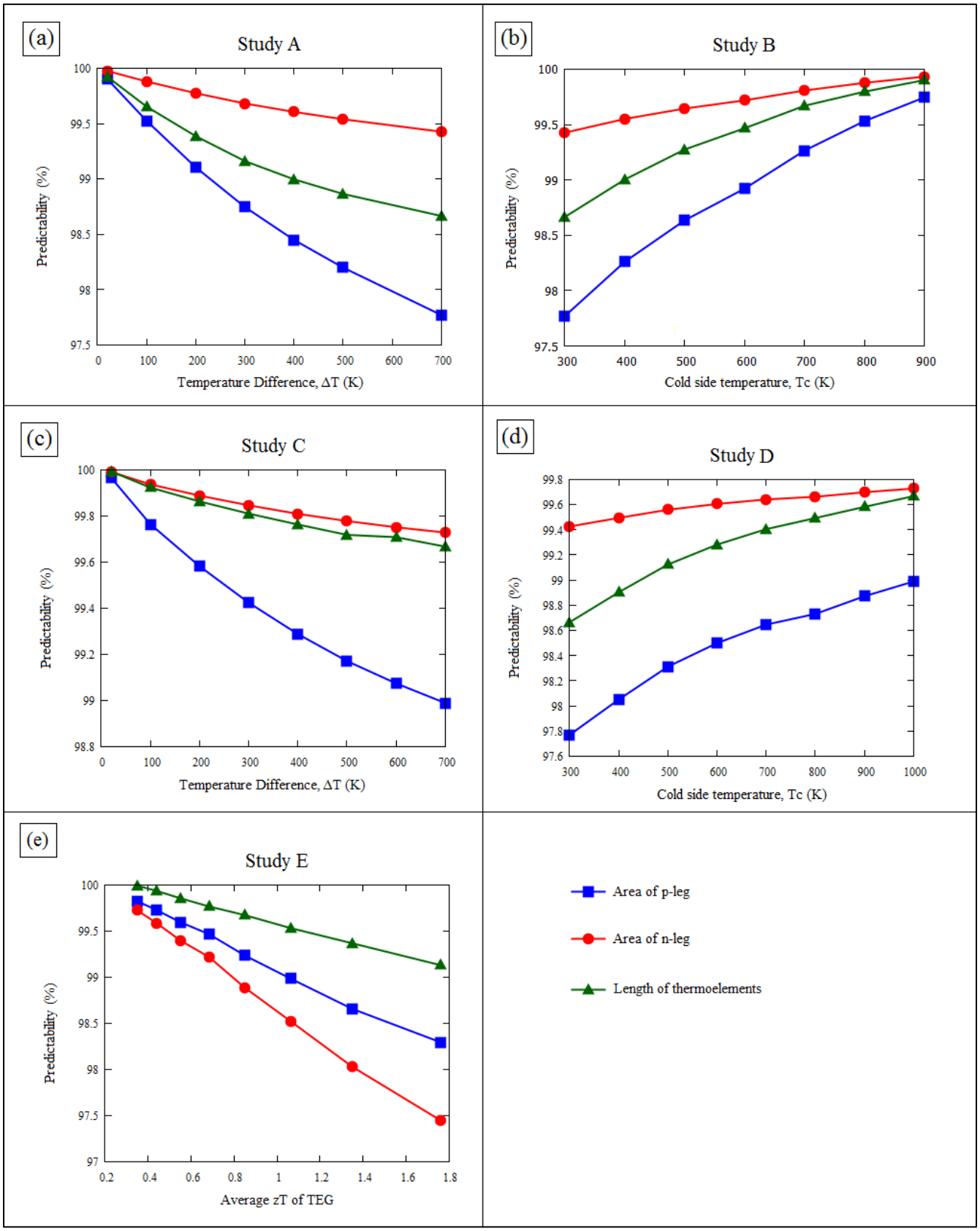

Figurer 6.3: Predictability of the TEG architecture by the new method comparing to the RCA for (a) Study A, (b) Study B, (c) Study C, (d) Study D, and (e) Study E

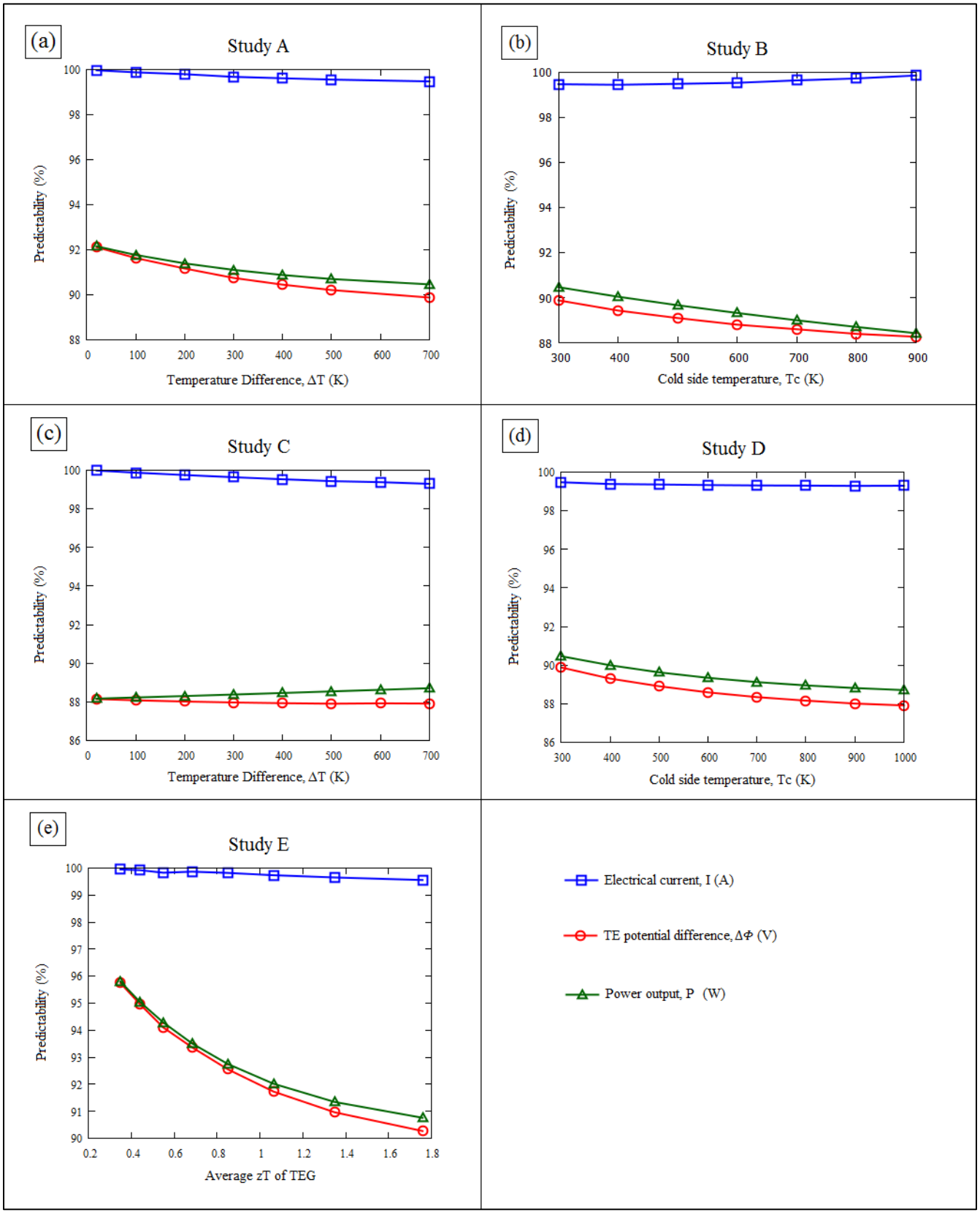

Figurer 6.4: Predictability of the TEG outputs by the new method comparing to the RCA for (a) Study A, (b) Study B, (c) Study C, (d) Study D, and (e) Study E

7. Conclusions

This PhD project focused on the development of a TEG design technique for high-temperature applications (about > 700 °C) using oxide TE materials. Furthermore the project focused on increasing the Volumetric Power Density (VPD) and reducing the cost-per-Watt of a TEG device. Since the project focuses on Oxide TE materials, one major challenge identified is that the p- and n-type oxide TE materials do not perform (zT values) at the same level. Thus, the TEG design technique proposed in this project should address this question in an appropriate manner. The project used an engineering approach to work with existing TEG design techniques and optimize those techniques to address the above question.

The project successfully managed to produce a TEG design technique whilst altering the well-known Reduced Current Approach (RCA) TEG design technique. This new method is appropriate for TE material combinations that have different performance levels (or zT values) to produce TEGs with higher volumetric power densities. This technique was called the Extended Reduced Current Approach (ERCA). For the TE materials used in the OTE-Power project (p-type $Ca_3Co_4O_9$ and n-type Al-doped ZnO), the ERCA managed to increase the VPD of the TEG by 42% when compared to the VPD given by the RCA. Thus this will reduce the cost-per-Watt of the TEG device produced under the OTE-Power project.

One of the main arguments in the TEG designing process is determining what should be the main focus when designing a TEG: is it efficiency or power output? So far, the answer has been at either extreme; some researchers vote for efficiency and others for power output. However, this project provides another viewpoint based on the RCA and ERCA. That is, at particular operating conditions, if the TE performances (or zT values) of two p- and n-type thermoelements in a TEG are compatible; the TEG design should focus on efficiency. However, at particular operating conditions, if the TE performances (or zT values) of two p- and n-type thermoelements in a TEG are not comparable; the TEG design should focus on power output.

This PhD project also focused on further solutions for the above question about thermoelectrically mismatched materials by replacing the weaker TE material with a conductor. This concept is called the Unileg-TEG (U-TEG) concept. One of the biggest issues when doing this replacement is the control of the heat flux through the conductor and the control over the potential thermal shortening effects, between the hot and cold side of the U-TEG. This control can be achieved by using an appropriate area ratio for the two legs. Thus, for the OTE-Power project, the n-type Al-doped ZnO in the conventional unicouple TEG design is replaced by Constantan. This U-TEG consisting of $Ca_3Co_4O_9$ and Constantan produces 65% more power and a 144% higher VPD than the conventional unicouple TEG design using $Ca_3Co_4O_9$ and Al-doped ZnO. This project further generalized this method using an idealized metal as the conductor in the U-TEG design. The U-TEG design with $Ca_3Co_4O_9$ and an idealized metal still managed to produce a higher volumetric power density than the conventional unicouple TEG design consisting of $Ca_3Co_4O_9$ and Al-doped ZnO. This U-TEG concept provides a valuable addition to the TEG design by reducing, by a half, the number of metal/semiconductor contacts in a conventional unicouple TEG. This result is a significant contribution to the reduction of the thermal and electrical contact resistance a TEG.

Furthermore, the PhD project focused on different TEG design techniques and their cost effectiveness. When considering Ioffe's method and RCA for the temperature independent TE properties, this PhD project showed

that both methods produce TEGs with same efficiency and power output at particular operating conditions, though the two methods do predict different most efficient area ratios for the p- and n-legs of the TEG. Therefore by just choosing the appropriate TEG design technique which gives the higher dominancy for the cheaper TE material, the cost-per-Watt of the TEG device could be reduced.

A simple TEG design technique based on RCA is proposed by this PhD project for TEGs with temperature-independent TE material properties. This new technique is a simplified version of the complex, time-consuming, and comprehensive RCA TEG design technique. This new technique is a straightforward technique to predict the architecture of a TEG with greater than 97% predictability when compared to the TEG architecture given by the RCA.

8. Future Work

Balancing the thermal and electrical circuits of a TEG is one of the main focuses of most of the present TEG design techniques. Although it is important to obtain a TEG with a higher power output and higher efficiency, a durable TEG design is also important. Because a TEG is a combination of semiconductors, conductors, and ceramics and works under considerable temperature gradients, the thermomechanical behaviour of the materials has a considerable influence on the mechanical stability of the TEG. Thus, it is important to have precise knowledge about the thermomechanical properties of the materials and their influences on the final TEG design. Therefore, future work could focus on the thermomechanical behaviour of the TEG design. Obtaining higher mechanical strengths in the contact areas of these different materials could enhance the electrical contact resistance at those joints. Therefore, when considering high mechanical stability, care should be taken with respect to the electrical contact resistance.

When focusing on high-temperature TEG applications, interleg radiation heat transfer could have an influence on the final temperature profile of a TEG. This influence should be considered as the subject of another future study. The interleg distance of a TEG is influenced by the thermal expansion of the TE materials. If the materials experience large thermal expansions, then at high temperatures, the thermoelements on the hot side of the TEG will have a smaller distance in between them than the cold side. At this point, the effects of radiative heat transfer could have an influence on the temperature profile of a thermoelement.

9. References

[1] Snyder GJ, Toberer ES. Complex thermoelectric materials. Nat Mater 2008;7:105–14. doi:10.1038/nmat2090.

[2] Rowe DM. General Principles and Basic Considerations. Thermoelectr. Handb. Macro to Nano, Boca Raton, USA: Taylor & Francis Group; 2006, p. 1–1 – 1–15.

[3] Snyder GJ. Small Thermoelectric Generators. Interface - Electrochem Soc 2008;17:54–6.

[4] Kim SJ, We JH, Cho BJ. A wearable thermoelectric generator fabricated on a glass fabric. Energy Environ Sci 2014;7:1959. doi:10.1039/c4ee00242c.

[5] Telkes M. Solar thermoelectric generators. J Appl Phys 1954;25:765–77. doi:10.1063/1.1721728.

[6] Goldsmid HJ, Giutronich JE, Kaila MM. Solar thermoelectric generation using bismuth telluride alloys. Sol Energy 1979;24:435–40.

[7] DURST T, HARRIS LB, GOLDSMID HJ. Studies of a thermoelectric generator operating from tubular solar collectors. Sol Eaergy 1983;31:421–5. doi:10.1016/s0379-0738(01)00508-4.

[8] Kugele R, Roth W, Schulz W, Steinhuser A. Thermoelectric generators in photovoltaic hybrid systems. 15th Int Conf Thermoelectr Proc ICT '96 1996:352–6. doi:10.1109/ICT.1996.553505.

[9] Naito H, Kohsaka Y, Cooke D, Arashi H. Development of a solar receiver for a high-efficiency thermionic/thermoelectric conversion system. Sol Energy 1996;58:191–5. doi:10.1016/S0038-092X(96)00084-9.

[10] Omer SA, Infield DG. Design optimization of thermoelectric devices for solar power generation. Sol Energy Mater Sol Cells 1998;53:67–82. doi:10.1016/S0927-0248(98)00008-7.

[11] Rockendorf G, Sillmann R, Podlowski L, Litzenburger B. PV-hybrid and thermoelectric collectors. Sol Energy 1999;67:227–37. doi:10.1016/S0038-092X(00)00075-X.

[12] Omer SA, Infield DG. Design and thermal analysis of a two stage solar concentrator for combined heat and thermoelectric power generation. Energy Convers Manag 2000;41:737–56. doi:10.1016/S0140-6701(00)93184-9.

[13] Maneewan S, Khedari J, Zeghmati B, Hirunlabh J, Eakburanawat J. Investigation on generated power of thermoelectric roof solar collector. Renew Energy 2004;29:743–52. doi:10.1016/j.renene.2003.10.005.

[14] Maneewan S, Hirunlabh J, Khedari J, Zeghmati B, Teekasap S. Heat gain reduction by means of thermoelectric roof solar collector. Sol Energy 2005;78:495–503. doi:10.1016/j.solener.2004.08.003.

[15] Khattab NM, El Shenawy ET. Optimal operation of thermoelectric cooler driven by solar thermoelectric generator. Energy Convers Manag 2006;47:407–26. doi:10.1016/j.enconman.2005.04.011.

[16] Crabtree GW, Lewis NS. Solar energy conversion. Phys Today 2007;60:37–42. doi:10.1063/1.2718755.

[17] Lertsatitthanakorn C, Khasee N, Atthajariyakul S, Soponronnarit S, Therdyothin a., Suzuki RO. Performance analysis of a double-pass thermoelectric solar air collector. Sol Energy Mater Sol Cells 2008;92:1105–9. doi:10.1016/j.solmat.2008.03.018.

[18] Tritt TM, Böttner H, Chen L. Thermoelectrics: Direct Solar Thermal Energy Conversion. MRS Bull 2008;33:366–8. doi:10.1557/mrs2008.73.

[19] Rodríguez a., Vián JG, Astrain D, Martínez a. Study of thermoelectric systems applied to electric power generation. Energy Convers Manag 2009;50:1236–43. doi:10.1016/j.enconman.2009.01.036.

[20] Deng Y, Zhu W, Wang Y, Shi Y. Enhanced performance of solar-driven photovoltaic–thermoelectric hybrid system in an integrated design. Sol Energy 2013;88:182–91. doi:10.1016/j.solener.2012.12.002.

[21] Vorobiev Y, González-Hernández J, Vorobiev P, Bulat L. Thermal-photovoltaic solar hybrid system for efficient solar energy conversion. Sol Energy 2006;80:170–6. doi:10.1016/j.solener.2005.04.022.

[22] Lin W, Shih T-M, Zheng J-C, Zhang Y, Chen J. Coupling of temperatures and power outputs in hybrid photovoltaic and thermoelectric modules. Int J Heat Mass Transf 2014;74:121–7. doi:10.1016/j.ijheatmasstransfer.2014.02.075.

[23] Fisac M, Villasevil FX, López AM. High-efficiency photovoltaic technology including thermoelectric generation. J Power Sources 2014;252:264–9. doi:10.1016/j.jpowsour.2013.11.121.

[24] Liao T, Lin B, Yang Z. Performance characteristics of a low concentrated photovoltaic–thermoelectric hybrid power generation device. Int J Therm Sci 2014;77:158–64. doi:10.1016/j.ijthermalsci.2013.10.013.

[25] Sark WGJHM Van. Feasibility of photovoltaic – Thermoelectric hybrid modules. Appl Energy 2011;88:2785–90. doi:10.1016/j.apenergy.2011.02.008.

[26] Killander A, Bass JC. A Stove-top Generator For Cold Areas. 15th Int. Conf. Thermoelectr. 1996, n.d., p. 390–3.

[27] Nuwayhid RY, Shihadeh A, Ghaddar N. Development and testing of a domestic woodstove thermoelectric generator with natural convection cooling. Energy Convers Manag 2005;46:1631–43. doi:10.1016/j.enconman.2004.07.006.

[28] Moser W, Friedl G, Haslinger W, Hofbauer H. Small-Scale Pellet Boiler with Thermoelectric Generator. 25th Int. Conf. Thermoelectr. 2006, IEEE; 2006, p. 349–53. doi:10.1109/ICT.2006.331221.

[29] Lertsatitthanakorn C. Electrical performance analysis and economic evaluation of combined biomass cook stove thermoelectric (BITE) generator. Bioresour Technol 2007;98:1670–4. doi:10.1016/j.biortech.2006.05.048.

[30] Qiu K, Hayden ACS. Development of a thermoelectric selef-powered residential heating system.pdf. J Power Sources 2008;180:884–9. doi:10.1016/j.jpowsour.2008.02.073.

[31] Vican J, Gajdeczko BF, Dryer FL, Milius DL, Aksay I a., Yetter R a. Development of a microreactor as a thermal source for microelectromechanical systems power generation. Proc Combust Inst 2002;29:909–16. doi:10.1016/S1540-7489(02)80115-8.

[32] Funahashi R, Mihara T, Mikami M, Urata S, Ando N. Power generation of thermoelectric oxide modules. 24th Int Conf Thermoelectr ICT, Proc 2005;2005:295–302. doi:10.1109/ICT.2005.1519947.

[33] Posthill J, Reddy A, Siivola E, Krueger G, Mantini M, Thomas P, et al. Portable power sources using combustion of butane and thermoelectrics. 24th Int Conf Thermoelectr ICT, Proc 2005:520–3. doi:10.1109/ICT.2005.1520000.

[34] Yoshida K, Tanaka S, Tomonari S, Satoh D, Esashi M. High-energy density miniature thermoelectric generator using catalytic combustion. J Microelectromechanical Syst 2006;15:195–203. doi:10.1109/JMEMS.2005.859202.

[35] Smith CWS, Newton CM, Gassman R. Fuel Flexible thermoelectric micro-generator. Pub. No.: US 2006/0027258 A1, 2006.

[36] Federici J a., Norton DG, Brüggemann T, Voit KW, Wetzel ED, Vlachos DG. Catalytic microcombustors with integrated thermoelectric elements for portable power production. J Power Sources 2006;161:1469–78. doi:10.1016/j.jpowsour.2006.06.042.

[37] Karim a. M, Federici J a., Vlachos DG. Portable power production from methanol in an integrated thermoeletric/microreactor system. J Power Sources 2008;179:113–20. doi:10.1016/j.jpowsour.2007.12.119.

[38] Katsuki F, Tomida T, Nakatani H, Katoh M, Takata A. Development of a thermoelectric power generation system using reciprocating flow combustion in a porous FeSi2 element. Rev Sci Instrum 2001;72:3996–9. doi:10.1063/1.1405797.

[39] Adam C, Paul R, Uri F, Lars S, Eckart M, Steffen W. Microcombustor and combustion-based thermoelectric microgenerator, 2002.

[40] Crane D, Lagrandeur J, Jovovic V, Ranalli M, Adldinger M, Poliquin E, et al. TEG on-vehicle performance and model validation and what it means for further teg development. J Electron Mater 2013;42:1582–91. doi:10.1007/s11664-012-2327-8.

[41] Diuguid CA. GMZ Energy successfully demonstrates 1 kW thermoelectric generator for Bradley Fighting Vehicle n.d.

[42] Energy.gov. Could TEG Improve Your Car's Efficiency? n.d.

[43] GMZ Energy n.d. http://gmzenergy.com/applications/ (accessed January 27, 2015).

[44] Ota T, Tokunaga C, Fujita K. Development of thermoelectric power generation system for industrial furnaces. 25th Int Conf Thermoelectr 2006, ICT, Proc 2006:354–7. doi:10.1109/ICT.2006.331253.

[45] Auckland DW, Shuttleworth R, Luff AC, Axcell BP, Rahman M. Design of a semiconductor thermoelectric generator for remote subsea wellheads. IEE Proc - Electr Power Appl 1995;142:65–70. doi:10.1049/ip-epa:19951707.

[46] Caltech-Thermoelectrics. Brief History of Thermoelectrics 2014. http://www.thermoelectrics.caltech.edu/thermoelectrics/history.html (accessed September 28, 2014).

[47] Yadav GG, Susoreny J a, Zhang G, Yang H, Wu Y. Nanostructure-based thermoelectric conversion: an insight into the feasibility and sustainability for large-scale deployment. Nanoscale 2011;3:3555–62. doi:10.1039/c1nr10555h.

[48] Hung LT, Van Nong N, Linderoth S, Pryds N. Segmentation of low-cost high efficiency oxide-based thermoelectric materials. Phys Status Solidi 2015;8:n/a – n/a. doi:10.1002/pssa.201431626.

[49] Wu N, Holgate TC, Van Nong N, Pryds N, Linderoth S. Effects of Synthesis and Spark Plasma Sintering Conditions on the Thermoelectric Properties of Ca3Co4O9+δ. J Electron Mater 2013;42:2134–42. doi:10.1007/s11664-013-2546-7.

[50] Han L, Hung LT, van Nong N, Pryds N, Linderoth S. The Influence of Spark Plasma Sintering Temperature on the Microstructure and Thermoelectric Properties of Al,Ga Dual-Doped ZnO. J Electron Mater 2012;42:1573–81. doi:10.1007/s11664-012-2325-x.

[51] Snyder GJ. Thermoelectric Power Generation: Efficiency and Compatibility. Thermoelectr. Handb. Macro to Nano, Boca Raton, USA: Taylor & Francis Group; 2006, p. 9–1 – 9–26.

[52] Snyder G, Ursell T. Thermoelectric Efficiency and Compatibility. Phys Rev Lett 2003;91:148301. doi:10.1103/PhysRevLett.91.148301.

[53] Ioffe AF. Semiconductor thermoelements and thermoelectric cooling. London: Infosearch Ltd.; 1957.

[54] Min G. Thermoelectric Module Design Theories. Thermoelectr. Handb. Macro to Nano, Boca Raton, USA: Taylor & Francis Group; 2006, p. 11–1 – 11–5.

[55] Rowe DM, Min G. Design theory of thermoelectric modules for electrical power generation. IEE Proc - Sci Meas Technol 1996;143:351–6. doi:10.1049/ip-smt:19960714.

[56] Nemoto T, Iida T, Sato J, Sakamoto T, Hirayama N, Nakajima T, et al. Development of an Mg2Si Unileg Thermoelectric Module Using Durable Sb-Doped Mg2Si Legs. J Electron Mater 2013;42:2192–7. doi:10.1007/s11664-013-2569-0.

[57] Madan D, Chen A, Wright PK, Evans JW. Printed Se-Doped MA n-Type Bi2Te3 Thick-Film Thermoelectric Generators. J Electron Mater 2012;41:1481–6. doi:10.1007/s11664-011-1885-5.

[58] Madan D, Wang Z, Chen A, Juang R-C, Keist J, Wright PK, et al. Enhanced performance of dispenser printed MA n-type Bi_2 Te_3 composite thermoelectric generators. ACS Appl Mater Interfaces 2012;4:6117–24. doi:10.1021/am301759a.

[59] Wijesooriyage WD. Electrochemical Deposition and Characterization of Thermoelectric Thin Films of (Bi x Sb 1-x) 2 Te 3. Chalmers University of Technology, 2011.

[60] Minnich a. J, Dresselhaus MS, Ren ZF, Chen G. Bulk nanostructured thermoelectric materials: current research and future prospects. Energy Environ Sci 2009;2:466. doi:10.1039/b822664b.

[61] Tsuyoshi A, Matsuura K. A trial manufacture of a thermoelectric generator powered by high-temperature heat transfer medium oil. Electr Eng Japan 2002;141:36–44. doi:10.1002/eej.10042.

[62] McEnaney K, Kraemer D, Ren Z, Chen G. Modeling of concentrating solar thermoelectric generators. J Appl Phys 2011;110. doi:10.1063/1.3642988.

[63] Yang Y, Wei X-J, Liu J. Suitability of a thermoelectric power generator for implantable medical electronic devices. J Phys D Appl Phys 2007;40:5790–800. doi:10.1088/0022-3727/40/18/042.

[64] Damaschke JM. Design of a low input voltage converter for thermoelectric generator. IEEE Trans Ind Appl 1997;33:1203–7.

[65] Li Z, Zhao GL, Zhang P, Guo S, Tang J. Thermoelectric Performance of Micro / Nano-Structured Bismuth-Antimony-Telluride Bulk from Low Cost Mechanical Alloying. Mater Sci Appl 2012;3:833–7.

[66] Goldsmid H. Bismuth Telluride and Its Alloys as Materials for Thermoelectric Generation. Materials (Basel) 2014;7:2577–92. doi:10.3390/ma7042577.

[67] Ma Y, Wijesekara W, Palmqvist AEC. Electrochemical Deposition and Characterization of Thermoelectric Ternary (Bi x Sb1−x)2Te3 and Bi2(Te1−y Se y)3 Thin Films. J Electron Mater 2011;41:1138–46. doi:10.1007/s11664-011-1790-y.

[68] Wood C. Materials for thermoelectric energy conversion 1988;459.

[69] Chung D, Hogan T, Brazis P, Rocci-lane M, Kannewurf C, Bastea M, et al. CsBi 4 Te 6 : A High-Performance Thermoelectric Material for Low-Temperature Applications. Science (80-) 2000;287:1024–2027. doi:10.1126/science.287.5455.1024.

[70] Xiao F, Hangarter C, Yoo B, Rheem Y, Lee K-H, Myung N V. Recent progress in electrodeposition of thermoelectric thin films and nanostructures. Electrochim Acta 2008;53:8103–17. doi:10.1016/j.electacta.2008.06.015.

[71] Poudel B, Hao Q, Ma Y, Lan Y, Minnich A, Yu B, et al. High-thermoelectric performance of nanostructured bismuth antimony telluride bulk alloys. Science 2008;320:634–8. doi:10.1126/science.1156446.

[72] Venkatasubramanian R, Siivola E, Colpitts T, O'Quinn B. Thin-film thermoelectric devices with high room-temperature figures of merit. Nature 2001;413:597–602. doi:10.1038/35098012.

[73] Gelbstein Y, Dashevsky Z, Dariel MP. Highly efficient bismuth telluride doped p-type Pb0.13Ge0.87Te for thermoelectric applications. Phys Status Solidi – Rapid Res Lett 2007;1:232–4. doi:10.1002/pssr.200701160.

[74] Wood C. Materials for thermoelectric energy conversion. Reports Prog Phys 1988;51:459–539.

[75] Sootsman JR, Chung DY, Kanatzidis MG. New and old concepts in thermoelectric materials. Angew Chem Int Ed Engl 2009;48:8616–39. doi:10.1002/anie.200900598.

[76] Heremans JP, Jovovic V, Toberer ES, Saramat A, Kurosaki K, Charoenphakdee A, et al. Enhancement of Thermoelectric Efficiency in PbTe by Distortion of the Electronic Density of States. Science (80-) 2008;321:1457–61.

[77] Nolas GS, Poon J, Kanatzidis M. Recent Developments in Bulk Thermoelectric Materials. MRS Bull 2006;31:199–205. doi:10.1557/mrs2006.45.

[78] Zhai PC, Zhao WY, Li Y, Liu LS, Tang XF, Zhang QJ, et al. Nanostructures and enhanced thermoelectric properties in Ce-filled skutterudite bulk materials. Appl Phys Lett 2006;89:1–4. doi:10.1063/1.2234842.

[79] Snyder GJ. Application of the compatibility factor to the design of segmented and cascaded thermoelectric generators. Appl Phys Lett 2004;84:2436–8. doi:10.1063/1.1689396.

[80] Crane DT, Bell LE. Progress towards maximizing the performance of a thermoelectric power generator. 25th Int. Conf. Thermoelectr. ICT, Proc., 2006, p. 11–6. doi:10.1109/ICT.2006.331259.

[81] Yang J, Stabler FR. Automotive Applications of Thermoelectric Materials. J Electron Mater 2009;38:1245–51. doi:10.1007/s11664-009-0680-z.

[82] El-Genk MS, Saber HH. High efficiency segmented thermoelectric unicouple for operation between 973 and 300 K. Energy Convers Manag 2003;44:1069–88. doi:10.1016/S0196-8904(02)00109-7.

[83] Luan W, Tu S. Recent developments of thermoelectric power generation. Chinese Sci Bull 2004;49:1212–9. doi:10.1360/04we0037.

[84] Dasgupta T, Stiewe C, Sesselmann A, Yin H, Iversen BB, Mueller E. Thermoelectric studies in β-Zn4Sb3-the complex interdependence between thermal stability, thermoelectric transport, and zinc content. J Appl Phys 2013;113:103708 1–9. doi:10.1063/1.4794816.

[85] Cederkrantz D, Farahi N, Borup K a., Iversen BB, Nygren M, Palmqvist AEC. Enhanced thermoelectric properties of Mg2Si by addition of TiO2 nanoparticles. J Appl Phys 2012;111:023701 1–7. doi:10.1063/1.3675512.

[86] Satyala N, Vashaee D. Detrimental influence of nanostructuring on the thermoelectric properties of magnesium silicide. J Appl Phys 2012;112:093716–1 – 11. doi:10.1063/1.4764872.

[87] Morozova N V., Ovsyannikov S V., Korobeinikov I V., Karkin AE, Takarabe KI, Mori Y, et al. Significant enhancement of thermoelectric properties and metallization of Al-doped Mg2Si under pressure. J Appl Phys 2014;115:213705 1–9. doi:10.1063/1.4881015.

[88] Søndergaard M. Synthesis and characterization of inexpensive high-performance thermoelectric materials. Aarhus University, Denmark, 2013.

[89] Chen X, Weathers A, Salta D, Zhang L, Zhou J, Goodenough JB, et al. Effects of (Al,Ge) double doping on the thermoelectric properties of higher manganese silicides. J Appl Phys 2013;114. doi:10.1063/1.4828731.

[90] Uemura K. History of thermoelectricity development in Japan. J Thermoelectr 2002;3:7–16.

[91] Yu B, Zebarjadi M, Wang H, Lukas K, Wang H, Wang D, et al. Enhancement of thermoelectric properties by modulation-doping in silicon germanium alloy nanocomposites. Nano Lett 2012;12:2077–82. doi:10.1021/nl3003045.

[92] Joshi G, Lee H, Lan Y, Wang X, Zhu G, Wang D, et al. Enhanced thermoelectric figure-of-merit in nanostructured p-type silicon germanium bulk alloys. Nano Lett 2008;8:4670–4. doi:10.1021/nl8026795.

[93] Wang XW, Lee H, Lan YC, Zhu GH, Joshi G, Wang DZ, et al. Enhanced thermoelectric figure of merit in nanostructured n-type silicon germanium bulk alloy. Appl Phys Lett 2008;93:193121. doi:10.1063/1.3027060.

[94] Zhao L-D, Lo S-H, Zhang Y, Sun H, Tan G, Uher C, et al. Ultralow thermal conductivity and high thermoelectric figure of merit in SnSe crystals. Nature 2014;508:373–7. doi:10.1038/nature13184.

[95] Zhang H, Talapin D V. Thermoelectric tin selenide: The beauty of simplicity. Angew Chemie - Int Ed 2014;53:9126–7. doi:10.1002/anie.201405683.

[96] Kim G-H, Shao L, Zhang K, Pipe KP. Engineered doping of organic semiconductors for enhanced thermoelectric efficiency. Nat Mater 2013;12:719–23. doi:10.1038/nmat3635.

[97] Zhang K, Zhang Y, Wang S. Enhancing thermoelectric properties of organic composites through hierarchical nanostructures. Sci Rep 2013;3:3448. doi:10.1038/srep03448.

[98] Zhang Q, Sun Y, Xu W, Zhu D. Organic Thermoelectric Materials: Emerging Green Energy Materials Converting Heat to Electricity Directly and Efficiently. Adv Mater 2014:n/a – n/a. doi:10.1002/adma.201305371.

[99] Leclerc M, Najari A. Organic thermoelectrics: green energy from a blue polymer. Nat Mater 2011;10:409–10. doi:10.1038/nmat3032.

[100] Russ B, Robb MJ, Brunetti FG, Miller PL, Perry EE, Patel SN, et al. Power factor enhancement in solution-processed organic n-type thermoelectrics through molecular design. Adv Mater 2014;26:3473–7. doi:10.1002/adma.201306116.

[101] Søndergaard RR, Hösel M, Espinosa N, Jørgensen M, Krebs FC. Practical evaluation of organic polymer thermoelectrics by large-area R2R processing on flexible substrates. Energy Sci Eng 2013;1:81–8. doi:10.1002/ese3.8.

[102] Chen Y, Zhao Y, Liang Z. Solution processed organic thermoelectrics : towards flexible thermoelectric modules. Energy Environ Sci 2014;8:401–22. doi:10.1039/c4ee03297g.

[103] Terasaki I, Sasago Y, Uchinokura K. Large thermoelectric power in NaCo2O4 single crystals. Phys Rev B 1997;56:R12685–7. doi:10.1103/PhysRevB.56.R12685.

[104] Matsubara I, Funahashi R, Takeuchi T, Sodeoka S, Shimizu T, Ueno K. Fabrication of an all-oxide thermoelectric power generator. Appl Phys Lett 2001;78:3627–9. doi:10.1063/1.1376155.

[105] Choi S-M, Lee K-H, Lim C-H, Seo W-S. Oxide-based thermoelectric power generation module using p-type Ca3Co4O9 and n-type (ZnO)7In2O3 legs. Energy Convers Manag 2011;52:335–9. doi:10.1016/j.enconman.2010.07.005.

[106] Kabir R, Zhang T, Donelson R, Wang D, Tian R, Tan TT, et al. Thermoelectric properties of Yb and Nb codoped CaMnO 3. Phys Status Solidi 2014;211:1200–6. doi:10.1002/pssa.201330475.

[107] Zhan B, Lan J, Liu Y, Lin Y, Shen Y, Nan C. High Temperature Thermoelectric Properties of Dy-doped CaMnO3 Ceramics. J Mater Sci Technol 2014;30:821–5. doi:10.1016/j.jmst.2014.01.002.

[108] Shikano M, Funahashi R. Electrical and thermal properties of single-crystalline (Ca2CoO3)0.7CoO2 with a Ca3Co4O9 structure. Appl Phys Lett 2003;82:1851–3. doi:10.1063/1.1562337.

[109] Sotelo a., Constantinescu G, Rasekh S, Torres M a., Diez JC, Madre M a. Improvement of thermoelectric properties of Ca3Co4O9 using soft chemistry synthetic methods. J Eur Ceram Soc 2012;32:2415–22. doi:10.1016/j.jeurceramsoc.2012.02.012.

[110] Terasaki I. Physics of the thermoelectric oxide NaCo2O4: A guide to new thermoelectric oxides. Twenty-First Int Conf Thermoelectr 2002 Proc ICT '02 2002. doi:10.1109/ICT.2002.1190296.

[111] DiSalvo FJ. Thermoelectric Cooling and Power Generation. Science (80-) 1999;285:703–6. doi:10.1126/science.285.5428.703.

[112] Ono K, Suzuki RO. Thermoelectric power generation: Converting low-grade heat into electricity. Jom 1998;50:49–51. doi:10.1007/s11837-998-0308-4.

[113] Rowe DM. Thermoelectrics, an environmentally-friendly source of elelctrical power. Renew Energy 1999;16:1251–6.

[114] Min GMG, Rowe DM. Recent concepts in thermoelectric power generation. Twenty-First Int. Conf. Thermoelectr. 2002. Proc. ICT '02., 2002, p. 365–74. doi:10.1109/ICT.2002.1190341.

[115] Riffat SB, Ma X. Thermoelectrics: A review of present and potential applications. Appl Therm Eng 2003;23:913–35. doi:10.1016/S1359-4311(03)00012-7.

[116] Service RF. Temperature rises for devices that turn heat into electricity. Science 2004;306:806–7. doi:10.1126/science.306.5697.806.

[117] Mayer P, Ram RJ. Thin-film thermoelectric generator element characterization. Int Conf Thermoelectr ICT, Proc 2005;2005:265–8. doi:10.1109/ICT.2005.1519939.

[118] Schneider T, Alley R, Koester D, Lee S. Thin Film Thermoelectric Power Generation: Enabling Waste Heat Recovery in High Heat Flux Environments. 2007.

[119] Laird's. Laird's thin film thermoelectric materials 2015. http://www.lairdtech.com/product-categories/power-products/power-generators.

[120] Weinstein L a., McEnaney K, Chen G. Modeling of thin-film solar thermoelectric generators. J Appl Phys 2013;113. doi:10.1063/1.4803123.

[121] Fan P, Zheng ZH, Cai ZK, Chen TB, Liu PJ, Cai XM, et al. The high performance of a thin film thermoelectric generator with heat flow running parallel to film surface. Appl Phys Lett 2013;102:2013–6. doi:10.1063/1.4788817.

[122] Dresselhaus MS, Dresselhaus G, Sun X, Zhang Z, Cronin SB, Koga T, et al. the Promise of Low-Dimensional Thermoelectric Materials. Microscale Thermophys Eng 1999;3:89–100. doi:10.1080/108939599199774.

[123] Venkatasubramanian R, Colpitts T, Watko E, Lamvik M, El-Masry N. MOCVD of Bi2Te3, Sb2Te3 and their superlattice structures for thin-film thermoelectric applications. J Cryst Growth 1997;170:817–21. doi:10.1016/S0022-0248(96)00656-2.

[124] Mzerd a., Aboulfarah B, Giani a., Boyer a. Elaboration and characterization of MOCVD (Bi1- x Sb x)2 Te3 thin films. J Mater Sci 2006;41:1659–62. doi:10.1007/s10853-005-2033-5.

[125] Wang XH, Yamamoto a., Eguchi K, Obara H, Yoshida T. Thermoelectric properties of SiC thick films deposited by thermal plasma physical vapor deposition. Sci Technol Adv Mater 2003;4:167–72. doi:10.1016/S1468-6996(03)00015-9.

[126] Li F, Wang W. Electrodeposition of BixSb2-xTey thermoelectric thin films from nitric acid and hydrochloric acid systems. Appl Surf Sci 2009;255:4225–31. doi:10.1016/j.apsusc.2008.11.013.

[127] Holgate TC, Han L, Wu N, Bøjesen ED, Christensen M, Iversen BB, et al. Characterization of the interface between an Fe-Cr alloy and the p-type thermoelectric oxide Ca3Co4O9. J Alloys Compd 2014;582:827–33. doi:10.1016/j.jallcom.2013.08.096.

[128] Zhao D, Geng H, Chen L. Microstructure contact studies for skutterudite thermoelectric devices. Int J Appl Ceram Technol 2012;9:733–41. doi:10.1111/j.1744-7402.2011.02703.x.

[129] García-Cañadas J, Powell A V., Kaltzoglou A, Vaqueiro P, Min G. Fabrication and evaluation of a skutterudite-based thermoelectric module for high-temperature applications. J Electron Mater 2013;42:1369–74. doi:10.1007/s11664-012-2241-0.

[130] Wijesekara W, Rosendahl L, Brown DR, Snyder GJ. Unileg Thermoelectric Generator Design for Oxide Thermoelectrics and Generalization of the Unileg Design Using an Idealized Metal. J Electron Mater 2014. doi:10.1007/s11664-014-3569-4.

[131] Vining CB. An inconvenient truth about thermoelectrics. Nat Mater 2009;8:83–5. doi:10.1038/nmat2361.

[132] Wijesekara WP, Rosendahl LA, Wu N, Han L, Bjørk R, Nong N V. Unpublished data - Performance and Stress Analysis of Oxide Thermoelectric Module Architecture Designed for Maximum Power Output. Aalborg, Denmark: 2013.

[133] Onsager L. Reciprocal relations in irreversible processes. I. Phys Rev 1931;37:405–26. doi:10.1103/PhysRev.37.405.

[134] Callen HB. The application of onsager's reciprocal relations to thermoelectric, thermomagnetic, and galvanomagnetic effects. Phys Rev 1948;73:1349–58. doi:10.1103/PhysRev.73.1349.

[135] Dqmenicali CA. Irreversible Thermodynamics of Thermoelectricity. Rev Mod Phys 1954;26:237–75.

[136] Boerdijk AH. Contribution to a general theory of thermocouples. J Appl Phys 1959;30:1080–3. doi:10.1063/1.1776982.

[137] Boerdijk AH. Diagrams Representing States of Operation of a General Thermocouple. J Appl Phys 1960;31:1141–4. doi:10.1063/1.1735791.

[138] Boerdijk AH. Zero, First, and SecondOrder Theories of a General Thermocouple. J Appl Phys 1961;32:1584–9. doi:10.1063/1.1728400.

[139] Ure RW, Heikes RR. Materials requirements for segmented thermoelectric materials. Adv Energy Convers 1962;2:177–81. doi:10.1016/0365-1789(62)90022-X.

[140] Harman TC. Multiple stage thermoelectric generation of power. J Appl Phys 1958;29:1471–3. doi:10.1063/1.1722971.

[141] Snyder GJ. Application of the compatibility factor to the design of segmented and cascaded thermoelectric generators. Appl Phys Lett 2004;84:2436–8. doi:10.1063/1.1689396.

[142] Chen L, Gong J, Sun F, Wu C. Effect of heat transfer on the performance of thermoelectric generators. Int J Therm Sci 2002;41:95–9. doi:10.1016/S1290-0729(01)01307-2.

[143] Xuan XC, Ng KC, Yap C, Chua HT. A general model for studying effects of interface layers on thermoelectric devices performance. Int J Heat Mass Transf 2002;45:5159–70. doi:10.1016/S0017-9310(02)00217-X.

[144] Mayer PM, Ram RJ. Optimization of Heat Sink–Limited Thermoelectric Generators. Nanoscale Microscale Thermophys Eng 2006;10:143–55. doi:10.1080/10893950600643063.

[145] Rollinger CN, Sunderland JE. The performance of a convectively cooled thermoelement used for power generation. Solid State Electron 1961;3:268–77. doi:10.1016/0038-1101(61)90009-0.

[146] Ybarrondo LJ, Sunderland JE. Effects of surface heat transfer on the performance of a thermoelectric generator. Solid State Electron 1962;5:143–54. doi:10.1016/0038-1101(62)90005-9.

[147] SUNDERLAND JE, BURAK NT. The influence of the Thomson effect on the performance of a thermoelectric power generator. Solid State Electron 1964;7:465–71. doi:10.1016/j.ijheatmasstransfer.2004.05.040.

[148] Tai-ko Shaw D. The static temperature distribution of a thermoelement with temperature varying parameters. Adv Energy Convers 1966;6:57–65. doi:10.1016/0365-1789(66)90012-9.

[149] Sandoz-Rosado EJ, Weinstein SJ, Stevens RJ. On the Thomson effect in thermoelectric power devices. Int J Therm Sci 2013;66:1–7. doi:10.1016/j.ijthermalsci.2012.10.018.

[150] Brennan WD. Experiment in Thermoelectricity. Am J Phys 1959;27:427. doi:10.1119/1.1934889.

[151] Lucke WH. Reply to Experiment in Thermoelectricity. Am J Phys 1960;28:563. doi:10.1119/1.1935887.

[152] Landecker K. Some aspects of the performance of refrigerating thermojunctions with radial flow of current. J Appl Phys 1976;47:1846–51. doi:10.1063/1.322903.

[153] Şişman A, Yavuz H. The effect of joule losses on the total efficiency of a thermoelectric power cycle. Energy 1995;20:573–6. doi:10.1016/0360-5442(94)00085-H.

[154] Chua HT, Ng KC, Xuan XC, Yap C, Gordon JM. Temperature-entropy formulation of thermoelectric thermodynamic cycles. Phys Rev E - Stat Nonlinear, Soft Matter Phys 2002;65:1–6. doi:10.1103/PhysRevE.65.056111.

[155] Hodes M. On One-Dimensional Analysis of Thermoelectric Modules (TEMs). IEEE Trans COMPONENTS Packag Technol 2005;28:218–29.

[156] Pramanick a. K, Das PK. Constructal design of a thermoelectric device. Int J Heat Mass Transf 2006;49:1420–9. doi:10.1016/j.ijheatmasstransfer.2005.09.028.

[157] Naji M, Alata M, Al-Nimr M a. Transient behaviour of a thermoelectric device. Proc Inst Mech Eng Part A J Power Energy 2003;217:615–21. doi:10.1177/095765090321700604.

[158] Alata M, Al-Nimr M a., Naji M. Transient behavior of a thermoelectric device under the hyperbolic heat conduction model. Int J Thermophys 2003;24:1753–68. doi:10.1023/B:IJOT.0000004103.26293.0c.

[159] Mahan G. Density variations in thermoelectrics. J Appl Phys 2000;87:7326–32. doi:10.1063/1.372988.

[160] Bitschi A. Modelling of thermoelectric devices for electric power generation. 2009.

[161] Sherman B, Heikes RR, Ure RW. Calculation of Efficiency of Thermoelectric Devices. J Appl Phys 1960;31:1. doi:10.1063/1.1735380.

[162] Brandt JA. Solutions to the differential equations describing the temperature distribution, thermal efficiency, and power output of a thermoelectric element with variable properties and cross sectional area. Adv Energy Convers 1962;2:219–30.

[163] Lyon WC, Bustard TS. Degital computation of thermoelement operational parametrs. Adv Energy Convers 1962;2:197–208.

[164] Moore RG. Exact computer solution of segmented thermoelectric devices. Adv Energy Convers 1962;2:183–95.

[165] Mahan GD. Inhomogeneous thermoelectrics. J Appl Phys 1991;70:4551–4. doi:10.1063/1.349091.

[166] Schilz J, Helmers L, Müller WE, Niino M. A local selection criterion for the composition of graded thermoelectric generators. J Appl Phys 1998;83:1150. doi:10.1063/1.366808.

[167] Helmers L, Müller E, Schilz J, Kaysser WA. Graded and stacked thermoelectric generators—numerical description and maximisation of output power. Mater Sci Eng B 1998;56:60–8. doi:10.1016/S0921-5107(98)00211-6.

[168] Müller E, Walczak S, Seifert W, Stiewe C, Karpinski G. Numerical performance estimation of segmented thermoelectric elements. 24th Int Conf Thermoelectr ICT, Proc 2005:352–7. doi:10.1109/ICT.2005.1519959.

[169] Min G. Thermoelectric Energy Harvesting. In: Beeby S, White N, editors. Energy Harvest. Auton. Syst., 2010, p. 135–57.

[170] Rowe DM, Min G. Evaluation of thermoelectric modules for power generation. J Power Sources 1998;73:193–8. doi:10.1016/S0378-7753(97)02801-2.

[171] Snyder GJ. Application of the compatibility factor to the design of segmented and cascaded thermoelectric generators. Appl Phys Lett 2004;84:2436. doi:10.1063/1.1689396.

[172] Funahashi R, Mihara T, Urata S, Hisazumi Y, Kegasa A. Preparation and properties of thermoelectric pipe-type modules. 25th Int. Conf. Thermoelectr. ICT, Proc., 2006, p. 58–61. doi:10.1109/ICT.2006.331269.

[173] Preis K, Biro O, Dyczij-Edlinger R, Richter KR, Badics Z, Riedler H, et al. Application of FEM to coupled electric, thermal and mechanical problems. IEEE Trans Magn 1994;30:3316–9. doi:10.1109/20.312647.

[174] Kubo M, Shinoda M, Furuhata T, Kitagawa K. Optimization of the incision size and cold-end temperature of a thermoelectric device. Energy 2005;30:2156–70. doi:10.1016/j.energy.2003.10.017.

[175] Span G, Wagner M, Holzer S, Grasser T. Thermoelectric Power Conversion using Generation of Electron-Hole Pairs in Large Area p-n Junctions. 25th Int. Conf. Thermoelectr. 2006, 2006, p. 23–6. doi:10.1109/ICT.2006.331261.

[176] Iwasaki Y, Takeda M. Development of flexible thermoelectric device: Improvement of device performance. 25th Int. Conf. Thermoelectr. 2006, 2006, p. 562. doi:10.1007/s11664-009-0657-y.

[177] Min G, Rowe DM. Ring-structured thermoelectric module. Semicond Sci Technol 2007;22:880–3. doi:10.1088/0268-1242/22/8/009.

[178] Ebling D, Bartholomé K, Bartel M, Jägle M. Module geometry and contact resistance of thermoelectric generators analyzed by multiphysics simulation. J Electron Mater 2010;39:1376–80. doi:10.1007/s11664-010-1331-0.

[179] Jang B, Han S, Kim J-Y. Optimal design for micro-thermoelectric generators using finite element analysis. Microelectron Eng 2011;88:775–8. doi:10.1016/j.mee.2010.06.025.

[180] Yang T, Xiao J, Li P, Zhai P, Zhang Q. Simulation and optimization for system integration of a solar thermoelectric device. J Electron Mater 2011;40:967–73. doi:10.1007/s11664-010-1471-2.

[181] Kim R-Y, Lai J-S, York B, Koran A. Analysis and Design of Maximum Power Point Tracking Scheme for Thermoelectric Battery Energy Storage System. IEEE Trans Ind Electron 2009;56:3709–16. doi:10.1109/TIE.2009.2025717.

[182] Ziolkowski P, Poinas P, Leszczynski J, Karpinski G, Müller E. Estimation of thermoelectric generator performance by finite element modeling. J Electron Mater 2010;39:1934–43. doi:10.1007/s11664-009-1048-0.

[183] Wang F, Zhou J, Wang G, Zhou X. Simulation on thermoelectric device with hydrogen catalytic combustion. Int J Hydrogen Energy 2012;37:884–8. doi:10.1016/j.ijhydene.2011.04.029.

[184] Bjørk R, Christensen DV, Eriksen D, Pryds N. Analysis of the internal heat losses in a thermoelectric generator. Int J Therm Sci 2014;85:12–20. doi:10.1016/j.ijthermalsci.2014.06.003.

[185] Ebling D, Jaegle M, Bartel M, Jacquot A, Böttner H. Multiphysics Simulation of Thermoelectric Systems for Comparison with Experimental Device Performance. J Electron Mater 2009;38:1456–61. doi:10.1007/s11664-009-0825-0.

[186] COMSOL. Comsol Multiphysics User's Guide 2012.

[187] Saber HH, El-Genk MS. Optimization of segmented thermoelectric for maximizing conversion efficiency and electric power density. Twenty-First Int. Conf. Thermoelectr. 2002. Proc. ICT '02., IEEE; n.d., p. 404–7. doi:10.1109/ICT.2002.1190347.

[188] Apertet Y, Ouerdane H, Goupil C, Lecoeur P. Comment on "Effective thermal conductivity in thermoelectric materials" [J. Appl. Phys. 113, 204904 (2013)]. J Appl Phys 2014;115:126101. doi:10.1063/1.4869138.

[189] Baranowski LL, Jeffrey Snyder G, Toberer ES. Effective thermal conductivity in thermoelectric materials. J Appl Phys 2013;113:204904. doi:10.1063/1.4807314.

[190] Baranowski LL, Jeffrey Snyder G, Toberer ES. Response to "Comment on 'Effective thermal conductivity in thermoelectric materials'" [J. Appl. Phys. 113, 204904 (2013)]. J Appl Phys 2014;115:126102. doi:10.1063/1.4869140.

[191] Yee SK, LeBlanc S, Goodson KE, Dames C. $ per W metrics for thermoelectric power generation: beyond ZT. Energy Environ Sci 2013;6:2561. doi:10.1039/c3ee41504j.

[192] Cengel YA, Turner RH, Cimbala JM. Steady heat conduction. Fundam. Therm. - fluid Sci. 3rd ed., Singapore: McGraw Hill Higher Education; 2008, p. 653–722.

[193] Muta H, Kurosaki K, Uno M, Yamanaka S. Thermoelectric properties of constantan / spherical SiO 2 and Al 2 O 3 particles composite. J Alloys Compd 2003;359:326–9.

[194] Cagran C, Hüpf T, Pottlacher G, Lohöfer G. High-Temperature Metallic Melts – Resistivity Intercomparison for Space Applications. Int J Thermophys 2007;28:2176–87. doi:10.1007/s10765-007-0245-4.

[195] Brückner W, Baunack S, Reiss G, Leitner G, Knuth T. Oxidation behaviour of Cu-Ni(Mn) (constantan) films. Thin Solid Films 1995;258:252–9. doi:10.1016/0040-6090(94)06358-3.

[196] The Physics Hypertextbook. Electric Resistance n.d. http://physics.info/electric-resistance/.

[197] Smith DR, Fickett FR. Low-Temperature Properties of Silver. J Res Natl Inst Stand Technol 1995;100:119–71.

[198] Snyder GJ, Ursell TS. Thermoelectric efficiency and compatibility. Phys Rev Lett 2003;91:148301. doi:10.1103/PhysRevLett.91.148301.

[199] Saramat a., Svensson G, Palmqvist a. EC, Stiewe C, Mueller E, Platzek D, et al. Large thermoelectric figure of merit at high temperature in Czochralski-grown clathrate Ba 8Ga 16Ge 30. J Appl Phys 2006;99:2–6. doi:10.1063/1.2163979.

[200] Nagira T, Ito M, Katsuyama S, Hara S. Thermoelectric Properties of NaxCo2O4 Prepared by the Polymerized Complex Method and Spark Plasma Sintering. Mater Trans 2003;44:1866–71. doi:10.2320/matertrans.44.1866.

[201] Puyet M, Dauscher a., Lenoir B, Dehmas M, Stiewe C, Müller E, et al. Beneficial effect of Ni substitution on the thermoelectric properties in partially filled Ca[sub y]Co[sub 4−x]Ni[sub x]Sb[sub 12] skutterudites. J Appl Phys 2005;97:083712. doi:10.1063/1.1868083.

[202] He Z, Stiewe C, Platzek D, Karpinski G, Müller E, Li S, et al. Thermoelectric properties of hot-pressed skutterudite CoSb3. J Appl Phys 2007;101. doi:10.1063/1.2538036.

[203] American Elements. American Elements - Lead Telluride 2015. https://www.americanelements.com/pbte.html (accessed August 3, 2015).

[204] Wijesekara W, Rosendahl L. Expanding the reduced-current approach for thermoelectric generators to achieve higher volumetric power density. Phys Status Solidi 2015;212:591–9. doi:10.1002/pssa.201431335.